European Research Community On Flow, Turbulence And Combustion

www.ercoftac.org

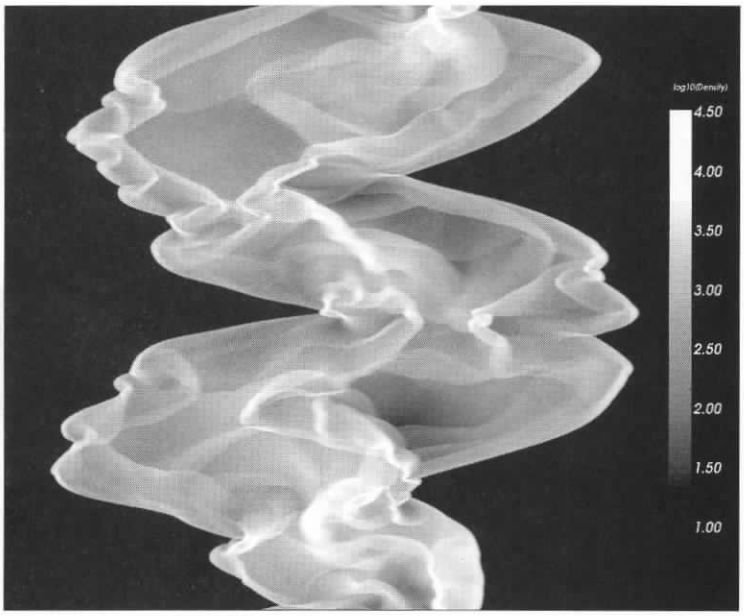

THEME - TURBULENCE IN COMPRESSIBLE FLOWS

ERCOFTAC bulletin

70

SEPTEMBER 2006

ERCOFTAC

Honorary Presidents

Mathieu J., Spalding D.B., Vittoz B., Zienkiewicz O.

Managing Board Members

Executive Committee:

Oliemans R.V.A.	***Chairman*** — Multiphase Flow B.V., Bilthoven, NL Tel.: +31.30.229.1719, Fax: +31.15.278.2838
Rodi W.	***Deputy Chairman*** — Universität Karlsruhe, Karlsruhe, D
Hirsch Ch.	***Deputy Chairman*** —NUMECA, Brussels, B
Duursma R.P.J.	***Treasurer*** — CORUS, Amsterdam, NL
Ooms G.	***Deputy Treasurer*** — J.M. Burgers Centre, Delft, NL
Hunt J.	University College — London, UK
Hutton A.G.	QinetiQ — Farnborough, GB
Jacquin L.	ONERA-DAFE — Meudon, F
Laurence D.	UMIST — Manchester, UK / EDF — Chatou, F
Leschziner M.	Imperial College — London, UK

Anderson H.	NTNU — Trondheim, N
Binninger B.	ITM, RWTH — Aachen, D
Bonnet J.P.	Univ. de Poitiers — Poitiers, F
Bontoux P.	Univ. de Aix-Marseille — Marseille, F
Cambon C.	ECL/LMFA — Ecully, F
Carey Ch.	Fluent Europe Ltd — Sheffield, UK
Castilla R.	UPC — Barcelona
Chmielniak T.	Silesian Tech. Univ. — Gliwice, PL
Courty J.-C.	Dassault Aviation — Saint Cloud, F
Doerffer P.	Polish Academy of Sciences — Gdansk, PL
Eggels R.	Rolls Royce Deutschland — Dahlewitz, D
Haas J.-F.	CEA-DIF — Bruyères-le-Châtel, F
Kozel K.	CTU — Prague, CZ
Knörzer D.	CEC — Brussels, B
Kuhlmann H.	TU Wien — Vienna, A
Macek J.	CTU — Prague, CZ
Martelli F.	University of Florence — Florence, I
Menter F.	AEA Technology — Otterfing, D
Monkewitz P.	EPFL-LMF — Lausanne, CH
Redondo J.M.	UPC — Barcelona, E
Sick M.	VATECH — Zurich, CH
Spathopoulos T.	Hellenic Aerospace Industry — Schmitari, GR
Torre A.	Ansaldo Energia — Genova, I
Tatschl R.	AVL List GmbH — Graz, A
Van den Braembussche R.	VanKarman Institute — Rhode-St-Genèse, B
Vlachos N.	University of Thessaly — Volos, GR
Wagner C.	DLR — Göttingen, D
Wallin S.	FOI — Stockholm, S

Secretary ***Ursenbacher T.*** — ERCOFTAC Coordination Centre

Industrial Advisory Committee

Hutton A.G. ***Chairman*** — QinetiQ, Farnborough, GB
Tel.: + 44 (0) 1252.395.568
Fax: +44 (0) 1252.395.322
E-mail: aghutton@QinetiQ.com

Laurence D. ***(Deputy Chairman),*** UMIST — Manchester, GB

The members of the IAC are the representatives of industrial members of ERCOFTAC.

Scientific Programme Committee

Leschziner M. ***(Chairman)***
Imperial College — London, UK
Tel.: + (0) 44.20.7594.5061
Fax: + (0) 44.20.7584.8120

Andersson H. — NTNU, Trondheim, N
Aupoix B. — ONERA, Toulouse, F
Braza M. — IMFT-CNRS, Toulouse, F
Cambon C. — ECL/LMFA, Ecully, F
Carey Ch. — Fluent Europe, Sheffield, UK
Cartage T. — Solvay S.A., B
Castro I. — Univ. of Southampton, UK
Choi K.S. — Univ. of Nottingham, UK
Courty J.-C. — Dassault Aviation, F
Dick E. — Universiteit, Gent, B
Doerffer P. — Polish Academy of Sciences, Gdansk, PL
Drobniak S. — TU-Czestochowa, PL
Duursma R.P.J. — CORUS, NL
Flohr P. — ALSTOM Ltd., Baden-Daettwil, CH
Geurts B.J. — Univ. Twente, Enschede NL
Haas J.F. — CEA, Bruyères-le-Châtel, F
Haase W. — EADS, München, D
Hanjalic K. — TU - Delft, NL
Hirsch Ch. — NUMECA, Brussels, B
Hunt J.C.R. — Univ. College London, UK
Kozel K. — CTU, Prague, CZ
Kuhlmann H. — TU Wien, Vienna, A
Menter F. — AEA Technology, D
Métais O. — IMG-LEGI, Grenoble, F
Monkewitz P. — EPFL-LMF, Lausanne, CH
Morvan H. — Univ. of Nottingham, UK
Oliemans R.V.A. — Multiphase Flow B.V., NL
Ooms G. — JMBC, Delft, NL
Orlandi P. — Universita di Roma, I
Peters B. — AVL GmbH, Graz, A
Peters N. — RWTH, Aachen, D
Redondo J. — UPC, Barcelona, E
Rodi W. — Universität Karlsruhe, D
Savill A.M. — Cranfield Univ. Cranfield, UK
Stelling G.S. — TU Delft, Delft, NL
Turan A. — UMIST, Manchester, UK
Van Steenhoven A. — TUE, Eindhoven, NL
Wagner C. — DLR, Göttingen, D

Secretary: Ursenbacher T.
Director : Monkewitz P.A.
ERCOFTAC Coordination Centre

LISTE OF CONTENTS

PAGE

EDITORIAL 5
P. Comte

THEME

Compressible Turbulence of Supersonic Flows: Actions and Interactions 7
J.-P. Dussauge

Compressible Mixing Layers: Data Analysis and Modelling 13
B. Aupoix, H. Bézard

Is Compressibility Always Stabilizing and Why? Open Issues 19
C. Cambon , L. Jacquin

On compressiblity effects on Hypermixing strategies 27
E. Collin, M. Ndoye, J.-P. Bonnet

Introduction to Turbulent Combustion 33
D. Veynante

Aspects of Turbulence in Astrophysics 43
R. Walder, D. Folilni, J. Favre

BULLETIN THEMES AND PC REPORTS 49
Past and Futur

ERCOFTAC SPECIAL INTEREST GROUPS 50
Contacts E-mails, Faxes and Phone Numbers

ERCOFTAC PILOT CENTRES AND OFFICES 51
Addresses, E-mails and Phone Numbers

EDITORIAL BOARD

Editor - T. Ursenbacher
EPF-Lausanne

E. Dick, ***Chairman***
Univ. of Gent

B.J. Geurts
Univ. of Twente

W. Elsner
TU Czestochowa

ADDRESS:
ERCOFTAC BULLETIN
ERCOFTAC C.C.
EPFL STI ISE ERCOFTAC
ME B2 495, Station 9
CH-1015 Lausanne
Tel: +41.21.693.5305
Fax: +41.21.693.5307
E-Mail: ercoftac@epfl.ch
http://www.ercoftac.org

SUBSCRIPTION FEE:
ERCOFTAC members: Free*
Non-members in Europe: € 140.-
Institutes outside Europe: € 75.-
*€ 60.- after first ten subscriptions per member organisation.
Libraries: enquiries to the above address.

The reader should note that the Editorial Board cannot accept responsibility for the accuracy of statements made by individual contributing authors.

CIRCULATION: 850 copies

TEXT PROCESSING AND LAYOUT:
Ruth Fiaux

FRONT COVER PICTURE:
Supersonic turbulence in hypersonic flow collision, shown in density. Dissipation is due to a network of shocks that scales with the interaction zone. Courtesy R. Walder, D. Folini and J. Favre, Observatoire de Strasbourg, Strasbourg / Institute of Astronomy, ETH-Zürich / CSCS, Manno
(see paper "Aspect of Turbulence in Astrophysics", pp. 43-47 in this Special Issue).

Call for contributions

Deadline for submission of papers, announcements, letter to the editor

October 20, 2006

Next issue scheduled for December 2006

ERCOFTAC

Introductory Course to Design Optimisation

Universitå degli Studi di Trieste, Trieste, Italy

April 18 - 20, 2007

Organised by

Università degli Studi di Trieste, ERCOFTAC SIG on Design Optimisation in Association with the von Karman Institute (Belgium)

Computer-optimisation of engineering designs is a powerful emerging technology. Currently, technical designs are based on the intuition and the experience of design engineers. In the future, computer optimisation will assist in the search for optimal technical solutions.

Automated design optimisation technology has already been applied to numerous problems. Many of the applications are in the area of Computational Structural Mechanics (CSM). Computational Fluid Dynamics (CFD) has not been a natural first candidate for the application of optimisation methods, due to the high CPU requirements for CFD simulations. This is a challenge, as optimisation methods require a significant number of solution points in parameter space in order to arrive to an improved design. However, substantial effort has been devoted in recent years to this problem and efficient solution strategies have been developed.

Acknowledging the growing importance of Design Optimisation to industrial CFD applications, ERCOFTAC has established a Special Interest Group (SIG) on this subject at its Pilot Centre in Munich. It is intended as a platform for the information exchange from science to industry.

In the present course, experts will offer an introduction to the basic methods used in design optimisation. The presentations will cover:

- Genetic Algorithms
- Evolution Strategies
- Gradient-based Methods
- Sensitivity Analysis
- Meta-models / Neural networks
- Optimisation Set-Up
- Commercial Optimisation Tools
- Test Cases for Demonstration on "How It Works"

Furthermore, code vendors will be invited to demonstrate the capabilities of their codes, and to develop basic skills in problem definition, in set-up of applications, in the use of different methods and solution evaluation (maybe you could bring your own application?) on various test cases via hands-on/on-line training. This will help to enable participants to compare different software tools and their suitability for own applications.

Special Interest Group Committee:

- N. Adams (chair), (TU München, Germany)
- R. van den Braembussche (von Karman Institute, Belgium)
- K.C. Giannakoglou (NTU Athens, Greece)
- W. Haase (EADS-MAS, Germany)
- F. Menter (ANSYS Germany GmbH, Germany)
- J. Periaux (Dassault, Pole Scientifique, France)
- C. Poloni (University Trieste, Italy)
- G. Winter (IUSIANI/ULPGC, Spain)

For more information please visit the SIG's Web site on Design Optimisation
www.aer.mw.tum.de/ERCOFTAC/

or simply e-mail to:
info@smileservice.it

For on-line registration:
www.congress.net/ercoftac-ts2007

EDITORIAL

P. Comte

LEA, UMR 6609 CNRS, Université de Poitiers, ENSMA, Poitiers, France

Pierre.Comte@lea.univ-poitiers.fr

The effect of compressibility on turbulence and mixing has been a burning issue ever since the early projects of Advanced Supersonic Transport airplanes and Single Stage to Orbit launchers. Indeed, whereas wall-bounded turbulent flows apparently seem to resist high speeds quite well, as implied by the Strong Reynolds Analogy and the Morkovin hypothesis, the spreading rate of mixing layers is dramatically reduced when the convective Mach numbers (based upon the velocity difference between the vortical structures and each of the two free streams) exceed about 0.7. This, added to the obvious fact that, at a given temporal growth rate, the spatial growth rate decreases as the average between the velocities of the two free streams increases, makes the necessary length for reactants to mix at molecular scales (mixing transition) impractical for planes and launchers, and many European research projects went down, with this reason put forward. However, on Nov. 16, 2004, NASA's X-43A, a 4m long unmanned vehicle equipped with a scramjet engine, reached Mach 9.6 for about 10 seconds.

The ERCOFTAC SIG4 had to react in some way, with its own means. A Summer School on "Turbulence and Mixing in Compressible Flows" was held in Strasbourg, July 7-11 2005, and the first Conference on Turbulence and Interactions, TI 2006, 29 May – 2 June 2006, held in Porquerolles, France, was organized in the form of a 3-day conference followed by a 2-day SIG 4 workshop.

Opportunity has thus been given to revisit and update our knowledge regarding the effects of compressibility on turbulence in the light of recent experiments and simulations, and also to recast the importance of this topic in the general context of industrial, geophysical and astrophysical flows.

This theme issue stems from these two events. Six contributions have been selected, the first three devoted to the understanding of compressibility effects on turbulence, and the last three gradually broadening the scope, almost to the edges of the universe, should there be any.

"Compressible turbulence of supersonic flows: actions and interactions", by Jean-Paul Dussauge, gives an appetizing review of situations in which turbulence not only is modified by compressibility effects, but also modifies the driving flow, causing for example shock unsteadiness and buffeting on an airfoil. The main course could not fit in this bulletin. Readers are thus advised to check out the second issue of "Turbulent Shear Layers in Supersonic Flows", Smits A.J. and Dussauge J.P., Springer Verlag, 2006.

"Compressible mixing layers: data analysis and modelling", by Bertrand Aupoix and Hervé Bézard, assesses the results available both from experiments and simulations and proposes a way of taking into account the reduction of the growth rate as a function of the convective Mach number in RANS models, which is not done yet.

"Is compressibility always stabilizing and why? Open issues", by Claude Cambon and Laurent Jacquin, applies Rapid Distorsion Theory and compares different linear limits in homogeneous turbulence with irrotational main strain or plane shear. It is in particular concluded that, in mixing layers, the linear and non-linear parts of the pressure terms are likely to react differently to compressibility, which requires a more subtle analysis than that permitted by Reynolds stress modelling.

"On compressibility effects on hypermixing strategies", by Erwan Collin, Malick Ndoye and Jean-Paul Bonnet, shows experimental results of jets whose mixing is enhanced by smaller control jets in order to reduce noise. As a splendid answer to the question raised by the previous contribution, mixing is found to be enhanced by compressibility.

"Introduction to turbulent combustion", by Denis Veynante, manages to put a great deal of burning issues in a nutshell. Turbulence there has often to be ruled by combustion, that either damps it as heat release increases viscosity, or enhances it through the baroclinic torque in the vorticity transport equation. Incidentally, the second edition of "Theoretical and numerical combustion", by Poinsot, T. and Veynante, D., came out last year from Edwards Inc. Should I burn my copy of the first issue?

"Aspects of turbulence in astrophysics", by Rolf Walder, Doris Folini and Jean Favre, shows the role of turbulence within stellar objects, accretion disks around black holes and among supernovae. Mach numbers can exceed 100, turbulent Mach numbers are above 1 and dissipation is mostly due to shocks. A 'golden age' of turbulence research in astrophysics is foreseen, in which SIG4 should naturally participate.

Recent Tables of Contents of Flow Turbulence and Combustion

An International Journal Published in Association with ERCOFTAC

Board of Editors: J.C.R. Hunt, K. Hanjalic, L. Vervisch & W. Rodi

TABLE OF CONTENTS VOLUME 76 NO 1, JANUARY 2006

A. H. Herbst and D. S. Henningson
The Influence of Periodic Excitation on a Turbulent Separation Bubble
pp. 1 - 21

G. Kramm and F. Herbert
The Structure Functions of the Velocity and Temperature Fields from the Perspective of Dimensional Scaling
pp. 23 - 60

Z. Wu, A. R. Masri, R. W. Bilger
An Experimental Investigation of the Turbulence Structure of a Lifted H2/N2 Jet Flame in a Vitiated Co-Flow
pp. 61 - 81

J. J. Wang, P. F. Zhang, S. F. Lu, K. Wu
Drag Reduction of a Circular Cylinder Using an Upstream Rod
pp. 83 - 101

TABLE OF CONTENTS VOLUME 76 NO 2, MARCH 2006

K. Lodefier and E. Dick
Modelling of Unsteady Transition in Low-Pressure Turbine Blade Flows with Two Dynamic Intermittency Equations
pp. 103 - 132

I. S. Kim and E. Mastorakos
Simulations of Turbulent Non-Premixed Counterflow Flames with First-Order Conditional Moment Closure
pp. 133 - 162

R. J. E. Walpot, J. G. M. Kuerten, C. W. M. van der Geld
Experimental Determination of Lagrangian Velocity Statistics in Turbulent Pipe Flow
pp. 163 - 175

K.-U. Schildmacher, R. Koch, H.-J. Bauer
Experimental Characterization of Premixed Flame Instabilities of a Model Gas Turbine Burner
pp. 177 - 197

M. Mortensen and B. Andersson
Presumed Mapping Functions for Eulerian Modelling of Turbulent Mixing
pp. 199 - 219

COMPRESSIBLE TURBULENCE OF SUPERSONIC FLOWS: ACTIONS AND INTERACTIONS

Jean-Paul Dussauge

IUSTI, UMR CNRS - Université de Provence 6595, Marseille, France

Jean-Paul.Dussauge@polytech.univ-mrs.fr

Abstract

We propose here a brief review of supersonic flows, in which energy is injected into the turbulent field through distortions. Some peculiarities of compressible turbulence in shear flows are firstly recalled. Some situations in which turbulence do not modify the source of energy injection, typically rapid distortions are recalled and show the peculiarities introduced by compressibility, with the particular role played by pressure. Finally, a number of shock wave/ boundary layer interactions are discussed. A classification is proposed, according to their ranges of influence. Attention is paid to supersonic interactions for which the origin of the observed interactions is discussed.

1 Introduction

When considering an action on turbulence, it is supposed that some turbulent field is subjected to an external influence or forcing. This results in modification of turbulence through the amplitude of the fluctuations, the shape and dynamics of the eddies, producing changes of the rms levels, of the spectra, and in general, of the characteristic scales of turbulence. The notion of interaction implies that the external forcing will be in turn modified by turbulence. Such complex feedback mechanisms are considered here or at least their macroscopic manifestations in the case of supersonic flows; in this case, compressible turbulence can be found, and the external causes of the actions can assume very particular forms, such as shock waves, expansions, etc. Firstly, a short reminder will be proposed to describe how turbulence can be compressible. Some simple cases of 'actions' will be recalled, in which turbulence is subjected to some distortion, which remains constant. Finally, a short review of some other cases will be made, corresponding to interactions, in situations typical of compressible flows: shock vortex interactions, shock/boundary layer interactions.

2 Elements of compressible turbulence

From a formal point of view, compressible turbulence may be characterized by the nature of the instantaneous velocity field, and therefore, the level of fluctuating velocity divergence should be assessed. A dimensional evaluation was proposed in Smits & Dussauge 2006 [1]. For that purpose, a situation of weak compressibility was made, in order to obtain first departures from incompressibility of the fluctuating motion. The divergence of fluctuating velocity was evaluated from the continuity equation in terms of pressure and entropy. The sources of entropy are of course related to viscous heating and molecular heat conduction. A low compressibility hypothesis was made and consisted in assuming that pressure contribution is negligible, and that velocity divergence is produced by the strong heating related to the high level of dissipation occurring at high speeds. Some terms involving temperature fluctuations are present in the final expression, which are expressed in terms of velocity fluctuations through relationships given by the Strong Reynolds Analogy for adiabatic boundary layers. Finally, the following expression is obtained:

$$\frac{div\,u'}{u'/\Lambda} \sim 10\,(\gamma-1)\,m_t^2\left(1+\frac{M^2}{2\gamma}\right),$$

where m_t is the turbulent Mach number based on rms velocity. The first factor of the right hand side member is due to dissipation into heat, the second one represents the contribution of temperature fluctuations. The dependence in m_t^2 is consistent with the results of [2] and [3]. Taking typical values for adiabatic flat plate boundary layers or even in supersonic mixing layers suggests that producing a significant level of velocity fluctuation divergence through dissipations necessitates very high Mach numbers. At rather high, probably hypersonic Mach numbers, velocity divergence may be high because of dissipation, of an increase of the acoustic mode and probably of the apparition of shocklets. Finally this analysis is consistent with the findings of [4] in direct simulations: in mixing layers, it seems that the main effect of compressibility is felt on pressure fluctuations, which in turn modify the anisotropy of turbulence, but it does not act directly on velocity divergence. A conclusion is that in many supersonic situations without heat sources, it may be expected that the divergence free approximation will be good enough to describe the turbulence of the shear flows or of boundary layers.

3 Actions

In this section, the particular properties of turbulence subjected to an external constraint which injects energy into the flow, without possible feedback from turbulence

on this source of energy are considered: they are considered as an action on turbulence. These are typically rapid distortion situations. They are not considered for themselves, but just as constitutive elements of interactions in which they can take place.

This situation is basically simpler than interactions. Typically we consider some global evolution imposed for example by geometry producing some pressure gradient. Considering the mean momentum equation ,far from walls, the mean distortion is independent from the turbulent field if the pressure gradient is much larger than the friction force. This leads to the condition

$$\gamma m_t^2 \frac{\bar{p}}{\Delta p} \frac{L}{\delta} << 1$$

L is the distortion length, δ the turbulent flow thickness and Δp the pressure jump in the distortion. In many supersonic flows, m_t~0.1 and in most rapid distortions L/δ is of the order of 1, so that the previous condition becomes

$$\frac{\Delta p}{\bar{p}} >> 10^{-2},$$

a condition easily matched with isentropic expansion or compression waves in usual supersonic situations. Note that this condition is valid only far from walls, since at the wall, the non-slip condition imposes that friction and pressure forces are comparable, and this condition is felt in most of the inner layer. The external part of boundary layers however, can be safely computed by Euler equations, and therefore does not depend on the turbulence evolving in the distortion.

Many examples of such flows can be found in the literature. We will refer here to two of them, which show clearly the particular role of pressure fluctuations in supersonic flows. The first one is from Dussauge & Gaviglio [5] who studied a turbulent boundary layer subjected to an expansion fan at a Mach number of 1.8. Using a hypothesis of solenoidal fluctuating field, which has been justified in the previous section, they showed essentially that in this case the evolution of the Reynolds stresses in the distortion could be described by low speed modelling, emphasizing that the pure volume changes have an action which is not limited by pressure fluctuations. The other example is taken from Debiève [6], [7]. In this work, shock relations for Reynolds stresses were investigated for a steady shock wave. From the equation for the Reynolds stresses, they retained only the production term and could defined a quantity invariant along the mean motion, and then derived the shock relationships, which are in good agreement with experimental observations. The reason why we could neglect the pressure can be probably found in the works of Durbin & Zeman [8] and from Jacquin et al. [9]. These authors examined linearised problems, and showed that a 'gradient Mach number' M_g , based on the velocity difference across an integral scale in the distortion, can be large in the case of a shock. They suggested that, in this case, pressure terms can be neglected in the linear problem. This can justify, or explain the good behaviour of Debiève's shock formulae, and shows again that even in rather simple linearised problems and even with assumptions of incompressible fluctuating field, the structure of pressure fluctuations is altered, with observable necessary modifications in the pressure strain terms of the Reynolds stress equations.

3 Interactions

3.1 Introduction

In supersonic flows, many studies have been devoted to shock/boundary layer interactions. We will discuss here to what respect these problems can be considered as interactions. The first thing to be examined is the academic case of the interaction of a vortex with a shock wave. We know from theory that in such a situation, the vorticity is altered downstream of the shock, and that there is a loss of energy by acoustic radiation. There is no real input of energy in the system, so that Lighthill [10] considered that there was a redistribution of energy among the different elements. As a consequence, he considered that the energy of shock waves was scattered by the eddies. This is an interesting point of view, since now we considered that the intensity of the shock is modified when the eddy passes through it. Experimental pioneering work [11], gave evidence of this property. Note however that no complete energy budget has been performed in a shock vortex (or shock turbulence) interaction, so that many aspects have never been verified. In general, we may have to consider that a shock wave can be modified by turbulence, even if this phenomenon is often of little consequence. For further discussion of the influence of incoming perturbations on the intensity of shock waves, see for example Cambon & Sagaut [12].

3.2 Attempts of classification

Now, we can consider the interactions of shock waves with wall layers in different cases, and we can propose a first classification. We can list elementary situations, which are of common practice, as follows: interaction on a profile leading to buffeting, interaction with a plane shock in a channel, reflection of a shock and compression ramp flow.

In all these cases, shocks are often strong enough to make the layer separate, and in general the resulting flow is 'unsteady', i.e. the whole flow experiences random motions at frequencies much lower than the energetic frequencies identified in the flow. One of the problems of such interactions is to find the origin of these low frequencies.

We can try to classify and characterize the previous situations. The buffeting problem appears in the transonic regime, with large subsonic zones in the external flow, through which acoustic waves can propagate upwards and produce a coupling. It is often assumed that the perturbations caused by large eddies at the trailing edge are noise sources sufficiently efficient to provoke a synchronization between the edge and the shock wave producing separation. In this case, there is a

feedback by almost all the parts of the external flows, and these cases correspond to long range propagating interactions. A second configuration is the interaction with a plane shock in a channel. The plane shock is generally produced by choking the wind tunnel. Close to the wall a lambda shock is formed. The external flow downstream of the interaction is subsonic. Now, the path of communication by acoustic wave is limited to the flow downstream of the interaction, but perturbations from downstream can contribute to make the shock move in the external flow, while the unsteadiness related to separation can act as an excitation for the legs of the lambda shock: this case can be called mixed range interactions. Finally, in the case of oblique shock reflection or in compression ramp flows in the supersonic regime, a subsonic zone exists, but is almost limited to the separated region: downstream of reattachment, the layer reaccelerates rapidly, so that the subsonic part becomes small, hindering the backwards communication; these flows can be considered as short range interactions. It is believed that these cases are of simpler analysis, since only contributions in a rather close neighbourhood have to be taken in account. Attention will be focused on the latter cases, which may include physical elements for the understanding of more complicated coupling or dependences.

What problems can be found in such interactions? Observations from visualizations and from the interpretation of measurements show that the shock system is in general wrinkled and unsteady. In the separated zone, inflectional structures are formed and shed into the downstream flow; their spacing and size seems to be only in weak relation with the upstream layer, but apparently depends on the size of the separated zone. The shock is subjected to the unsteady conditions related to the incoming boundary layer and to the downstream flow, and its motion depends on its response to these constraints, with possible acoustic couplings.

3.3 Short range interactions

Shock motions

Firstly, some properties of shock motion can be recalled. They have been derived from linearised theories, [13], [14]. It is known that shock waves can move under the influence of upstream and downstream conditions, and therefore can move under these two influences. Shocks are in general stable or neutral, and can be often considered as low pass filters: they are less stable for lower frequencies. Depending on the downstream conditions, shocks may be frequency selective or not; in general in supersonic flows, experimental observations do not show frequency selection. Moreover, it is found that strong shocks are less stable than weak shocks. A last property is useful for interpreting experimental results. If an oblique shock is considered, perturbations propagate along the shock with the direction of the tangential velocity [14]. These ingredients provide some keys for interpreting some observations: if a shock emanating from a wall, produced by a compression ramp or by a wall reflection is considered, the turbulent structures perturb randomly the foot of the shock. It is found that the perturbations propagate along the shock to the outer flow where it is oblique and therefore weaker and more stable: the fluctuations are damped as they move outwards. This corresponds to usual observations or measurements in supersonic interactions. This is also consistent with the results of simulations [15], [16], in which it appears that the shock corrugations due to the turbulent eddies are damped when moving outwards. However, the fined grained corrugations are probably not energetic enough or involve too high frequencies to explain the large fluctuations of the position of the shock. Recent visualisations [17] suggest that the large amplitude motions of the shock are directly linked to large amplitude motions in the separated zone, which seems to act as a sliding corner, pushing the shock system forth and back. The point of the origin of the shock motion has been discussed for years (see for example [18] [19], [20] among others). Some small scale motions have been detected by some authors; this is of course possible, since if the shocks act as low pass filter, they may have a rather progressive roll-off, so that higher frequencies corresponding to the energetic eddies are not totally damped, and can be detected and studied. However, it will be shown that in many cases that these frequencies, corresponding to the energetic eddies in the incoming boundary layer, are to high to give a sufficient excitation to the shock system.

Some characteristic scales

The low frequencies of the shock motion seem to be found in many interactions. We want here to explore this point more precisely, and more quantitatively: is there some Strouhal number which would have a universal value, whatever the interaction? Note that the answer is not obvious: if the shock motion results from the excitations provoked by upstream and downstream fluctuations, we may find values depending on each separation case.

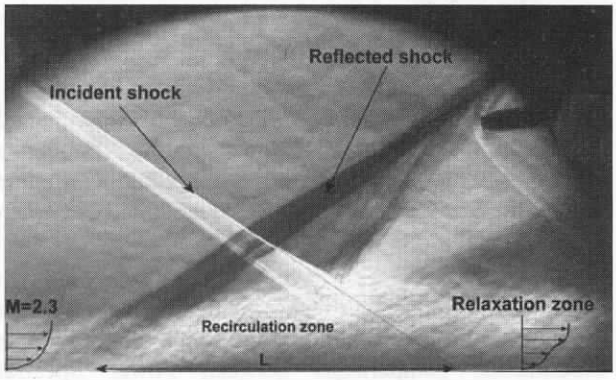

Figure 1: Shock reflection experiment at Mach number 2.3

An experiment of oblique shock reflection was studied at IUSTI (see for example [21], [22], and Figure 1). It is an interaction at a nominal Mach number of 2.3, at a Reynolds number R_θ of 5070. In this experiment wall pressure fluctuations were measured. Measurements at

the vicinity of the foot of the reflected shock have shown clearly the unsteadiness of the reflected shock. From their frequency spectra $E(f)$, a characteristic frequency F was defined in the usual way, from the maximum of $fE(f)$. A Strouhal number was formed $S_L=fL/U_\infty$, where L is the length of the interaction defined from the foot of the mean reflected shock and the reattachment point, and U_∞ is the external velocity in the upstream flow. This was made for several shock intensities producing separation, namely for flow deflections from 7 to 9.5 degrees.

These results have been compared to other flow cases in which experimental results are available. Figure 2 (from [21]) presents some results obtained from experiments in the following configurations: incident shock wave (M=2.3, θ=7° to 9.5°, wall reflection [22]); compression ramp (2.2<M<5, 20°<θ<45°: Erengil & Dolling [23], Thomas et al. [24], Dolling and Or [25], Dolling and Brusniak [26], Bonnet et al. [27], Coe et al.[28]); blunt fin interaction (interaction with a cylinder: Dolling and Smith [29], Dolling and Brusniak [26]); over expanded nozzles with restricted shock separation (Nguyen [30], Bourgoing [31]).

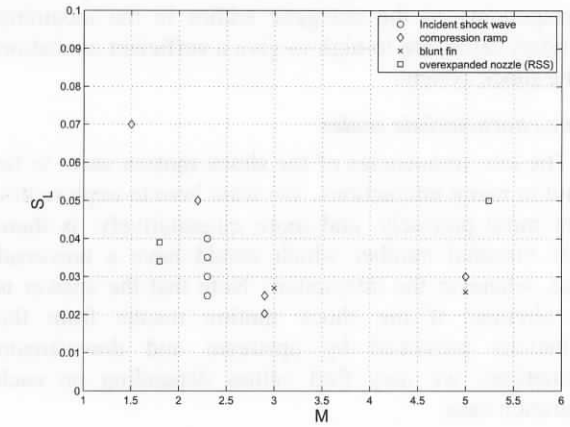

Figure 2: Shock Strouhal numbers in various interactions, from Dussauge et al. 2006 [21].

It can be seen that for this wide range of experimental conditions, the defined dimensionless frequency $S_L=fL/U_e$ groups these experiments together with some scatter: the Strouhal number is found essentially between 0.02 and 0.05.

Such low values have to be compared to characteristic frequencies inside the detached zone which develops downstream the unsteady shock wave. For our experiments, comparisons between Power Spectral Density (PSD) of wall pressure signals in the vicinity of the foot of the shock and inside the recirculating zone showed that nergetic scales involved in two regions are totally different (S_L ≈0.5 for the recirculation). Nevertheless, in the recirculation, low frequencies in the range involved by shock motion contribute for about 25% to the total energy of the signal: this is not completely negligible, and there is no real scale separation between the separated bubble and the shock motion.

The question of the moderately high frequencies (S_L~0.5 or 0.6) found in the separated zone is not totally clarified. At the end of the separated bubble, the Strouhal number is almost constant, and the influence of the involved frequency band is found far downstream. This phenomenon is interpreted as vortex shedding. In the IUSTI experiment, it has been found that the Strouhal number of this shedding frequency increases with shock intensity (see [22]). The value of this Strouhal number has been examined. In subsonic separations, it is about 0.6, while in IUSTI experiments, it varies with the shock intensity. Recent numerical work [20] has examined such an interaction at the same Mach number and at a lower Reynolds number. By analogy with cavity flows, they propose to interpret this Strouhal number as the result of an acoustic feedback mechanism in the separated zone. A difference however is that in separated flows, we find no peaks in spectra, but only bumps. It seems however that this explanation does not account for all phenomena, since the predicted frequency varies with shock intensity, while the experimentally observed one does not. Finally, such simulations found a shock motion in phase with the passage of large eddies through the shock foot. On the opposite, recent visualisations [17] of the shock reflection flow suggest that shock fluctuations of large amplitudes occur at the same time as large amplitude fluctuation of the separated zone: the mechanism probably leading to low frequencies seems to be related to some global motion of the separated bubble, rather than from a local, convective perturbation.

Three dimensional aspects

In this particular case of shock reflection, it was possible to make spanwise PIV measurements, and to get velocity fields in planes x-z parallel to the wall. When exploring the separated bubble, it was obvious that the interaction is fully three-dimensional in the case θ=9.5°, with a pair of tornadoes located symmetrically with respect to the axis of the wind tunnel.

An example is given in Figure 3, taken in a plane located at y= 1 mm from the wall. It shows the 3-d character of the separation- and of the reattachment lines, with the convergence of the streamlines. Further analysis suggests that the tornadoes are as high as about one half of the initial boundary layer thickness.

Now, the question is to know if such vortices play a real energetic role, or if we can just ignore them. It was noticed that the large amplitudes shock motions seemed to result from some global behaviour of the separated zone, and the tornadoes participate in the organization of this zone. Mean velocity measurements were performed in the tornadoes. It is found that the value of the inverse of the maximum velocity gradient is of same order as the average frequency of the shock motion. This resembles some subsonic situations, as pointed out by Jacquin [33]. He recalled that, at low speeds, a pair of two-dimensional vortices produces collective instabilities, with a frequency of the order of the inverse of the maximum

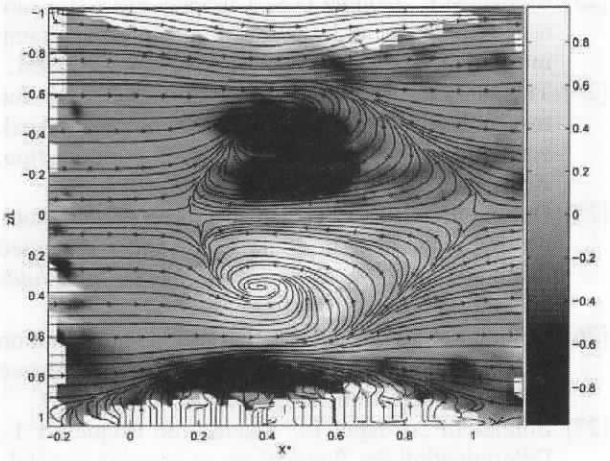

Figure 3: Velocity field on the interaction. x-z plane parallel to the wall; θ=9.5°;y=1 mm. The solid lines are a 2-d representation of the streamlines. Grey scale indicates the level of vorticity normal to the plane. From [32]

velocity gradient in the vortex. It is therefore tempting to speculate that the three dimensional organisation of the separated zone contain an efficient process to produce fluctuations in a frequency range to which the shock motion is particularly receptive.

Does this scenario bring all the comprehensive elements to explain the low, almost "universal", Strouhal number value shown in figure 3? The existence of tornado vortices has been reported in some other interactions, in particular with a plane shock [34], [35]. The case of the leading shock in an interaction produced by a blunt fin [28] reveals a rather complicated vortical structure, very different from our tornado pair. The other question is about the intrinsic character of the three-dimensional structure: is the formation of the vortices inherent to the interaction or to the separation, or is it fortuitously related to the presence of side walls? Can we extrapolate the results found in 2-d situations to an axisymmetric nozzle? This point needs some more investigation. We have some elements in the compression ramp experiments performed at Princeton University. They studied a 24° compression ramp flow, at M=2.9. To minimize the interference between the shock wave and the side wall, they designed the compression ramp with a spanwise gap of about one boundary layer thickness; side plates of limited height were used to preserve the two-dimensionality of the flow. In this flow, no tornadoes were detected. What was found instead was a wavy pattern on the separation and on the reattachment lines. It was conjectured that this undulation was the sign of the development of Görtler vortices in the concavely curved part of the layer. The surprising thing is that in this configuration, the Strouhal number is of the same order of magnitude as in other interactions. A possible guess is that in all cases the shock motion is related to the fluctuations in the separated zone, which is much larger than the boundary layer thickness and therefore implies much lower frequencies. As the shock acts as a low pass filter, differences in the excitation are probably smoothed out and this leads to Strouhal number values lying in the same range. It is clear that some more elements are required to explain and to predict these low frequencies in our supersonic interactions.

4 Conclusions

In the analysis of turbulent shear flows subjected to shock waves, some properties of compressible turbulence have been recalled, with their consequences on the behaviour of turbulence when experiencing mean distortions. Cases of interactions (i.e. cases when there is mutual modification of turbulence and of the distortion) have been defined and a classification of the shock/boundary layer interactions usually found in high speed flows has been proposed. It is shown that, independently of the geometry of the particular configurations, these situations seem to share some common properties, like the characteristic frequency of the shock system motion conveniently normalized. It is shown from some particular cases that this motion cannot be explained only by simple feedback acoustic loops. It is proposed to explore the influence of the global organization of the separated bubbles on the shock motion, including their three-dimensional aspects. However, it is clear that such questions require further efforts of investigation, including at least the structure of a separated zone in supersonic flow, with the associated frequencies, and the transfer function of a curved shock in such conditions.

References

[1] Smits A.J., Dussauge J.P., Turbulent Shear Layers in Supersonic Flow, Springer Verlag, 2006.

[2] Ristorcelli J.R. A pseudo-sound constitutive relationship for the dilatational covariances in compressible turbulence, *Journal of Fluid Mechanics*, 347, pp.37-70, 1997.

[3] Fauchet G., Bertoglio J.P., An analytical expression for the spectrum of compressible turbulence in the low Mach number limit, *Advances in turbulence VII*, U. Frisch Ed., Kluwers, 1998.

[4] Vreman A.W., Sandham N.D., Luo K.H., Compressible mixing layer growth rate and turbulence characteristics, *Journal of Fluid Mechanics*, 320, pp. 235-258, 1996.

[5] Dussauge J.P., Gaviglio J., The rapid expansion of a supersonic turbulent flow: role of the bulk dilatation, *Journal of Fluid Mechanics*, 174, pp.81-112, 1987.

[6] Debiève J.F., Etude d'une interaction turbulence/onde de choc, Thèse de Doctorat d'Etat, Univ. D'Aix-Marseille II, 1983.

[7] Debiève J.F., Gouin H., GaviglioJ., Evolution of the Reynolds stress tensor in a shock/turbulence interaction, *Indian Journal of Technology*, 20, pp. 90-97, 1982.

[8] Durbin P.A., Zeman O., Rapid distortion theory for homogeneous compressible turbulence with application to modelling, *Journal of Fluid Mechanics*, 242, pp. 349-370, 1992.

[9] Jacquin L., Cambon C., Blin, E., Turbulence amplification by a shock wave and rapid distortion theory, *Physics of Fluids A*, 5, 2539-2550, 1993.
[10] Lighthill M. J., On the energy scattered from the interaction of turbulence with sound or shock waves, *Proc. Cambridge Philos. Soc.*, 49, 531, 1953.
[11] Dosanj D.S., Weeks T.M., Interaction of a starting vortexas well as a vortex street with a travelling shock wave, *AIAA Journal*, 3, 216, 1965.
[12] Cambon C., Sagaut P., Spectral approach to compressible turbulence. Linear and weakly non-linear theory and modelling, ERCOFTAC Summerschool on Compressible turbulence and mixing, Strasbourg, July 7-11, 2005.
[13] Culick F.E.C., Rogers T., The response of normal shocks in diffusers, *AIAA Journal*, 21(10), pp. 1382-1390, 1983.
[14] Robinet J.C., Casalis G., Critical interaction of a shock wave with an acoustic wave, *Physics of Fluids*, 13(4), Avril 2001.
[15] Knight D., Yan H., Panaras A., Zheltovodov A., Advance in CFD prediction of shock wave turbulent boundary layer interactions, *Progress in Aerospace Sciences*, 39, pp. 121-184, 2003.
[16] Garnier E., Sagaut P., Deville M., Large eddy simulation of shock/boundary layer interaction, *AIAA Journal*, 40(10), pp. 1935-1944, 2002.
[17] Sidorenko A., Piponniau S., Dupont P., Debiève J.F., Unpublished work, IUSTI, 2006.
[18] Dolling D.S., Fifty years of shock wave/boundary layer interaction research: what next?, *AIAA Journal*, 39(8), August 2001.
[19] Pirozzoli S., Grasso F., Gatski T.B., DNS Analysis of shock wave/turbulent boundary layer interaction at M=2.25, *TSFP4*, Virginia, June 27-29, pp. 1207-1211, 2006.
[20] Grasso F., Pirozzoli S., To appear, *Physics of Fluids*, 2006.
[21] Dussauge J.P., Dupont P., Debiève J.F., Unsteadiness in shock wave boundary layer interactions with separation, To appear, *Aeronautical Science and Technology*, 2006.
[22] Debiève J.F., Dupont P., Some multi time-scale aspects in shock wave/boundary layer interaction, *Conference on Turbulence and Interactions*, May 29-June 2, 2006, Porquerolles, France.
[23] Erengil M.E., Dolling D.S., Unsteady wave structure near separation in a Mach 5 compression ramp interaction, *AIAA Journal*, 29(5), pp. 728-735, 1991.
[24] Thomas F.O., Putman C.M., Chu H.C., On the mechanism of unsteady shock oscillation in shock wave/turbulent boundary layer interaction, *Experiments in Fluids*, 18, pp.69-81, 1994.
[25] Dolling D.S., Or C.T., Unsteadiness of the shock wave structure in attached and separated compression ramp flows, *Experiments in Fluids* Vol.3, N°24-32 , 1985.
[26] Dolling D.S., Brusniak L., Separation shock motion in fin, cylinder, and compression ramp-induced turbulent interaction, *AIAA Journal*, 27(6), 1989.
[27] Bonnet J.P., Chaput E., Alaziary de Roquefort T., Détermination des fluctuations de pression pariétale dans une interaction onde de choc-couche limite turbulente en écoulement supersonique, Rapport final, Convention ONERA 20.391/SAT.2.CDC, Mai 1986.
[28] Coe C.F., Chyu W.J., Dods Jr. J.B., Pressure fluctuations underlying attached and separated supersonic turbulent boundary layers and shock waves, AIAA Paper 73-996, *AIAA Aeroacoustics Conference*, Seattle, Wash., October 15-17, 1973.
[29] Dolling D.S., Smith D.R., Unsteady shock-induced separation in Mach 5 cylinder interactions, *AIAA Journal*, 27(12), pp.1598-1706, 1989.
[30] Nguyen AT., Décollement instationnaire et charges latérales dans les tuyères propulsives, Thèse de Doctorat, Université. de Poitiers, 10/06 2003.
[31] Bourgoing A., Instationnarité et dissymétrie d'un écoulement supersonique décollé dans une tuyère plane, Thèse de doctorat de l'Université Paris 6, Juin 2002.
[32] Piponniau S., Rapport de stage de DEA, IUSTI, Université de Provence, 2005.
[33] Jacquin L., Communication privée, 2005.
[34] Bourgoing A., Reijasse P., Experimental investigation of an unsteady and asymmetrical supersonic separated flow, CASI, 8th Aerodynamic Session Symposium; Toronto, 29 April - 2 May 2001.
[35] Doerffer P. and Szwaba R., Shock wave- boundary layer interaction control by streamwise vortices, 11th ICTAM Symposium; Warsaw, Poland. 15-21 August 2004.

COMPRESSIBLE MIXING LAYERS: DATA ANALYSIS AND MODELLING

Bertrand Aupoix, Hervé Bézard

Office National d'Etudes et de Recherches Aérospatiales
Aerodynamics and Energetics Department
BP 4025 - 2, Avenue E. Belin - 31055 Toulouse Cedex 4, France

Bertrand.Aupoix@onera.fr , Herve.Bezard@onera.fr

1 Introduction

Compressible mixing layers occur in a wide variety of flows. Often, the best mixing capabilities are looked for as, e.g. in combustion chambers or in nozzle jets, to reduce the infrared signature in that last case. However, in some cases as in wall cooling by tangential blowing or film cooling, the lowest possible mixing is wanted.

The prediction of the spreading rate of a mixing layer and of its entrainment remains a key challenge for turbulence models. As mixing layers quickly get close to a self-similar state, a simple and relevant test case is the prediction of self-similar mixing layers.

For self-similar mixing layers, the velocity profile can be expressed as

$$\frac{u-u_2}{u_1-u_2} = f\left(\frac{y}{\delta(x)}\right) \tag{1}$$

where u is the local velocity, u_1 and u_2 the velocities on both edges of the mixing layer, subscripts $_1$ and $_2$ respectively referring to high- and low-speed streams, y the distance along the mixing layer thickness and δ a characteristic mixing layer thickness. Standard definitions of this mixing layer thickness are:

- $\delta_{1\%}$ (resp. $\delta_{10\%}$) defined as the distance between the points where the ratio $\frac{u-u_2}{u_1-u_2}$ is equal to 1% (resp. 10%) and 99% (resp. 90%),

- Stanford thickness δ_S defined as the distance between the points where the ratio $\frac{u-u_2}{u_1-u_2}$ is equal to $\sqrt{0.1}(\approx 0.32)$ and $\sqrt{0.9}(\approx 0.95)$,

- the vorticity thickness δ_ω defined as the ratio of the velocity difference divided by the maximum velocity gradient

$$\delta_\omega = \frac{u_1-u_2}{\left(\frac{\partial u}{\partial y}\right)_{max}} \tag{2}$$

Of course, for compressible flows, not only the velocity but also the density, temperature or mass fractions profiles can be recast in a self-similar form similar to (1). Therefore, all the above thicknesses are proportional, their ratios weakly depend upon the flow conditions. The vorticity thickness will be used in the following.

For self-similar mixing layers, the standard argument (see e.g. Bonnet et al. (1998) or Dimotakis (1991) and references herein) is that, in a frame linked to the coherent structures, the spreading rate $\frac{d\delta}{dt}$ is proportional to the only available velocity scale, the velocity difference across the layer $u_1 - u_2$. In the laboratory reference frame, the spreading rate is thus proportional to the ratio of the velocity difference to the advection speed u_c of these coherent structures, i.e.

$$\frac{d\delta}{dx} \propto \frac{u_1-u_2}{u_c} \quad . \tag{3}$$

The advection speed u_c is determined by considering equilibrium of the stagnation pressure at the stagnation point between coherent structures, in a reference frame moving with the structures. So, it can be stated that the spreading rate depends upon three parameters:

- the velocity ratio of the two streams $r = \frac{u_2}{u_1}$,

- the density ratio of the two streams $s = \frac{\rho_2}{\rho_1}$,

- the convective Mach number M_c which characterizes the compressible character of the turbulent motion. For gases of identical isentropic exponents, it reduces to $M_c = \frac{u_1-u_2}{c_1+c_2}$ where c is the speed of sound.

The standard analysis yields the following expression for the mixing layer spreading rate

$$\delta' = \frac{d\delta}{dx} = C_\delta(M_c)\frac{(1-r)(1+\sqrt{s})}{2(1+\sqrt{s}r)} \tag{4}$$

This paper first deals with the modelling of the compressibility effect, i.e. the variation of the coefficient $C_\delta(M_c)$ with the convective Mach number. Experimental references for low-speed will first be briefly discussed to compare with high-speed mixing layers data. Modelling issues will then be addressed.

2 Experimental references for incompressible flows

For low speed, constant density flows, a selection of good quality experiments was collected. Figure 1 shows the spreading rate versus the velocity ratio, or more precisely versus $\frac{u_1-u_2}{u_1+u_2} = \frac{1-r}{1+r}$ to which the spreading rate should be proportional, according to equation (4). For the sake of room, experiments are not listed here, the reader is referred to the figure caption. The expected linear dependence is retrieved, but with a significant scatter. A best fit of the available data gives an average value of the coefficient C_δ for incompressible flows about 0.175-0.185.

A more interesting representation is proposed in figure 2 where the values of the coefficient C_δ are directly plotted for each experiment. A large scatter is so evidenced. This is unavoidable when the velocity ratio $\frac{u_1-u_2}{u_1+u_2}$ is small but remains significant when this ratio is close to unity. This figure shows that the C_δ coefficients range from 0.15 to 0.22, i.e. roughly a ±20% scatter.

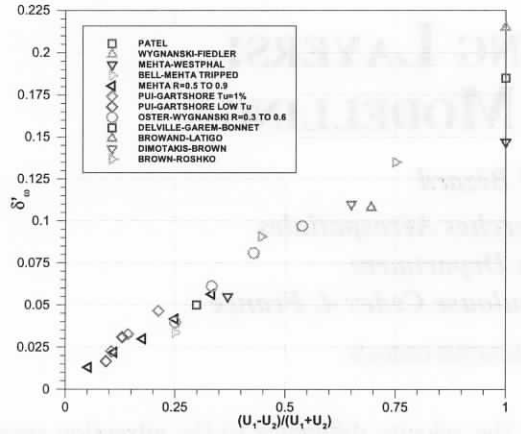

Figure 1: Experimental spreading rate coefficients versus velocity ratio.

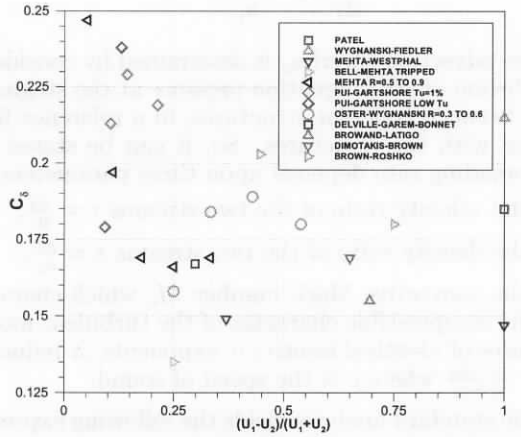

Figure 2: Experimental spreading rate coefficients versus velocity ratio

Experimental data also support equation (4) concerning the influence of density ratio. The reader is referred to Brown and Roshko (1974).

3 Experimental references for compressible flows

A large set of compressible mixing layer experiments was analyzed. It includes experiments by Samimy et al. (1990, 1992), Chinzei et al. (1986), Goebel and Dutton (1991), Papamoschou and Roshko (1988), Hall et al. (1993), Clemens and Mungal (1995), Bonnet and Debisschop (1992) and Barre et al. (1994) (labelled *Dussauge* in figure 8 and 9).

Goebel and Dutton provided values for $\delta_{10\%}$, Chinzey et al. for the Stanford thickness, Papamoschou and Roshko used the Pitot thickness based upon stagnation pressure profiles while Clemens and Mungal or Hall et al. first considered a visual thickness. All these thicknesses were converted into vorticity thickness, sometimes by the authors.

All experiments were compared to proposed correlations, as shown in figures 3 to 8. As convective Mach number acts only as a multiplicative factor since in equation (4), $C_\delta(M_c) = C_\delta(M_c = 0)f(M_c)$ the coefficient $C_\delta(M_c)$ is plotted versus the convective Mach number using a semi-logarithmic representation. Therefore, a change in the reference $C_\delta(M_c = 0)$ is just a vertical shift.

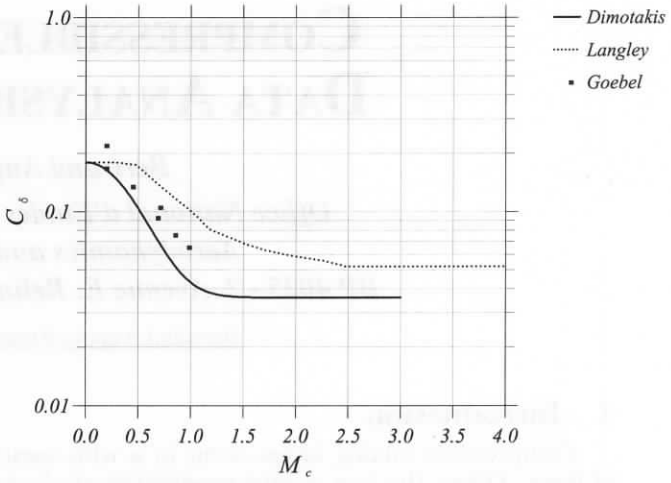

Figure 3: Spreading rate coefficients versus convective Mach number for the Goebel and Dutton experiment

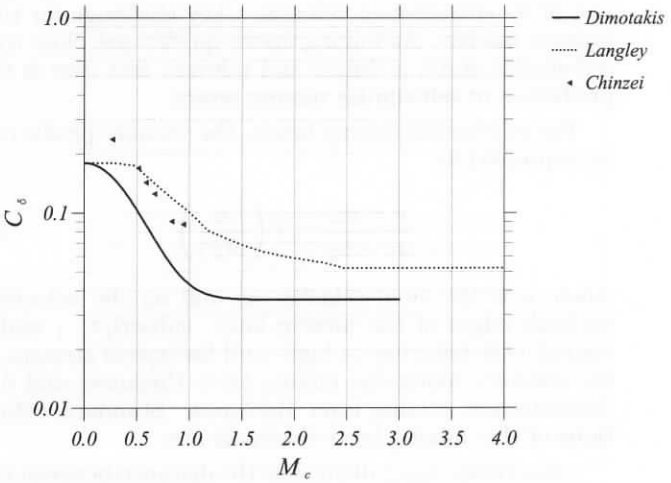

Figure 4: Spreading rate coefficients versus convective Mach number for the Chinzei et al. experiment

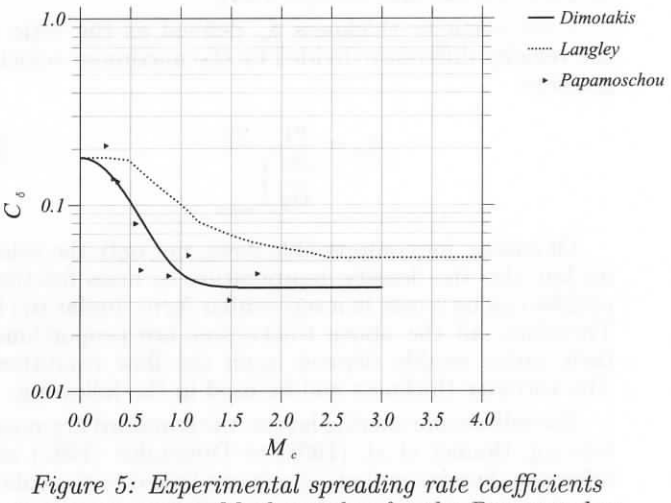

Figure 5: Experimental spreading rate coefficients versus convective Mach number for the Papamoschou and Roshko experiment

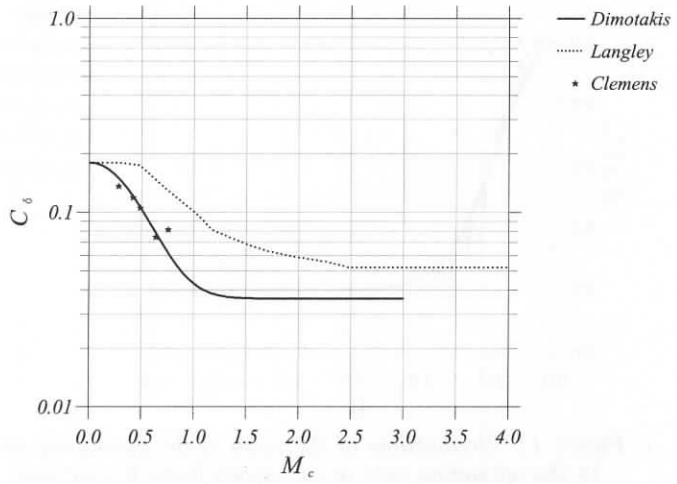

Figure 6: Spreading rate coefficients versus convective Mach number for the Clemens and Mungal experiment

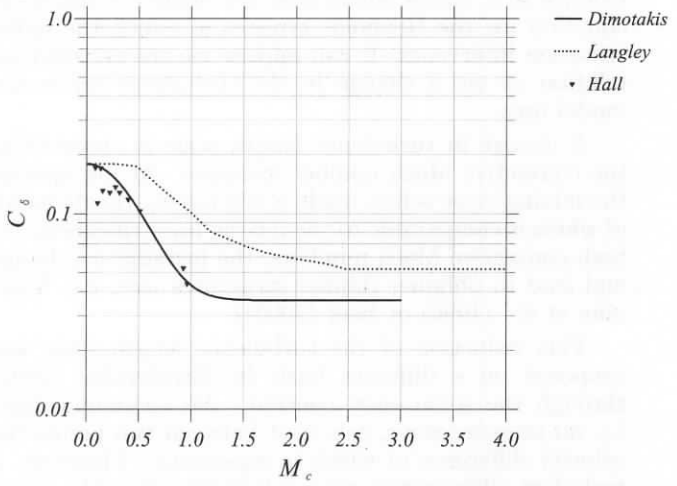

Figure 7: Spreading rate coefficients versus convective Mach number for the Hall et al. experiment

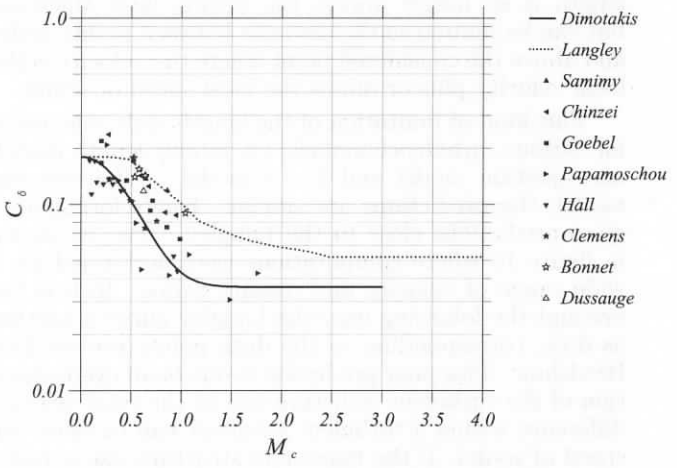

Figure 8: Experimental spreading rate coefficients versus convective Mach number

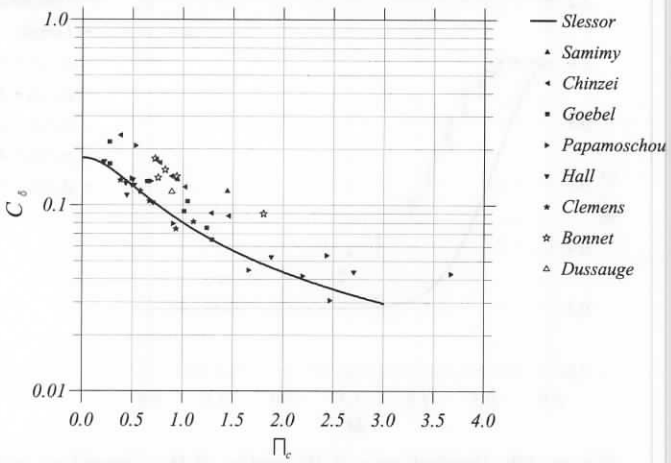

Figure 9: Experimental spreading rate coefficients versus Slessor et al. Mach number

The two available correlations are also plotted in these figures. The dotted line is the well-known "Langley curve", taken from Bradshaw in Kline et al. (1980, pp. 364-368). As only few points were available, this line seems rather broken. The solid line is the curve fit proposed by Dimotakis (1991)

$$\frac{\delta'_\omega}{\delta'_\omega(M_c{=}0)} = \frac{C_\delta}{C_\delta(M_c{=}0)} = 0.2 + 0.8\exp(-3M_c^2) \quad (5)$$

Both reference curves are plotted for a value of $C_\delta(M_c{=}0)$ of 0.18.

Figures 3 to 7 give examples for five typical experiments. All the data are plotted together in figure 8.

The analysis of each experiment evidences that the rapid decrease of the spreading rate with the convective Mach number is in better agreement with Dimotakis' curve than with Langley curve (do not forget the log scaling so that slopes have to be compared, not values).

However figures 3 and 4 as well as figure 8 show that the reference level $C_\delta(M_c = 0)$ is noticeably higher than 0.18 for some experiments. Values ranging from 0.18 to 0.32 were obtained, i.e. higher values and more scatter than for incompressible flows. These differences cannot be blamed only upon the conversion from the given thickness into the vorticity thickness and upon the scatter already observed in incompressible flows. A plausible cause for these higher values could be the free stream turbulence and noise levels which are known to be high in supersonic wind tunnels and to trigger instabilities in mixing layers, as already pointed out by Chandrsuda et al. (1978) or Bonnet et al. (1998).

Slessor et al. (2000) criticized the use of the convective Mach number, pointing out that, if the temperatures of the two streams are strongly different, and hence the speeds of sound c, the convective Mach number M_c is ruled by the hottest flow, which usually is the slowest, while it should mainly be ruled by the high speed flow where compressibility effects are expected to be larger. As the Mach number is the ratio of the kinetic to internal energy since $\frac{u^2}{2h} = \frac{\gamma-1}{2}M^2$, they introduced another Mach number:

$$\Pi_c = \max_{i=1,2}\left[\frac{\sqrt{\gamma_i - 1}}{c_i}\right](u_1 - u_2) \quad (6)$$

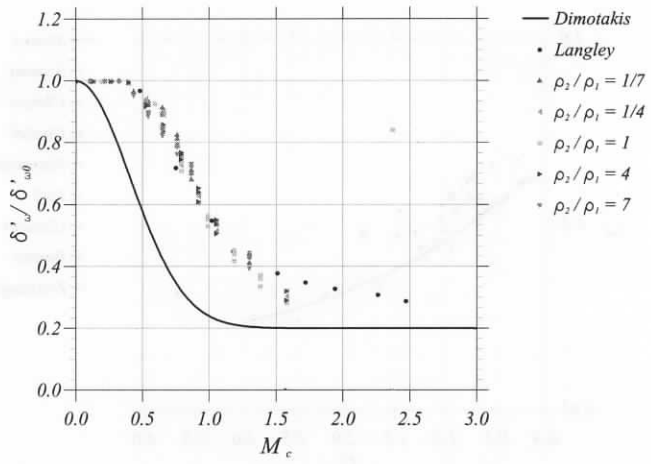

Figure 10: Predictions of the ratio of the spreading rate to the spreading rate in low-speed flows for various velocity and density ratios, using Kim's model

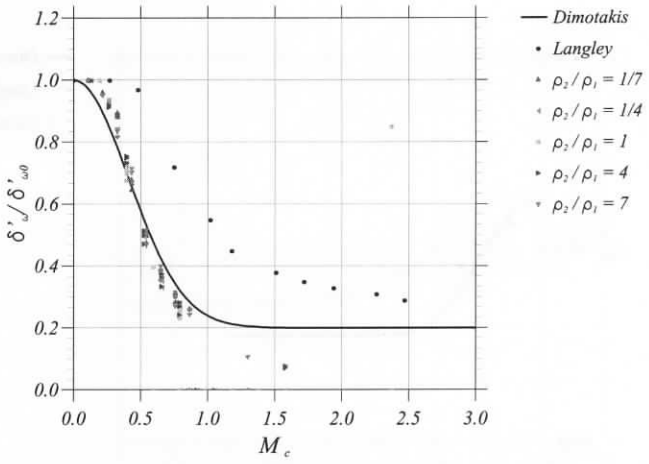

Figure 11: Predictions of the ratio of the spreading rate to the spreading rate in low-speed flows for various velocity and density ratios, using the proposed revision of Kim's model

In figure 9, experiments are compared to the Slessor et al. (2000) curve fit (solid line)

$$\frac{\delta'_\omega}{\delta'_\omega(\Pi_c = 0)} = \frac{C_\delta}{C_\delta(\Pi_c = 0)} = \frac{1}{\sqrt{1 + 4\Pi_c^2}} \qquad (7)$$

This figure shows that the use of Slessor parameter Π_c does not significantly reduce the scatter, even when each experiment is considered solely. Therefore, Dimotakis' curve fit will be used to characterize compressibility effects.

4 Compressibility effects modelling

The ability of turbulence models to predict the influence of the velocity and density ratio on the mixing layer spreading rate is discussed in Aupoix (2004). Only the key conclusions will be recalled.

Models usually predict a nearly linear growth of the spreading rate with respect to $\frac{u_1-u_2}{u_1+u_2}$ but slightly underestimate it, yielding values of C_δ in the range 0.135–0.16. Concerning density effects, transport equation models predict no influence or even a slight but opposite one.

Using standard turbulence models, there is no information about the speed of sound in the set of equations, once written in self-similar form. Therefore, whatever the turbulence model used, no reduction of the spreading rate is observed as the convective Mach number is increased.

Corrections were proposed, based upon models for the dilatational dissipation and the pressure-dilatation correlation by Sarkar (1991) and Zeman (1990). These models give predictions close to the Langley curve and therefore underestimate the spreading rate reduction as the convective Mach number increases.

Direct numerical simulations by Freund et al. (2000) and Pantano and Sarkar (2002) showed that indeed the rôle of the dilatational terms is negligible and that the main effect of compressibility is via a reduction of the redistribution due to pressure fluctuations. The energy transfer from $\langle \rho u''^2 \rangle$ to $\langle \rho v''^2 \rangle$ is reduced, and therefore the production of the shear stress $\langle -\rho u'' v'' \rangle$ is lowered and hence the turbulence production and the spreading rate. This alteration of the redistribution was previously suggested by Goebel and Dutton (1991) on experimental grounds.

A change in the redistribution seems difficult to introduce in a model which does not solve the transport equation for the Reynolds stresses in which the redistribution intervenes. It can appear via the constitutive relation or via a change in the turbulence scales the model uses.

A change in turbulence length scale is observed as the convective Mach number increases. At low speeds, the mixing layer is first made of big rollers, the diameter of which is comparable to the mixing layer thickness. At high convective Mach numbers, the instabilities change and lead to oblique, thinner structures (see, e.g. Vreeman et al. (1996) or Beer (2003)).

This reduction of the turbulence length scale was proposed on a different basis by Breidenthal (1992) through the sonic eddy concept. No communication, i.e. no pressure wave, can exist between two points the velocity difference of which is supersonic. Therefore, a turbulent eddy cannot extend beyond points the velocity difference of which is sonic.

This sonic eddy concept was adapted to the mixing length model by Kim (1990). In Kim's model, the mixing length is proportional to a reference length linked to the size of the energy containing eddies. This reference length is no longer always the mixing layer thickness but can be limited to the distance between points under and above the considered point where the velocity is the local velocity plus or minus the local speed of sound.

This kind of limitation of the length scale was tested for various turbulence models, i.e. mixing length model, one-equation model and $k - \varepsilon$ model. Whatever the model, the predictions are similar. Kim's formulation gives predictions close to the Langley curve, as shown in figure 10 where computations were performed for a wide range of velocity and density ratios. In this figure and the following one, the Langley curve is plotted as dots, corresponding to the data points provided by Bradshaw. This poor prediction is due to an overestimation of the turbulent structure size as the total velocity difference within a turbulent structure can be twice the speed of sound. If the maximum structure size is really reduced to a velocity difference equal to the speed of sound, i.e. reducing the reference length to the distance between points where the velocity is the local velocity

plus or minus half the speed of sound, the prediction is in good agreement with Dimotakis' curve as shown in figure 11. Here again, the conclusion holds whatever the turbulence model.

This kind of model requires to identify the mixing layer and can be easily applied in a parabolic or a self-similarity code, not in a general Navier-Stokes solver. A more general and non-local modification of the turbulence model is required. The reader is referred to Aupoix (2004) for such a proposal.

5 Conclusion

Analysis of low speed mixing layer data supports the classical analysis but evidences a large scatter on the mixing layer growth rate.

Analysis of high speed mixing layers data shows that Dimotakis' and Slessor's curves are good estimates of the spreading rate reduction, not the Langley curve. Slessor et al. approach does not significantly reduce the scatter. Higher values for the reference growth rate $C_\delta(M_c 0)$ are found, which could be related to noise in supersonic wind tunnels.

Standard models predict no reduction of the spreading rate as the convective Mach number increases. Corrections based upon dilatational terms do not rely upon the right physics and were tuned to reproduce the Langley curve so that they under-predict the reduction. A reduction of the turbulence length scale, which sounds logical and is supported by DNS, allows to predict the growth rate reduction without any ad-hoc tuning. Such a reduction of the turbulence length scale should surely also be included in models solving the Reynolds stress transport equations and accounting for the reduction of the redistribution.

Bibliography

[1] Aupoix B., Modelling of Compressibility Effects in Mixing Layers, *Journal of Turbulence*, 5, February 2004.

[2] Barre S., Quine C., and Dussauge J.P., Compressibility effects on the structure of supersonic mixing layers: Experimental results, *Journal of Fluid Mechanics*, 259:47–78, January 1994.

[3] Beer A., Étude par simulation numérique temporelle des effets de compressibilité en couche de mélange plane turbulente, PhD Thesis, Université Joseph Fournier, Grenoble, May 2003.

[4] Bonnet J.P. and Debisschop J.R., Analyse expérimentale de la turbulence dans les couches de mélange supersoniques, *Revue Scientifique et Technique de la Défense*, pages 65–83, 1992.

[5] Bonnet J.P., Moser R.D. and Rodi W., Free shear flows, *A Selection of Test Cases for the Validation of Large-Eddy Simulations of Turbulent Flows – AGARD Advisory Report 345*, chapter 6, pages 29–36. April 1998.

[6] Breidenthal R.E., Sonic eddy – A model for compressible turbulence, *AIAA Journal*, 30(1):101–104, January 1992.

[7] Brown G.L. and Roshko A., On density effects and large structure in turbulent mixing layers, *Journal of Fluid Mechanics*, 64(4):775–816, July 1974.

[8] Chandrsuda C., Mehta R.D, Weir A.D. and Bradshaw P., Effects of free-stream turbulence on large structure in turbulent mixing layers, *Journal of Fluid Mechanics*, 85(4):693–704, April 1978.

[9] Chinzei N., Masuya G., Komuro T., Murakami A., and Kudou K., Spreading of two-stream supersonic turbulent mixing layers, *Physics of Fluids*, 29(5):1345–1347, May 1986.

[10] Clemens N.T. and Mungal M.G., Large-scale structure and entrainment in the supersonic mixing layer. *Journal of Fluid Mechanics*, 284:225–236, 1995.

[11] Dimotakis P.E., Turbulent free shear layer mixing and combustion, In S.N.B Murthy and E.T. Curran, editors, *High-Speed Flight Propulsion Systems – Progress in Astronautics and Aeronautics – Volume 137*, chapter 5, pages 265–340. AIAA, 1991.

[12] Freund J.B., Lele S. and Moin P., Compressibility effects in a turbulent annular mixing layer. Part 1. Turbulence and growth rate, *Journal of Fluid Mechanics*, 421:229–267, October 2000.

[13] Goebel S.G. and Dutton J.C., Experimental study of compressible mixing layers, *AIAA Journal*, 29(4):538–546, 1991.

[14] Hall J.L., Dimotakis P.E., and Rosemann H., Experiments in non-reacting compressible shear layers, *AIAA Journal*, 31(12):2247–2254, December 1993.

[15] Kim S.C., New mixing-length model for supersonic shear layers, *AIAA Journal*, 28(11):1999–2000, November 1990.

[16] Kline S.J., Cantwell B.J. and Lilley G.M., editors *The 1980-81 AFOSR–HTTM–Stanford Conference on Complex Turbulent Flows : Comparison of Computation and Experiment – Volume I – Objectives, Evaluation of Data, Specification of Test Cases, Discussion and Position Papers*, Thermosciences Division, Mechanical Engineering Department, Stanford University, California, 3-6 September 1980.

[17] Pantano C. and Sarkar S., A study of compressibility effects in the high-speed turbulent shear layer using direct simulation, *Journal of Fluid Mechanics* , 451:329-371, 2002.

[18] Papamoschou D. and Roshko A., The compressible turbulent shear layer : An experimental study, *Journal of Fluid Mechanics*, 197:453–477, 1988.

[19] Samimy M. and Elliot G.S., Effects of compressibility on the characteristics of free shear layers, *AIAA Journal*, 28(3):439–445, March 1990.

[20] Samimy M., Reeder M.F. and Elliott G.S., Compressibility effects on large structures in free shear flows, *Physics of Fluids (A*, 4(6):1251–1258, June 1992.

[21] Sarkar S., Erlebacher G., Hussaini M.Y. and Kreiss H.O., The analysis and modelling of dilatational terms in compressible turbulence, *Journal of Fluid Mechanics*, 227:473–493, 1991.

[22] Slessor M.D., Zhuang M. and Dimotakis P.E. Turbulent shear-layer mixing: Growth-rate compressibility scaling, *Journal of Fluid Mechanics*, 414:35–45, July 2000.

[23] Vreman A.W., Sandham N.D. and Luo K.H., Compressible Mixing Layer Growth Rate and Turbulence Characteristics, *Journal of Fluid Mechanics*, 320:235–258, 1996.

[24] Zeman O., Dilatation dissipation : The concept and application in modeling compressible mixing layers. *The Physics of Fluids A*, 2(2):178–188, February 1990.

SPECIAL INTERESTING GROUP ON TURBULENCE MODELLING – SIG 15

12TH ERCOFTAC WORKSHOP ON REFINED TURBULENCE MODELLING

TECHNICAL UNIVERSITY BERLIN, GERMANY
OCTOBER 12-13, 2006

http://www.cfd.tu-berlin.de/ercoftac-workshop06.html

BACKGROUND

Computational Fluid Dynamics (CFD) has developed to a key technology which plays an important role in design, development and optimization in engineering practice. The ERCOFTAC Workshops on Refined Turbulence Modelling aim to bring together scientists, researchers, users and developers from industry and from the academic field. Similar to the previous workshops in Lyon (1992,1993), Lisabon (1994), Karlsruhe (1995), Chatou/Paris(1996), Delft (1997), Manchester (1998), Helsinki (1999), Darmstadt (2001), Poitiers (2002) and Gothenburg (2005), some fundamental phenomena, but also some industrially relevant problems have been chosen as test cases for this workshop.

TEST CASES

The workshop focuses on four test cases involving numerous features of scientific and engineering relevance (three-dimensionality, unsteady wake regions, periodicity, separation and reattachment, swirling effects, turbulent mixing, etc.):

CASE 11.1:

Flow over a wall-mounted, 2-D hump with oscillatory zero-mass-flux jet or suction through a thin slot (Exp.: Greenblat et al., 2005)

Coordinator S. Saric: Saric@sla.tu-darmstadt.de

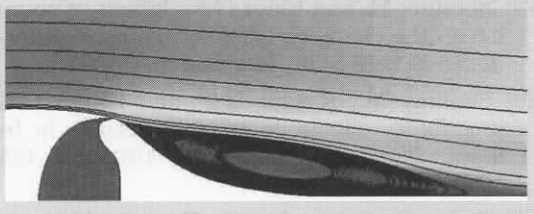

CASE 11.2:

Flow over a 3-D hill (Exp.: Simpson et al., 2002)

Coordinator M. Leschziner: Mike.Leschziner@imperial.ac.uk

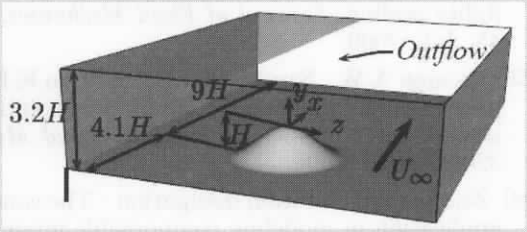

CASE 12.1:

Tip-gap turbulent flow in a low-speed, linear compressor cascade (Exp.: Tang and Simpson 2004)

Coordinator F. Menter: Florian.Menter@ansys.com

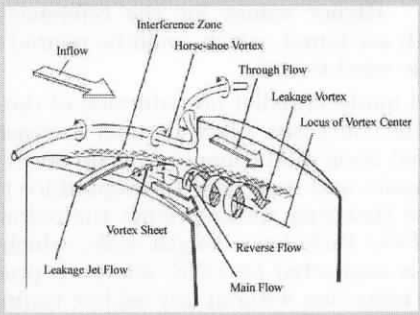

CASE 12.2:

Flow and mixing in a model of swirl combustor (Exp.: Palm et al., 2005)

Coordinator S. Jakirlic: S.Jakirlic@sla.tudarmstadt.de

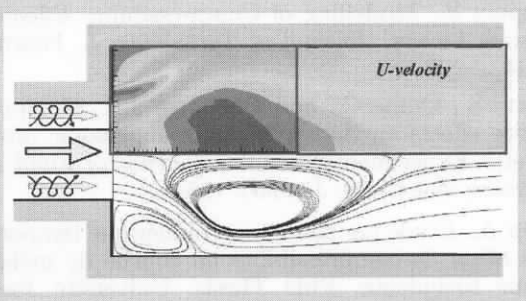

SIG-15 STEERING COMMITTEE

Prof. K. Hanjalic, Dr. S. Jakirlic, Prof. B.E. Launder, Prof. D. Laurence, Prof. M.A. Leschziner, Dr. R. Manceau, Dr. F. Menter, Prof. W. Rodi and Dr. S. Wallin

LOCAL ORGANIZING COMMITTEE

Prof. F. Thiele, O. Frederich and D. Eschricht

IMPORTANT DATES

Results submission: September 1, 2006

Registration: September 1, 2006

CONTACT:

Prof. F. Thiele, Hermann-Foettinger Institute for Fluid Mechanics, Technical University Berlin, Mueller-Breslau Strasse 8, D-10623 Berlin, Germany, Frank.Thiele@cfd.tuberlin.de

Is Compressibility Always Stabilizing and Why? Open Issues

Claude Cambon [1], Laurant Jacquin [2]

[1] Laboratoire de Mécanique des Fluides et d'Acoustique, UMR 5509, Ecole Centrale de Lyon, 69134 Ecully Cedex, France, [2] Office National d'Etudes et Recherches Aérospatiales, France

Claude.Cambon@ec-lyon.fr

1 Context and issues

Compressibility induced effect on turbulence is an important topic for several engineering applications, particularly in the field of propulsion and supersonic aerodynamics which is concerned by jets or wakes subjected to large velocity and density gradients. The compressible plane mixing layer is a generic problem for these applications, and explaining and modelling how compressibility reduces turbulent mixing in a shear layer that motivated the large research effort devoted to this topic during the 80-90. Mixing usually refers to interpenetration of two streams and it is characterized by two scales, a lengthscale δ and a velocity scale ΔU evaluating respectively the thickness of the interface and intensity of the fluctuations. In this context, reduction of mixing by compressibility is illustrated on Fig. 1, from Pantano & Sarkar, in which δ is the above mentioned thickness and $M_c = \Delta U/c$ is the convective Mach number, with c the averaged sonic speed.

More generally, there is now a consensus in the literature that the 'intrinsic compressibility' (nonzero velocity divergence, Mach number dependent flows) of a turbulent velocity field tends to reduce the amplification rate of turbulent kinetic energy produced by mean velocity gradients, with respect to the solenoidal case. These effects were particularly investigated in shear flows, with both experimental and numerical studies of the mixing layer, mentioned above, and DNS of homogeneous shear flows. In addition to Sarkar 1995 [2], Simone et al. (1997) [3] for the latter studies, the reader is referred to the review by Lele (1994) [4] and references therein.

Two preliminary questions immediately follow: 1) To what extent homogeneous turbulence is relevant to explain such mechanisms in inhomogeneous flows ? 2) Is compressibility always stabilizing (reducing the turbulent kinetic growth rate) in homogeneous turbulence? The answer to the first question is somewhat difficult, and this issue partly motivates this article, but the answer to the second question is simple: no.

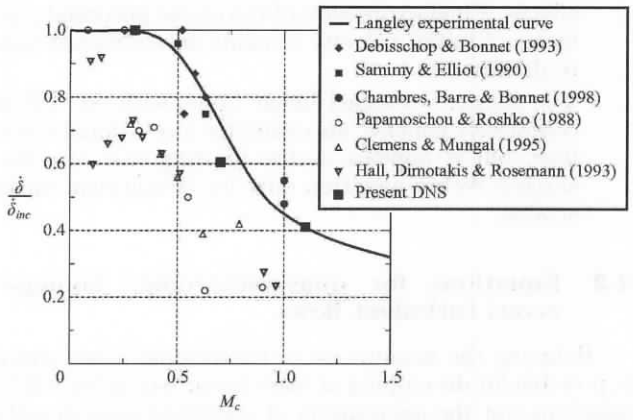

Figure 1: Dependence of shear layer growth rate on convective Mach number. DNS and experimental results from [1]

The main argument for explaining a 'stabilizing effect' of compressibility, at least in the context of fully turbulent flows, is the alteration of the dynamics of pressure fluctuation, resulting in the 'mollification' of pressure-strain rate tensor in the equations for the Reynolds stress tensor. On the one hand, we agree that this argument is more relevant that the one based on the role of explicit compressible terms, such as pressure-dilatation and dilatational dissipation terms, and that the main parameter for quantifying the effect of compressibility is the distortion, or gradient, Mach number, recalled below. On the other hand, we have found flow cases in which the mollification of pressure-strain rate at increasing distortion Mach number is not the right explanation, since it results in *increasing* the turbulent kinetic energy growth rate. These flow cases include irrotational strain and even shear flows, but at moderate elapsed time, using Rapid Distortion Theory and DNS. In addition, the conventional stabilizing effect was recovered for homogeneous shear at larger elapsed times, but the explanation was different from the one only based on the reduction of pressure-strain terms [2, 1], as extensively rediscussed below.

First of all, it is necessary to discuss what is compared: linear or nonlinear effects (or "rapid" or "slow" in the context of Reynolds Stress Modelling), or really incompressible and compressible ? In order to avoid misunderstanding only based on terminology, we will speak of "solenoidal" and "dilatational" modes (rather than incompressible and compressible) for the velocity fluctuation u_i, in agreement with the Helmholtz decomposition. For instance

$$u_i = u_i^{(s)} + u_i^{(d)} \,, \qquad (1)$$

the first term being divergencefree and the second one having zero curl. In the same way, the pressure fluctuation p will be possibly expressed via the Poisson equation in the pure incompressible limit, and denoted $p^{(s)}$ in this limit and in this limit only. Finally, the terminology "Rapid Distortion Theory" being ambiguous given the multi-time scale nature of the problem in the compressible case, we will use "Linear theory" instead. Recall that at least two "rapid" time-scales can be used, the inverse of a typical shear rate (or mean gradient) S, and the sonic time-scale L/c at a lengthscale L. Of course, their ratio gives the "distortion" Mach number [7], or gradient Mach number [2]

$$M_d = \frac{LS}{c} \quad , \qquad (2)$$

c being the sonic speed.

The paper is organised as follows. Three linear limits are defined in section 2, from the simplest to the most complex:

- Pressure released linear limit,
- Solenoidal linear limit,
- Quasi-isentropic compressible linear limit.

The main results obtained for irrotational mean compression are recalled and rediscussed in the same section 2. The case of pure plane shear flow will be revisited in section 3, following the analysis by [3] and a recent one by Tacker et al. [5]. Open issues for more realistic, statistically inhomogeneous, flows are investigated in section 4, after a brief recap of conclusions from our analysis of canonical flows.

2 Governing equations and relevant linear limits

2.1 The pressure-released limit. Relevance for irrotational mean flows

Linearizing Euler equations for velocity and pressure fluctuations (u_i, p) around a mean flow with velocity U_i and discarding the pressure fluctuation term yields the following solution (e.g. [6]):

$$u_i^{(pr)}(\boldsymbol{x}, t) = H_{ij}(\boldsymbol{X}, t, t_0) u_j(\boldsymbol{X}, t_0) \; , \qquad (3)$$

where $\boldsymbol{x}$ is the position of a fluid particle at time t having the position $\boldsymbol{X}$ at time t_0, following a mean trajectory. The matrix H_{ij} is closely linked to The Cauchy matrix, or semi-Lagrangian displacement gradient matrix, $\mathbf{F}$, which characterizes the distortion of a bi-point along the mean trajectory equation $x_i = \tilde{x}_i(\boldsymbol{X}, t, t_0)$, in accordance with

$$dx_i = U_i dt + F_{ij} dX_j, \quad \text{or} \quad F_{ij} = \frac{\partial x_i}{\partial X_j} \; , \qquad (4)$$

so that H_{ij} and F_{ij} reflects a time-accumulated effect of mean velocity gradients, solving

$$\dot{F}_{ij} = \frac{\partial U_i}{\partial x_m} F_{mj}, \quad F_{ij}(\boldsymbol{X}, t_0, t_0) = \delta_{ij} \qquad (5)$$

$$\dot{H}_{ij} = -\frac{\partial U_i}{\partial x_m} H_{mj}, \quad H_{ij}(\boldsymbol{X}, t_0, t_0) = \delta_{ij} \qquad (6)$$

In eq. (3), one has $H_{ij} = F_{ji}^{-1}$ only if the mean velocity gradient matrix is symmetric, whereas a transposed mean velocity gradient matrix must be used in eq. (5) to connect H_{ij} to the modified $\mathbf{F}$ in the general, rotational, case.

More generally, the linear response to an *irrotational* mean flow can be expressed using a linearized Weber equation

$$u_i(\boldsymbol{x}, t) = F_{ji}^{-1}(\boldsymbol{X}, t, t_0) u_j(\boldsymbol{X}, t_0) + \frac{\partial \varphi}{\partial x_i} \; , \qquad (7)$$

in which the scalar potential accounts for effects of fluctuating pressure, with a related equation for the vorticity fluctuation

$$\omega_i(\boldsymbol{x}, t) = \frac{1}{Det\mathbf{F}} F_{ij}(\boldsymbol{X}, t, t_0) \omega_j(\boldsymbol{X}, t_0). \qquad (8)$$

Both equations are valid not only in the solenoidal case ($u_{i,i} = 0$), but also in various barotropic compressible cases (the vorticity equation is not valid in the presence of a linearized baroclinic torque, for instance). These equations were used by several authors, including Hunt, Goldstein, Durbin and Zeman.

As conjectured in [7] and rediscussed in [8, 3], the solenoidal linear response, or $u^{(s)}$ obtained by applying the Helmholtz decomposition to eq. 7, gives the minimum kinetic energy growth rate, whereas its pressure-released counterpart gives the maximum, suggesting a linear compressible model as

$$\boldsymbol{u} = \boldsymbol{u}^{(s)} + \underbrace{f(M_d)\left(\boldsymbol{u}^{(pr)} - \boldsymbol{u}^{(s)}\right)}_{\boldsymbol{u}^{(d)}} \; ,$$

yielding for the linear history of the turbulent kinetic energy (e.g. [8])

$$q^2 = q^{2(s)} + \underbrace{f(M_d)\left(q^{2(pr)} - q^{2(s)}\right)}_{q^{2(d)}} \qquad (9)$$

for the turbulent kinetic energy, where the modelled factor $f(M_d)$ varies monotonically from 0 (zero M_d) to one (largest M_d). This simple scheme was verified for homogeneous turbulence, as we will rediscuss further, and is reasonable if the pressure-released limit is more energetic than the solenoidal limit, as it often does. Incidentally, one can mention that a simple model by Debiève (1982) for the Reynolds stress tensor passing through a shock wave can be derived from equation (3); the reader is referred to [7] for the related context.

This preliminary analysis has the advantage not to need Fourier space and detailed expressions for the Helmholtz decomposition, but the extraction of $\boldsymbol{u}^{(s)}$ from eq. (7) implies to solve a Poisson equation, or

$$\nabla^2 \varphi = -\frac{\partial u_i^{(pr)}}{\partial x_i} \; ,$$

as usual when pressure is called into play. More generally, two aspects must be kept in mind:

- The linearized Weber equation is only valid for *irrotational* mean flows with no occurence of baroclinic effects. Final expression of the scalar potential φ in terms of initial velocity remains an additional task to do anyway.
- The pressure-released linear limit, with eq. (3) is completely general, also valid for a rotational mean flow, but it appears as the limiting case of a linearized Weber equation only for irrotational mean strains.

2.2 Equations for quasi-isentropic, homogeneous turbulent flows

Relaxing the assumption of irrotational mean strain is possible for developing at least linear (so-called RDT) solutions but the assumption of statistical homogeneity must be stated. Even if this assumption is much less constraining than it is generally admitted (thanks to the use of WKB developments for zonal RDT, use of Fourier modes for the linear response to a shock wave of

various disturbances without any homogeneity assumption), the fact that the mean flow is only characterized by its spatial gradient matrix $A_{ij} = \frac{\partial U_i}{\partial x_j}$ has important consequences. First of all, it is not possible to define a length scale and a velocity scale for the mean flow (such as δ and ΔU in the shear layer), only a time-scale. This explains why linearization is not justified, as in conventional linear stability analysis, by a (small) ratio of disturbance-to-base velocity scale, but by an assumption of small elapsed time. S being a typical (inverse time) scalar scale for $\mathbf{A}$ magnitude, the validity of the linear solution is only expected for small St, but the maximum St for validity depends crucially on the initial "shear rapidity" as SL/u', where L and u' are typical scales for the disturbance flow, and so on. Our experience is that the validity of RDT cannot be predicted a priori, in terms of only St and initial SL/u': in contrast, in some extreme cases (rotating turbulence with angular velocity Ω, low Rossby number $Ro = u'/(2\Omega L)$), the nonlinearity become significant only after a very long time, such as $\Omega t = Ro^{-2}$ (this is partly explained by the depletion of nonlinearity due to phase mixing by dispersive inertial waves at small Rossby number). This misleading "rapid" adjective in RDT is even more irrelevant here with at least two "rapid" time scales, $1/S$ and L/c. In brief, short time is a sufficient condition for the linear solution to be valid, not a necessary one.

Compressible isentropic equations are found writing conservation of mass, momentum and entropy, in terms of density, velocity and pressure. A 'mean' state is given by space-uniform density $\rho_0(t)$, pressure $P(t)$ and mean velocity gradients

$$U_i = A_{ij} x_j \ ,$$

and we are interested in the equations for the disturbance (or fluctuating) flow characterized by (fluctuating) density ρ, pressure p and velocity u_i. Additional simplifications are found if we consider that the fluctuations of density and pressure are weak with respect to their 'mean' reference state, and a simplified system of two equations is found as

$$\dot{u}_i + A_{ij} u_j + \frac{1}{\rho_0} \frac{\partial p}{\partial x_i} = -u_j \frac{\partial u_i}{\partial x_j} \tag{10}$$

$$\frac{D}{Dt}\left(\frac{p}{\gamma P}\right) + \frac{\partial u_i}{\partial x_i} = -u_j \frac{\partial}{\partial x_j}\left(\frac{p}{\gamma P}\right) \tag{11}$$

where

$$c^2 = \gamma \frac{P}{\rho_0} \ , \tag{12}$$

is the square of the sonic speed, assuming $p = c^2 \rho$. The 'overdot', possibly replaced by the symbol $\frac{D}{Dt}$ if applied to long formulae, holds for a substantial derivative following the mean flow. Viscous terms are omitted, in agreement with isentropic assumption, but can be added for numerical convenience. These equations, with possible viscous terms, are the starting point for both the nonlinear (statistically isotropic) approach by Bertoglio and coworkers [12] in the absence of mean velocity gradient, and our linear approaches [7, 3] in the presence of $\mathbf{A}$. The more general "linear" case was addressed by [3], including mean compression/dilatation $A_{ii} \neq 0$, resulting in a possible volumetric ratio $J(t)$ $(= Det\mathbf{F})$ and time-depending sonic speed $c(t)$. In addition, admissibility conditions were given for $A_{ij}(t)$, generalizing previous conditions given by Blaisdell and coworkers.

2.3 linear equations

Eq. (10) and (11) are linearized around the mean flow with space uniform gradient $\mathbf{A}$, so that their right-hand-sides are zero. As usual in RDT and in related stability analyses [13], the equations are simplified in terms of Lagrangian Fourier modes

$$(u_i, p)(\boldsymbol{x}, t) = \int (\hat{u}_i, \hat{p})(\boldsymbol{k}(t), t) e^{\imath \boldsymbol{k}(t)\cdot\boldsymbol{x}} d^3\boldsymbol{k} \ ,$$

with

$$\dot{k}_i = -A_{ji} k_j \ . \tag{13}$$

The latter Eikonal-type equation has a solution

$$k_i = F^{-1}_{ji}(t) K_j \ , \tag{14}$$

which is very similar to the mean trajectory equation

$$x_i = F_{ij}(t) X_j \ . \tag{15}$$

Both equations give characteristic lines and are governed by the Cauchy matrix $\mathbf{F}$ (eq. (4) and (5) in general, with $t_0 = 0$ for simplicity) of the mean flow, symbolically

$$\mathbf{F} = \exp\left(\int_0^t \mathbf{A}(t')dt'\right) \ . \tag{16}$$

Lagrangian variables for the mean flow $\boldsymbol{X}$ are sometime called "Rogallo space". In addition to mean advection terms, Fourier space allows to treat the pressure-to-velocity relationship in a much simpler way for incompressible RDT. In the compressible case, at least the Helmholtz equation (1) amounts to a simple algebraic equation

$$\hat{\boldsymbol{u}} = \underbrace{u^{(1)}\boldsymbol{e}^{(1)} + u^{(2)}\boldsymbol{e}^{(2)}}_{\hat{\boldsymbol{u}}^s} + \underbrace{u^{(3)}\frac{\boldsymbol{k}}{k}}_{\hat{\boldsymbol{u}}^{(d)}} \ , \tag{17}$$

in agreement with the decomposition in physical space, the superscripts 's' and 'd' denotes solenoidal and dilatational modes, respectively. For convenience, the Craya-Herring frame of reference [9, 10] is used in order to define the two modes which represent the solenoidal part of the flow, toroidal $e^{(1)}$ and poloidal $e^{(2)}$ type. Let us just mention that $(\boldsymbol{e}^{(1)}, \boldsymbol{e}^{(2)}, \frac{\boldsymbol{k}}{k})$ form a direct orthonormal frame of reference. Accordingly, vortical (applying the Curl operator) and divergence (applying the divergence) velocity contributions have simple counterpart in Fourier, craya-Herring space

$$\hat{\boldsymbol{\omega}}(\boldsymbol{k}, t) = \imath k \left(u^{(1)}\boldsymbol{e}^{(2)} - u^{(2)}\boldsymbol{e}^{(1)}\right) \tag{18}$$

$$\widehat{u_{i,i}}(\boldsymbol{k}, t) = \imath k u^{(3)} \ . \tag{19}$$

The pressure term is scaled in a similar way by

$$u^{(4)} = \imath \frac{\hat{p}}{\rho_0 c} \ . \tag{20}$$

Linear solutions are then expressed in terms of $u^{(i)}, i = 1, 4$ components, solving the following linear system of ODE:

$$\begin{pmatrix} \dot{u}^{(1)} \\ \dot{u}^{(2)} \\ \dot{u}^{(3)} \\ \dot{u}^{(4)} \end{pmatrix} = \begin{pmatrix} * & * & m_{13} & 0 \\ & * & m_{23} & 0 \\ m_{31} & m_{32} & m_{33} & -ck \\ 0 & 0 & ck & \frac{3-\gamma}{2} A_{ii} \end{pmatrix} \begin{pmatrix} u^{(1)} \\ u^{(2)} \\ u^{(3)} \\ u^{(4)} \end{pmatrix} \quad (21)$$

or $\dot{u}^{(i)} = m_{ij} u^{(j)}, i = 1,4, j = 1,4$, the overdot denoting a time derivative including $\boldsymbol{k}(t)$, in close connection with its counterpart in physical space. Of course, the problem in four components in physical space (u_1, u_2, u_3, p) remains a four-components problem in Fourier, Craya-Herring, space, no reduction of the number of variables is found as in all other solenoidal cases, but at least, the matrix $m_{ij}, i = 1,4, j = 1,4$ has some zero components and the role of each nonzero component is clearer. The coefficients replaced by 'star' in (21) are the same as in solenoidal RDT [6]. All the coefficients in the 'velocity block' of the matrix above, or $m_{ij}, i = 1,3, j = 1,3$ depend on $\mathbf{A}$ (details in [3]) and therefore scale with S (a norm of $\mathbf{A}$); the acoustic terms m_{34} and m_{43} scale with the dispersion frequency of acoustic waves, or kc; accordingly, a spectral counterpart of the distortion Mach number is immediately found as being $S/(kc)$.

The solution of (21) is expressed as

$$u^{(i)}(\boldsymbol{k}(t), t) = J(t) g_{ij}(\boldsymbol{k}, t) u^{(j)}(\boldsymbol{K}, 0) \; . \quad (22)$$

As usual in RDT [11, 6], the deterministic function $g_{ij}, i = 1,4, j = 1,4$ can be obtained analytically, or numerically, solving the system of equations (21) for a set of arbitrary simple initial data (such as $u^{(i)} = \delta_{i1}, \delta_{i2}, \delta_{i3}, \delta_{i4}$ sequentially). Subsequent solutions for statistical moments are obtained through g-products, from the initial value of these statistical moments. Simplified forms of these initial values usually result from isotropy and acoustic equilibrium.

Recovering the acoustic regime

In the absence of mean flow, or $\mathbf{A} = \mathbf{0}$ in (21), the solenoidal mode is strictly conserved, whereas pressure and dilatational velocity modes are governed by

$$\left(u^{(3)} \pm \imath u^{(4)}\right)_t = e^{\pm ckt} \left(u^{(3)} \pm \imath u^{(4)}\right)_{t=0} \; . \quad (23)$$

up to diffusivity effects, not discussed here for the sake of brevity.

Recovering solenoidal and pressure-released limits

The solenoidal limit, also known as incompressible RDT, is found in solving only the block $i = 1,2, j = 1,2$, since $u^{(3)} = 0$ gives the solenoidal limit (e.g. eq. (19) and

$$u^{(4)} = u^{(4s)} = \frac{m_{3\alpha}}{kc} u^{(\alpha)} \quad (24)$$

gives the counterpart of the solution for the Poisson equation verified by the fluctuating pressure in this limit, or

$$\hat{p} = \hat{p}^{(s)} = -\frac{\imath}{\rho_0} m_{3\alpha} u^{(\alpha)}, \quad m_{3\alpha} = 2 \frac{k_i}{k} A_{ij} e_j^{(\alpha)} \; .$$

For convenience, Greek indices take the value one or two only, from now on, characterizing coupling with solenoidal modes only.

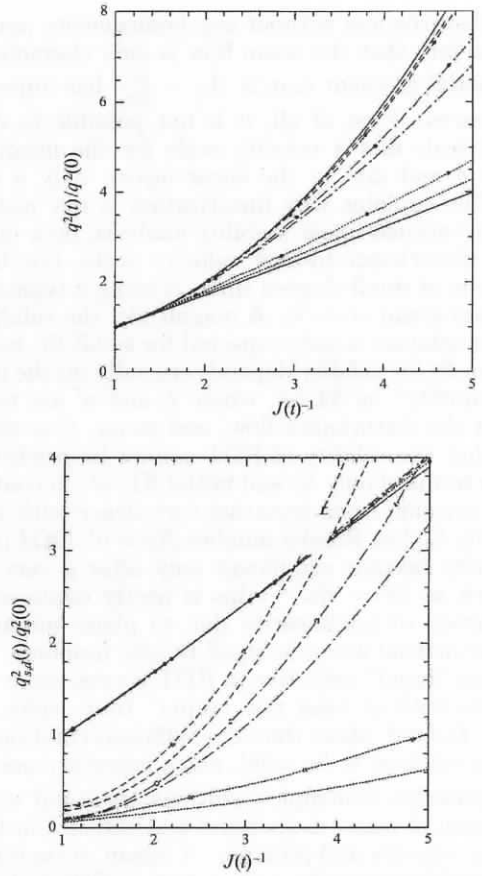

Figure 2: Turbulent kinetic energy histories at different M_d, axial compression. Full DNS (points) and linear theory (lines). Bottom: in addition, splitting into solenoidal and dilatational parts.[3]

Recovering the irrotational mean strain case

In addition to pure solenoidal coupling terms $m_{\alpha\beta}$, which are the same as in solenoidal RDT, and to 'acoustical' or 'pseudo-sound' terms $m_{34} = -ck$, $m_{43} = ck$, discussed above, very interesting terms are

$$m_{\alpha 3} = e_i^{(\alpha)} (A_{ij} - A_{ji}) \frac{k_j}{k} \; .$$

These terms represent a feedback from the dilatational mode to the solenoidal modes, and they are generated by the *rotational part* of the mean flow.

As an immediate consequence, the solenoidal flow is decoupled in the presence of an irrotational straining process. A second, less obvious, consequence, is that the kinetic energy growth rate is larger in compressible RDT than in solenoidal RDT, since the kinetic energy of the dilatational mode, always positive, is just added to the kinetic energy of the solenoidal mode, which is independent of compressibility in this context. The effect of fluctuating pressure is just to kill this dilatational contribution, in the solenoidal linear limit. Accordingly, as firstly demonstrated by Jacquin *et al.* (1993) [7], the kinetic energy growth rate increases monotonically with increasing distortion Mach number M_d, from solenoidal RDT to 'pressure released' (very simple) RDT, in complete agreement with eq. (9). These results were revisited and confirmed by full DNS [8], [4] for homogeneous axial compression ($A_{ij} = S(t)\delta_{i1}\delta_{j1}$), as shown on Fig. 2. For convenience, the time advancement parameter is not $S_0 t$ but the inverse of the mean volumetric ratio

$J(t)$, with $S(t) = -S_0/(1 - S_0 t) = -S_0/J(t)$. Energy contribution from the solenoidal mode corresponds to a quasi-linear growth in terms of the mean compression ratio J^{-1}, whereas dilatational contribution corresponds to a quasi-parabolic growth. One can retain that compressibility is always shown as destabilizing regarding RDT for irrotational mean flow. Of course, the general relevance of the result can be questioned from both the irrotational condition and the short time condition $S_0 t < 1$ in the case of axial compression.

3 Homogeneous pure plane shear

The case of pure plane shear is given by

$$A_{ij} = S\delta_{i1}\delta_{j2}; \quad F_{ij}(t) = \delta_{ij} + A_{ij}t \,, \qquad (25)$$

so that Eq. (14) reduces to

$$k_1 = K_1, \quad k_2 = K_2 - K_1 St, \quad k_3 = K_3 \,. \qquad (26)$$

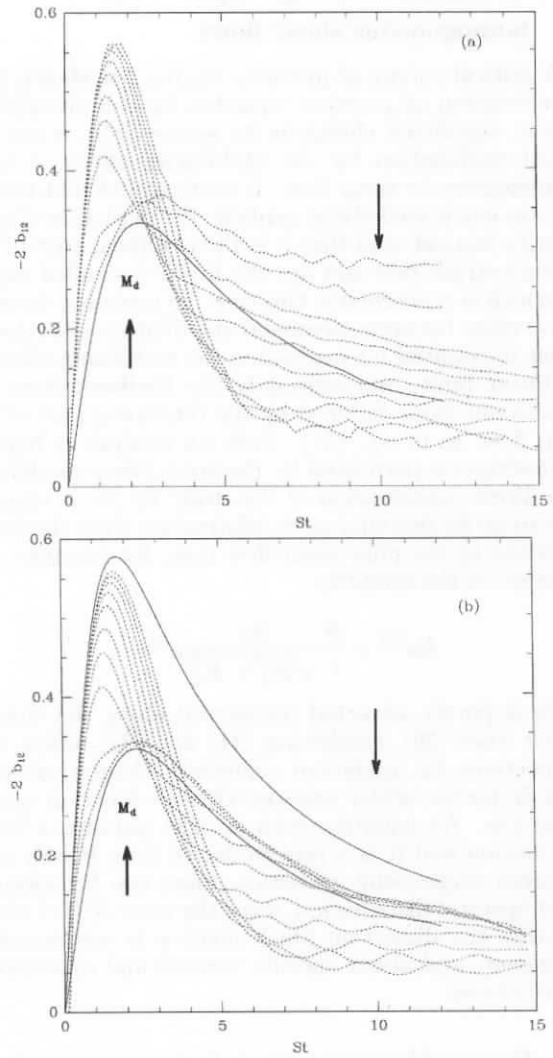

Figure 3: Histories of the nondimensional production term $-2b_{12}$, Full DNS (top) and linear quasi-isentropic compressible theory (bottom), so called (improperly) RDT. Upper and lower solid lines correspond to pressure-released limit and solenoidal limit, respectively. Initial M_d ranges from 4 to 67 for both DNS and RDT, arrows show trend with increasing M_d. From [3]

3.1 Qualitative results

Even for the case of pure shear, the pressure released limit is more energetic than the linear solenoidal limit. Accordingly, a reduction of pressure fluctuations, in the linear limit, would yield a monotonic increase of turbulent kinetic energy with increasing M_d, as for the case of irrotational mean straining ! The fact that the pressure-released growth rate is higher than the solenoidal one, in the linear limit, results from eq. (3), with (25), which yields a $(St)^2$ growth rate for kinetic energy. In the same conditions the solenoidal RDT only predicts a linear, St, growth rate (Rogers 1991 and Piquet's book). In a relevant nondimensional form, kinetic energy growth rate is characterized by

$$\Lambda = \frac{1}{Sq^2}\frac{dq^2}{dt}; \quad q^2(t) = \overline{u_i u_i} \,, \qquad (27)$$

and is given by

$$\Lambda = -2\left(b_{12} + \frac{\varepsilon^{(s)} + \varepsilon^{(d)} - \Pi_d}{Sq^2}\right) \qquad (28)$$

in the homogeneous shear flow case, b_{12} being the single component of the deviatoric part of the Reynolds stress tensor involved in the production term, the additional terms denoting the solenoidal dissipation rate, the dilatational one, and the pressure-dilatation term. The kinetic energy growth rate is equal to

$$\Lambda^{(pr)} = \frac{2St}{3 + (St)^2} \qquad (29)$$

in the pressure-released linear limit, started with isotropic initial data: this equation gives the upper solid curve in Fig. 3-bottom. The corresponding limit of solenoidal RDT is plotted in Fig. 3, as the lower solid curve. Is there a simple explanation for this 'stabilizing' effect of pressure in solenoidal RDT, without looking at RDT details ? as in all shear flow cases, the answer is given by the dynamics of the vertical velocity component: u_2 is only advected in the pressure-released linear limit, whereas its Laplacian, or $\nabla^2 u_2$ is advected in the RDT solenoidal limit. According to the corresponding RDT complete solution in Fourier space, $\frac{Dk^2\hat{u}_2}{Dt} = 0$, or $\hat{u}_2(\boldsymbol{k}, t) = \frac{K^2}{k^2}\hat{u}_2(\boldsymbol{K}, 0)$, yields decreasing u_2. Using the Craya-Herring frame with the polar axis parallel to the cross-gradient direction of the mean shear, the complete RDT solution (Cambon's thesis and [3]) is much simpler than the one given by, e.g. Townsend [11] in the fixed frame, but the corresponding equation concerning $u^{(2)}$ is

$$(k\dot{u}^{(2)}) = 0 \,, \qquad (30)$$

always consistent with the pure advection of $\nabla^2 u_2$ in physical space. Note that we only confirm that the role of the so-called 'rapid' pressure-strain rate tensor in Reynolds stress equations is stabilizing, *even in agreement with crude single-point modelling, where it is evaluated as reducing the production.* Using these simple arguments, a destabilizing effect of compressibility would be demonstrated, as shown in Fig. 3 for $St < 4$ for both full DNS and quasi-isentropic compressible linear theory. This result is very similar to what happened in the irrotational mean strain case, with a monotonic increase of Λ with increasing M_d, from the solenoidal to the pressure-released case.

3.2 General discussion

As shown in Fig. 3, the conventional 'stabilizing' behaviour of compressibility is recovered at largest time $St > 4$. It is therefore clear that this stabilizing behaviour is explained by the presence of the $m_{\alpha 3}$ coupling terms, at least in the linear limit. Fig. 3 shows the main part of the turbulent kinetic energy growth rate Λ in Eq. (27), which reduces to $-2b_{12}$, ignoring other terms, as justified by [2, 3]. More accurately, the key equation for the compressible shear flow case is

$$\left(k\dot{u}^{(2)}\right) = -S\frac{K_1}{\sqrt{K_1^2+K_3^2}}ku^{(3)}, \qquad (31)$$

as a special case of Eq. (21) for pure plane shear. Other important equations are

$$\dot{u}^{(4)} = ck(t)u^{(3)} \qquad (32)$$

and

$$\frac{D}{Dt}\left(\frac{\dot{u}^{(4)}}{k^2}\right) = c^2\left(u^{(4s)} - u^{(4)}\right) . \qquad (33)$$

as in [3], with $u^{(4s)}$ given by Eq. (24), equivalent to $\hat{p} = \hat{p}^{(s)}$ from the Poisson equation in Fourier space.

Going back to the (generally expected) stabilizing effect of compressibility, it is generally accepted, following [2, 1], that the weakening of pressure correlation is the only explanation. In fact, the weakening of pressure can be demonstrated from the solution of the equation (33), under a scalar Green's function for pressure to velocity

$$\hat{p}(\mathbf{k},t) = \int_{t_0}^{t} \mathcal{G}(\mathbf{k},t,t')\hat{p}^{(s)}(\mathbf{k},t')dt' . \qquad (34)$$

Recently, Thacker *et al.* [5] proposed an analytical solution for a similar scalar Green's function in the case of pure shear, generalizing the form $\mathcal{G} = \frac{\sin(ck(t-t'))}{ck}$ recovered in the shearless case (e.g. Pantano & Sarkar [1]). One can point out that this scalar Green's function is generated by the equation

$$\ddot{\hat{p}} + k^2c^2\hat{p} = k^2c^2\hat{p}^{(s)}$$

(using our own notations), which is simpler than eq. (33) — and less relevant to our opinion —. Both eq. (33), in which $u^{(4)}$ can be replaced by $\hat{p}$ since c is not time-dependent, and the one by Thacker et al. account for the time-dependency of k via (26), but the removal of the divergence term was not accurately obtained in [5]. In addition, the equation of type (34) was used to express the 'rapid' pressure-strain rate tensor in term of the velocity spectral tensor involved in $\overline{\hat{p}\hat{u}_i^{(s)}}$: a solenoidal spectral model for $\overline{\hat{u}_i^{(s)}\hat{u}_j^{(s)}}$ was used by [5] for this purpose (see also [14] for a discussion of this model).

We think that the explanation based on eq. (33), for stabilizing/destabilizing compressibility effects, is only a part of the whole story. This equation is also a byproduct of the general study based on the full system of linear equations in [3]. Conventional explanation is valid, for instance for accounting for the difference of the less compressible case in Fig. 3-top (almost constant production rate at largest St), which is also a fully nonlinear result, and the pressure released case (upper curve in solid line in Fig. 3-bottom). This 'explanation' is irrelevant when the curve of compressible RDT at large M_d and large elapsed time is found below the incompressible RDT limit curve (solid line in Fig. 3), in contrast with our explanation based on equation (31). As a final remark, let us recall that the argument on the weakening of pressure is always relevant in the irrotational 'mean' case, or at $St < 4$ in the shear case, but yields a *systematic destabilizing effect* because the pressure-released limit is always over the incompressible RDT limit ! Of course, looking at the Reynolds stress equations, the weakening of the *nonlinear* (so-called slow) pressure-strain rate tensor yields a stabilizing effect in the pure shear flow case, but this reflects more a depletion of nonlinearity at increasing M_d than a stabilizing effect of compressibility: in addition the ratio of "distortion" to "turbulent" Mach number, or M_d/M_t is nothing else than the ' shear rapidity', and increasing M_d without increasing M_t in the same proportion means depleting the nonlinearity. To be completely honest, the latter criticism holds for our DNS in Fig. 3, but not for pure linear theories.

4 Conclusion and perspectives

4.1 homogeneous shear flows

A critical survey of previous studies has shown that the alteration of pressure equation by compressibility, without significant change in its source term, is not the correct explanation for the 'stabilizing' effect, at least for homogeneous shear flow. It is suggested that the alteration mentioned above explains the depletion of nonlinearity instead, and that it is the nonlinear part of the pressure-strain rate and not the linear (so called rapid) one which is concerned in this case. In contrast, the subtle interplay between solenoidal and dilatational velocity modes is essential for explaining the stabilizing effect in the linear limit, and especially the feedback from the dilatational mode induced by the rotational part of the mean flow, as in eq. (31). Such an analysis is beyond the description permitted by Reynolds stress modelling. As a direct continuation of the study by [3], it remains work to do for deriving more information from the linear equations in the pure shear flow case; for instance, the existence of the quantity

$$ku^{(2)} + \frac{S}{c}\frac{K_1}{\sqrt{K_1^2+K_2^2}}u^{(4)} ,$$

which is purely advected (conserved along the characteristic lines (26), combining (31) and (32), offers new perspectives for analytical solutions. Analytical solutions [5] for the scalar pressure Green's function can be useful too. An equation such as (22) contains a lot of information and it is a pity to derive from it only conventional single-point statistics: more can be obtained about spectral distribution, since the ratio $S/(kc)$ which underlies the distortion Mach number is wavenumber-dependent, and about specific vortical and dilatational contributions.

4.2 Perspectives towards inhomogeneous shear flows

In an incompressible mixing layer, the velocity scale is unequally determined by the difference in the two stream velocities,$v_0 \sim \Delta U$ and variation in the length-scale unequally depends on the velocity ratio. Compressibility changes this dimensional rule by making the speed of sound a relevant parameter with the consequence that the two above scales now possibly depends on a Mach number (the gradient Mach number

$M_g \sim \Delta U/c$ or the turbulent Mach number $M_t \sim v_0/c$ with c an average of the two sound celerities). As already mentioned, the consensus that emerged from DNS of compressible mixing layers is that compressibility stabilises a mixing layer by decreasing its pressure fluctuations, see e.g. Pantano & Sarkar [1]. This leads in particular to reduction of the pressure-strain terms which produces the turbulent shear stress through redistribution among the Reynolds stresses of the energy provided by the work of the mean shear. Indeed, these DNS provided us with decisive results. But, according to our above analyses, the detailed sequence of mechanisms leading to the mixing layer stabilisation still escapes to our understanding. We pointed out that linear analyses of compressible flows are somewhat in contradiction with the proposed interpretations because given a shear rate $\Delta U/\delta$, damped pressure fluctuations should make both the kinetic energy and the shear stress *increased* instead of decreased, through contribution of dilatational velocity fluctuations growing with the gradient Mach number. This should remain effective in the conditions which hold in a mixing layer because one does not expect a strong imbalance between linear and non linear time scales in such a free flow (actually $\delta/\Delta U$ does not depart so much from δ/v_0 and mildly rapid shear conditions must prevail). This indicates that non-linear compressibility effects should be addressed, in particular the changes in the mechanism of "isotropisation" of the fluctuations by pressure which are essential for producing kinetic energy in a shear flow. Evaluation of the respective impact of compressibility on linear and non-linear pressure terms is required for understanding and modelling correctly the compressible mixing layer. Note at last that in this inhomogeneous flow transport terms are also deeply modified by the drop of pressure fluctuations. Namely, one observes that the decrease in the production of turbulent kinetic energy is almost compensated by an equivalent decrease in its transport, letting the dissipation rate ϵ almost unchanged.

This last result should also deserve attention. Favre average and normalization by ΔU and by the momentum thickness δ being used in the DNS, the result is that $\epsilon\delta/(\Delta U)^3$ poorly depends on compressibility. If at the same time the normalized kinetic energy $v_0^2/(\Delta U)^2$ is reduced by compressibility, basic dimensional analysis leaves us with the paradox that the rate of dissipation of the turbulent kinetic energy (proportional to $(\Delta U)^3/\delta$) exceeds by a factor proportional to $(\Delta U/v_0)^3$ the rate of injection of the kinetic energy into the cascade (proportional to v_0^3/δ).

Indeed, the reasoning is very crude, but it indicates that the detailed mechanisms fixing energetic equilibrium in compressible mixing layers are not yet fully asserted. This was addressed for instance by the results of Jacquin et al. 1996 [15] who observed that changing M_g thanks to variations in the total temperature of the interacting streams had almost no effect on mixing of the total pressure in their flow : poor variations in the total pressure spreading rate with compressibility were obtained and were also apparent in other experiments. This would be an indication that the dissipation processes, which set the losses (i.e. the transformation of mechanical energy into heat), weakly depends on compressibility in free compressible shear flows. If this were true, this should be integrated into our models. Though it is, it remains still much to make and to understand on the subject.

Finally, explanations based on the hydrodynamic stability, as the inhibition of Kelvin-Helmholtz instabilities by compressibility, cannot be ignored, even if our main theme here is developed turbulence. The reader is referred to [16] for the problems of compressibility in wall bounded flows.

Bibliography

[1] Pantano C., Sarkar S., A study of compressibility effects in the high-speed turbulent shear layer using DNS, *J. Fluid Mech.*, vol. 451, pp. 329–371, 2002.

[2] Sarkar S., The stabilizing effect of compressibility in turbulent shear flows, *J. Fluid Mech.*, vol. 282, pp. 163–286, 1995.

[3] Simone A., Coleman G.N., Cambon C., The effect of compressibility in turbulent shear flow: a RDT and DNS study, *J. Fluid Mech.*, vol. 330, pp. 307–338, 1997.

[4] Lele S.K., Compressibility effects on turbulence, *Annu. Rev. fluid Mech.*, vol. 26, pp. 211–254, 1994.

[5] Thacker W.D., Sarkar S., Gatski T.B., Analyzing the influence of compressibility on the rapid pressure-strain rate correlation in turbulent shear flow, TSFP4 meeting and TCFD journal, submitted.

[6] Cambon C., Teissèdre C., Jeandel D., Etude d' éffets couplés de déformation et de rotation sur une turbulence homogène, *J. Méc. Théor. Appl.*, vol. 4, pp. 629–657, 1985.

[7] Jacquin L., Cambon C., Blin E., Turbulence amplification by a shock wave and Rapid Distortion Theory, *Phys. Fluids A*, vol. 10, pp. 2539–2550, 1993.

[8] Cambon C., Coleman G.N., Mansour N.N., Rapid distortion analysis and direct simulation of compressible homogeneous turbulence at finite Mach number, *J. Fluid Mech.*, vol. 257, pp. 641–665, 1993.

[9] Written reports by Craya, Ph. D and P.S.T, in French, being unavailable or too abridged, more information can be obtained from the first author upon request.

[10] Herring J.R., Approach of axisymmetric turbulence to isotropy, *Phys. Fluids*, vol. 17, pp. 859–872, 1974.

[11] Townsend A.A., The structure of turbulent shear flow, Cambridge University Press, 1956/1976.

[12] Fauchet G., Shao L., Wunenberger R., Bertoglio J.-P., An improved two-point closure for weakly compressible turbulence, 11 Symp. Turb. Shear Flow, Grenoble, Sept. 8–10, 1997.

[13] Craik A.D.D., Criminale W.O., Evolution of wave-like disturbances in shear flows: a class of exact solutions of Navier-Stokes equations, *Proc. R. Soc. London Ser. A*, vol. 406, pp. 13–26, 1986.

[14] Cambon C., Rubinstein R., Anisotropic developments for homogeneous shear flows, *Phys. Fluids*, to appear.

[15] Jacquin L., Mistral S., Geffroy P., Cruaud F., Mixing of a heated supersonic jet with a parallel stream, *Advances in Turbulence V*, Springer-Verlag, 1996.

[16] Friedrich R., Effects of compressibility and heat release in turbulent wall-bounded and free shear flows, SIG4 ERCOFTAC and GST13 workshop, Porquerolles, France, June 1st.

PhD/Postgraduate positions

TECHNISCHE UNIVERSITEIT EINDHOVEN (TU/E)

Two PhD-students "Rapid Heating with Direct Steam Injection" (V35.348 and V35.349), at Thermo Fluids Engineering, Department of Mechanical Engineering.

In the project "Rapid heating with direct steam injection", which is funded by the Dutch Technology Foundation, a new physical model will be developed and validated that simulates the heating process of fluids by direct steam injection. In the project two PhD-students will cooperate, one of them focusing on numerical simulation (V35.348) and the other on experimental research (V35.349).

The aim of the numerical part of the project is the development of a Reynolds-averaged Navier-Stokes (RANS) model that describes rapid condensation of steam and rapid heating of a fluid. This model will be based on results of numerical simulation by means of a combination of large-eddy simulation and the diffuse-interface method. For a validation of the numerical model the experimental PhD-student will set up and utilize an experimental facility to accurately measure velocity components, temperatures and void fractions in a test rig in which steam is injected in a closed-loop water circuit. Experimental techniques to be used are micro-thermocouples, laser-induced fluorescence and particle image velocimetry.

More information can be obtained on: http://w3.wtb.tue.nl/. Send your application letter with extended curriculum vitae to: Mrs. Drs. A.J. Klomps (email: pzwtb@tue.nl), mentioning vacancy number 35.348 or 35.349.

J.M. BURGERS CENTRE FOR FLUID MECHANICS (THE NETHERLANDS) :

Postdoctoral position in Two-Phase Flow and Heat Transfer in Furnace tubes. The position for two years is available in the multiphase pipe flow group of the Kramers Laboratory at Delft University of Technology. Staff and students at the Kramers Laboratory are involved in numerous projects on multiphase flow, both experimental and numerical. The project with the vacancy is part of a long-term research program on the improvement of the flow regime dependent two-phase pipe flow models for use in industrial design and operation. Running projects deal with two-phase gas lift enhancement, liquid loading of gas wells, oil/water well logging, long liquid slugs in stratified flow and dispersed two-phase flow simulations in tubes.

More details on the position can be obtained from Prof. René Oliemans (r.v.a.oliemans@tnw.tudelft.nl). For further information on the Multi-Scale Physics Department, Delft University, and the Burgers Centre, please look at the web sites: http://msp.tudelft.nl, http://tudelft.nl, and http://jmburgerscentrum.org. Applications from both The Netherlands and abroad are welcome.

ON COMPRESSIBLITY EFFECTS ON HYPERMIXING STRATEGIES

Erwan Collin, Malick Ndoye, Jean-Paul Bonnet

Laboratoire d'Etudes Aéropdynamiques

UMR 6609 CNRS, Université Poitiers, ENSMA, France

erwan.collin@lea.univ-poitiers.fr

Abstract

A detailed experimental study of a fluidic device used for hypermixing is presented. A simplified version involving a single control jet/main jet interaction is analyzed through mean flow measurements and dynamical analysis of flow visualizations. Comparisons between subsonic and compressible (supersonic) flow configurations are given. One major observation is the flapping of the control jets. This flapping corresponds to a beating process between the local (Kelvin-Helmholtz) instability of the mixing layer of the main jet at the impact location of the Control Jet and the intrinsic instability (column mode) of the Control Jet itself. The interaction of the Control Jet and the mean flow results in an absolutely unstable configuration. The compressibility effects seem to have no strong influence on the global physical process itself, the major compressibility effects being observed on the amplitude of the unsteadiness. A complex behavior of the shock/mixing layer interaction in the supersonic configuration is evoked as an amplification mechanism of the whole unsteady process.

1 Introduction

Control of mixing of supersonic jets is an important issue for several industrial applications. Indeed, as the Mach number increases, the spreading rate of supersonic jets decreases dramatically, up to convective Mach numbers of order of 1 [1, 2]. Then, special care has to be given to compressible jets configurations if mixing has to be preserved or enhanced. Several methods have been used in order to improve the mixing properties of compressible jets. A first family of control methods is the use of special trailing edge geometries or tabs. These methods are known to modify the azimuthal organization of the flow and to add longitudinal vorticity within the mixing layers of the jet near the trailing edge, then enhancing mixing downstream [3, 4, 5, 6, 7, 8].

However, these methods present thrust losses when the hyper mixing is not mandatory (for example during the entire cruise). Pneumatic methods are then preferred due to the possibility of canceling their action when hypermixing is not required. Among these methods, several strategies can be used. For example, it is possible to create counter-flowing jets at the trailing edge, inducing then strong absolute instabilities that can excite the natural unstable modes of the main jet [9, 10]. Another method uses radial jets impinging the main jet in the immediate vicinity of the trailing edge where the receptivity of the mixing layer is maximum [11, 12]. This last strategy has been used in the present experimental study.

The present study deals with a hypermixing strategy that uses pneumatic injectors to manipulate an annular mixing layer. These injectors are located downstream of a main jet nozzle. Various geometries and control jets (CJs) configurations have been tested, both in incompressible and in supersonic regimes [13, 14]. One of the most efficient configurations consists of 4 CJs with rectangular nozzle at non zero sweep and roll angles. Photographies of this CJ configuration are given on Figure 1. The total mass flux of the CJs represents less than 1% of the main jet mass flux.

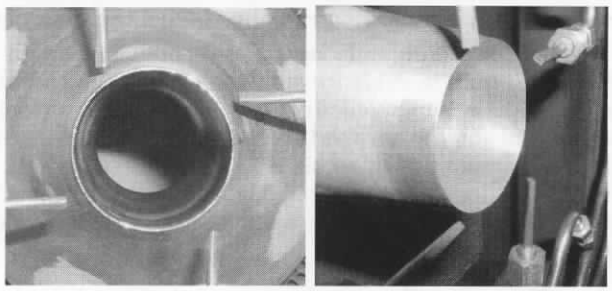

Figure 1: Photography of the 4 swept and rolled CJs configuration in the supersonic facility

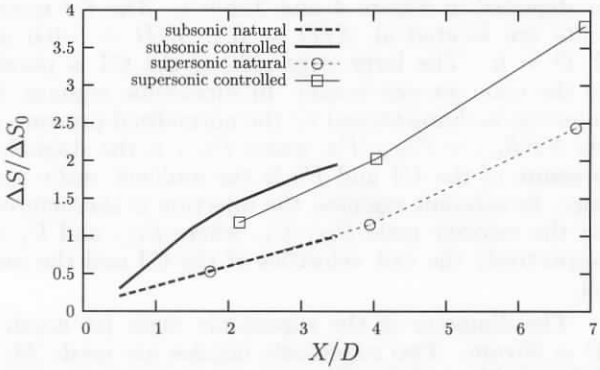

Figure 2: Longitudinal evolution of the mixing layer cross-section for the subsonic and supersonic regimes in the natural case and in the manipulated case with 4 swept and rolled CJs

A criteria that has been used to evaluate the hypermixing efficiency is the area of the mixing layer for each cross section of the flow. This area, which is noted ΔS, is defined as the area comprised between the iso-contours of the normalized velocity $U^* = (U - U_2)/\Delta U = 0.1$ and $U^* = 0.9$, where U is the local mean velocity magnitude, U_2 is the velocity magnitude of the external flow, $\Delta U = U_1 - U_2$, and U_1 is the velocity magnitude of the main jet. The parameter ΔS is normalized by ΔS_0 which is a mixing area arbitrary chosen to be the mixing area at $X/D = 3.5$ for the uncontrolled regime. A comparison between results obtained in subsonic (incompressible) and supersonic ($M_1 = 1.4$,

convective Mach number $M_c = 0.55$) regimes with similar CJ configurations is given on Figure 2. It appears clearly that the mixing efficiency in the supersonic case is of the same order as in the subsonic case. More, the hypermixing seems to occur only very near the injectors: no change of the spreading rate is detected downstream of $X/D = 2$.

The purpose of the present study is to analyze the flow characteristics in the near field of the pneumatic injection, to understand the mechanisms responsible of the hypermixing process, and to investigate the effects of compressibility on the hypermixing mechanisms. This study is performed using a simpler CJ configuration: a single steady CJ blowing radially toward the main jet.

The flow configurations are presented in section 2. Section 3 puts in evidence similarities between the subsonic and the supersonic regimes, for the mean velocity fields and for the unsteady behavior of the CJ-mixing layer interaction. In section 4, a parametric study is used in order to characterize the properties of the CJ-mixing layer interaction as a function of the flow conditions.

2 Flow configurations

The CJ configuration for the present study is depicted in Figure 3. The CJs consist of convergent only rectangular nozzles. Four CJ nozzle geometries are used, as depicted in Figure 4 and Table 1. The CJ nozzles exits are located at $X/D = 0.1$, $Y/D = -0.6$ and $Z/D = 0$. The large edge side of the CJ is parallel to the main jet exit nozzle. In supersonic regimes, the injection is characterized by the normalized pressure ratio $NPR_{CJ} = Pt_{CJ}/Ps$, where Pt_{CJ} is the stagnation pressure of the CJ and Ps is the ambient static pressure. In subsonic regimes, the injection is characterized by the velocity ratio U_{CJ}/U_1, where U_{CJ} and U_1 are respectively the exit velocities of the CJ and the main jet.

The diameter of the supersonic main jet nozzle is $D = 50\,mm$. Two supersonic nozzles are used: $M_1 = 1.4$ and $M_1 = 1.8$. The convergent-divergent nozzles are operated at ideally expanded conditions. So, the normalized pressure ratio for the main jet is $NPR_1 \equiv Pt_1/Ps = 3$ for the $M_1 = 1.4$ nozzle, and $NPR_1 = 5.7$ for the $M_1 = 1.8$ nozzle. The Mach number of the secondary flow is of the order of $M_2 = 0.13$ for both supersonic nozzle. The convective Mach number for the $M_1 = 1.4$ and $M_1 = 1.8$ jets are respectively $M_c = 0.55$ and $M_c = 0.68$.

For the low-subsonic regime, several velocity ratio for the main jet mixing layer are used, ranging from $U_2/U_1 = 0.05$ to $U_2/U_1 = 0.8$, with $U_1 \simeq 24\,ms^{-1}$.

The mean velocity field for each subsonic and supersonic non manipulated mixing layer is investigated. The vorticity thickness of the non manipulated main jet mixing layer at $X/D = 0.1$ is an important parameter for the control strategy, because it characterizes the shear encountered by the CJ. This thickness is noted $\delta_{\omega 0}$. Depending of the velocity ratio and the Mach number of the main jet, $\delta_{\omega 0}$ ranges between 2.9 and 6.1 mm. It can be noted that $\delta_{\omega 0}$ is of the order of the dimensions of most of the CJ nozzle that are studied.

3 Mean velocity fields and CJ penetration status

Mean velocity fields for the supersonic and subsonic regimes are presented on Figure 5. These results are

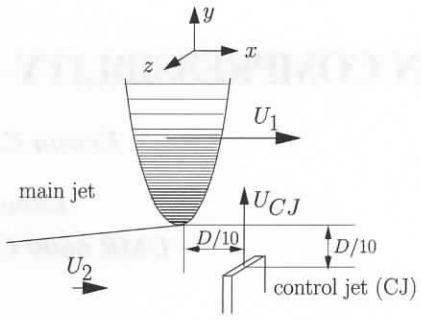

Figure 3: Schematic description of the flow configuration for the subsonic/supersonic comparative study

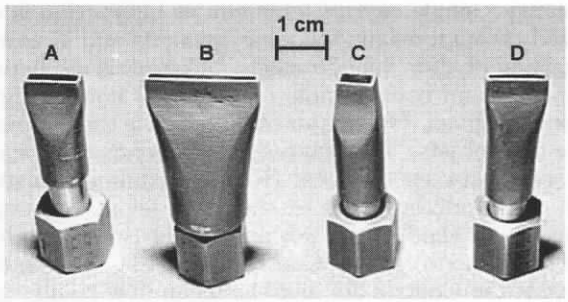

Figure 4: Photography of the CJ nozzles

Type	A	B	C	D
$L\,(mm)$	9.5	21	6	11
$l\,(mm)$	2	1	3	1

Table 1: Geometrical characteristics of the CJ nozzles (L: span length, l: thickness)

obtained with the same CJ operated conditions. Is is clearly visible that the distribution of the streamwise velocity is almost identical, whether the main jet is subsonic of supersonic. The manipulated mixing layer is characterized by a strong deformation just downstream of the CJ. The width and the depth of this deformation in the supersonic regime is very similar to the subsonic regime. The fact that the CJ should generate a shock-wave inside the potential core of the supersonic main jet does not seem to play an important part in the hypermixing process.

Calculations of mixing area for each cross section have been performed. The results, which are not shown here, show that the similarities between the subsonic and the supersonic regimes are typically the same as for the complex four swept and rolled CJ already discussed in §1. So, as well as for the complex CJ configuration, strong similarities arise between the subsonic and the supersonic regimes for the simpler CJ configuration.

Since most of the hypermixing process is achieved in the near field of the CJ-mixing layer interaction, close-up instantaneous visualizations are performed. These visualizations are performed using the optical part of a Dantec PIV system. The laser sheet is located in the $Z = 0$ plane. The CJ are seeded with solid particles in the supersonic regime, and with incense smoke in the subsonic regimes. Examples of instantaneous side views are given in Figure 6, 7 and 8. On these pictures, the

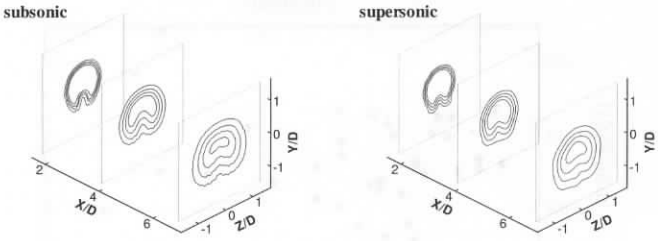

Figure 5: Distribution of the non-dimensional streamwise velocity magnitude (cross-sections are $X/D = 2$, 4 and 7; iso-contours correspond to $U^* = 0.2$, 0.4, 0.6 and 0.8; CJ type D; subsonic regime: $U_2/U_1 = 0.05$, $U_{CJ}/U_1 = 0.9$; supersonic regime: $M_1 = 1.4$, $NPR_{CJ}/NPR_1 = 0.85$)

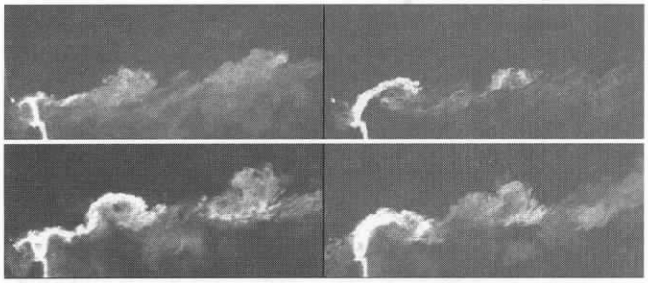

Figure 6: Examples of flow visualizations for situations corresponding to a strong flapping of the CJ in the supersonic regime (top: CJ type D, $M_1 = 1.4$, $NPR_{CJ}/NPR_1 = 0.85$ bottom: CJ type D, $M_1 = 1.8$, $NPR_{CJ}/NPR_1 = 1.5$)

main flow is from the left to the right, and the CJ is located in the bottom left of the field of view.

Every flow visualization acquired in the supersonic regime put forward the presence of a strong flapping of the CJ (see Figure 6). A similar behavior has been observed in previous works [14, 15]. Although this behavior occurs for each of the tested supersonic configurations, it is also noticed that the intensity of the flapping and the frequency are dependent of the dimensions of the CJ nozzle and of parameters NPR_{CJ}/NPR_1, $\delta_{\omega 0}$ and M_1.

The flapping of the CJ can also occur in the subsonic regime, as shown in Figure 7. However, this behavior is not evidenced for several flow conditions (see Figure 8). Of course, when shear in front of the CJ is weak ($U_2/U_1 = 0.8$ for instance), the CJ behaves as a standard jet in cross flow, without any flapping motion. But the absence of a flapping motion of the CJ is also noticed in some cases for which the mean shear in front of the CJ is strong.

The relationship between on one hand the flapping intensity and frequency and on the other hand the flow configurations is investigated using a parametric study in the next section.

4 Parametric study of the flapping of the CJ

4.1 Methodology

The parametric study is performed with the analysis of sets of instantaneous flow visualizations for a wide range of flow parameter, including the CJ geometry,

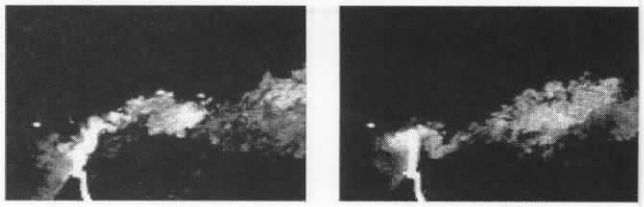

Figure 7: Example of flow visualizations for situations corresponding to a strong flapping of the CJ in the subsonic regime (CJ type D, $U_2/U_1 = 0.05$, $U_{CJ}/U_1 = 2$)

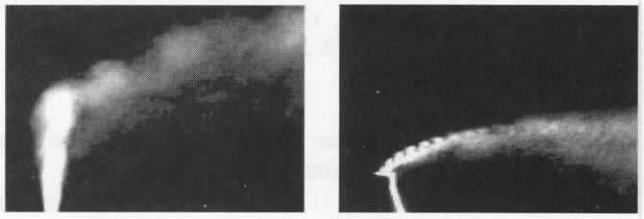

Figure 8: Examples of flow visualizations for situations without a strong flapping of the CJ in the subsonic regime (left: CJ type A, $U_2/U_1 = 0.05$, $U_{CJ}/U_1 = 1$; right: CJ type A, $U_2/U_1 = 0.8$, $U_{CJ}/U_1 = 0.5$)

U_{CJ}/U_1 or NPR_{CJ}/NPR_1, and U_1/U_2, M_1. Each visualization set contains 200 pairs of instantaneous snapshots that are acquired using the same set-up as in §3. The time delay between two images of a same pair is short enough to extract time derivatives of grayscale levels.

The frequency associated with the flapping motion is extracted using low-order dynamical systems of POD temporal coefficients. The dynamical systems are obtained using a polynomial identification. Details of this procedure can be found in [16]. Using this technique, a frequency can be extracted for each dataset. This frequency, which is related to the flapping motion of the CJ, is noted f_{CJ}.

The intensity of the flapping is a property that can not be easily extracted from the flow visualizations. Several criteria have been tested. The more confident indicator of the flapping intensity is based on the spatial auto-correlation function of the grayscale levels. The first step of the procedure is to extract the grayscale levels along the upper boundary of the CJ plume. Let $g(m, x)$ be this extracted grayscale series, where m is the number of the snapshot in a given dataset, and x is the streamwise location of an extracted pixel. A spatial auto-correlation function is built using $g(m, x)$:

$$R(\xi) = \left\langle \frac{\langle g(m,x) \cdot g(m,x+\xi) \rangle_X}{\langle g(m,x)^2 \rangle_X} \right\rangle_M$$

where $< >_X$ represents the ensemble average over the longitudinal position x, and $< >_M$ represents the ensemble average over the instantaneous realizations (i.e. average over m).

An example of $R(\xi)$ is plotted on Figure 9. When the CJ flaps, its plume contains puffs which are getting more and more distinct as the flapping intensity is increased. So, the minimal value of $R(\xi)$ is used as an indicator in order to detect the flapping intensity for a given series

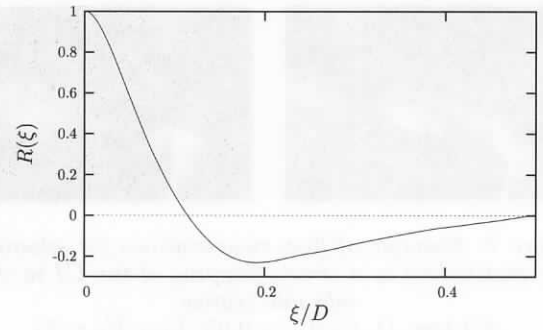

Figure 9: Example of spatial autocorrelation function extracted from a dataset of instantaneous visualizations (supersonic regime, CJ type A, $M_1 = 1.4$, $NPR_{CJ}/NPR_1 = 1.3$)

of visualizations. The more the flapping is intense, the more negative values of $\min(R(\xi))$ are obtained.

Both f_{CJ} and $\min(R(\xi))$ are used in order to extract the properties of the flapping behavior of the CJ.

4.2 Frequencies associated to the flapping motion

The results obtained in the subsonic and in the supersonic regime are plotted on Figure 10. The frequencies are expressed as a Strouhal number based on the vorticity thickness $\delta_{\omega 0}$ at $X/D = 0.1$ and the convective velocity U_c of the mixing layer. This normalization focuses on the dependency between the flapping frequency and the theoretical local frequency of the main mixing layer instabilities.

The results highlight that the most intense flapping of the CJ is associated to a flapping frequency that corresponds to the range $0.15 \leq f_{CJ}\,\delta_{\omega 0}/U_c \leq 0.25$ in the subsonic regime, and $0.18 \leq f_{CJ}\,\delta_{\omega 0}/U_c \leq 0.22$ in the supersonic regime. These ranges correspond to the Kelvin-Helmholtz instability mode of the mixing layer at the CJ impinging location. This result indicates that the perturbations of the incoming mixing layer can drive the flapping instability of the CJ.

These results also highlight that the range of the flapping frequency in the supersonic regime is a lot narrower than in the subsonic regime. This could indicate that the coupling between the flapping and the incoming Kelvin Helmholtz is stronger in the supersonic flow conditions.

4.3 Relations between the flapping frequency and the jet column mode instability of the CJ

Since the whole CJ flaps, it can be interesting to express f_{CJ} as a Strouhal number for the column mode of the CJ itself. This Strouhal number is based on a characteristic length of the CJ, and on the CJ exit velocity U_{CJ}. The exit velocity is computed assuming an isentropic expansion. Off course, this procedure is not rigorous: the flow coming out of the CJ is not isentropic for large values of NPR_{CJ}. The choice of a characteristic length to be used in the case of a rectangular jet column mode is not trivial too.

In order to help on this choice, specific measurements are performed. The CJ is placed outside of the wind tunnel test section, and operated in still air for several

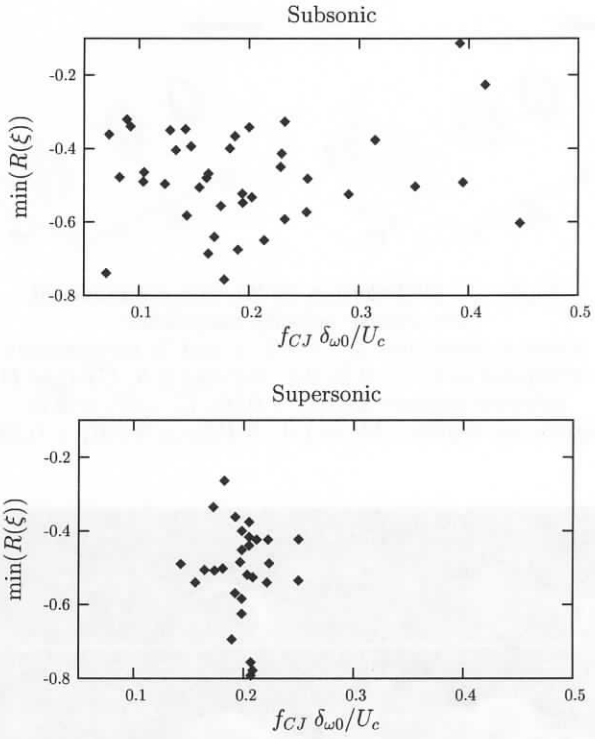

Figure 10: Characteristic frequencies of the flapping motion of the CJ plotted as a function of the minimal value of the auto-correlation $R(\xi)$ in the subsonic and supersonic regimes (frequencies expressed as a Kelvin Helmholtz Strouhal number based on the initial vorticity thickness of the mixing layer)

CJ geometries and three values of NPR_{CJ}. A simple way extract the frequency associated with the jet column mode is to measure the noise spectra of the jet. Usually, this noise is broadband, but higher energy levels are obtained in the range of the jet column mode. So, a microphone is positioned in the vicinity of the blowing CJ. The energy spectra of the radiated noise are computed. Several characteristic length scales are tested in order to collapse the spectra: L, l, hydraulic diameter... The best results are obtained by using the CJ span length L as the characteristic length scale (see Figure 11). The curves collapse well for $NPR_{CJ} = 2$ and 3: the obtained Strouhal number is in the range $[0.15\,;0.2]$ for these regimes. However, the results obtained at $NPR_{CJ} = 4$ put forward that the flow organization is getting more and more complex as the evolution of the CJ is getting less and less isentropic. More, the estimation of U_{CJ} in this regime is mistaken, because of the presence of shock waves in the plume. Nevertheless, in the following the CJ column mode is supposed to be characterized by the isentropic value of U_{CJ} and by the CJ span length L.

The results of the parametric study are now expressed using a Strouhal number based on L and U_{CJ} (see Figure 12). It appears that the most intense flapping situations (i.e. most negative values of $\min(R(\xi))$) are encountered in the range $0.08 \leq f_{CJ}L/U_{CJ} \leq 0.2$ in the subsonic regime, and $0.2 \leq f_{CJ}L/U_{CJ} \leq 0.3$ in the supersonic range.

A comparison between Figures 10 and 12 highlights that the flapping of the CJ can result of a resonance between the Kelvin Helmholtz mode of the mixing layer

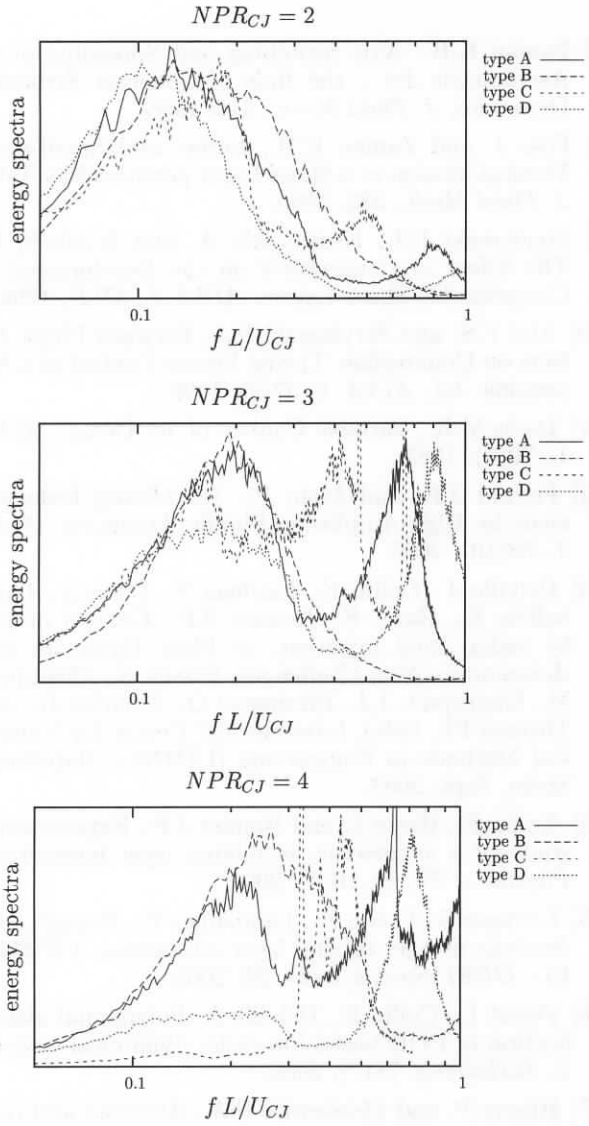

Figure 11: Energy spectra of the radiated jet noise of the CJ blowing in still air

at the CJ impinging location, and the jet column mode of the CJ itself.

Although the resonance mechanism certainly plays an important part for the intensity and the characteristic frequency of the flapping, these informations are not sufficient to explain the flapping itself. To investigate the origins of the flapping, we have to examine the flow characteristics just in front of the CJ, i.e. in the interstice between the main jet exit and the CJ nozzle. This has been performed in a previous study [14]. This region of the flow comprises a cross-stream vertical mixing layer, as depicted by the extracted profile in Figure 13. The shear layer developing at the upstream boundary of the CJ is characterized by vertical velocities $V_{min} = -0.2\Delta U$ and $V_{max} = 0.6\Delta U$. As a consequence, the vertical mixing layer in front of the CJ has a negative velocity ratio $(V_{max} - V_{min})/(V_{max} + V_{min}) = 2$. This value is above the theoretical threshold of the development of an absolute instability, as reported by Huerre and Monkewitz [17]. It has also to be noticed that the mean shear of this small vertical mixing layer is very strong: the difference of vertical velocity is of the order of $0.8\,\Delta U$.

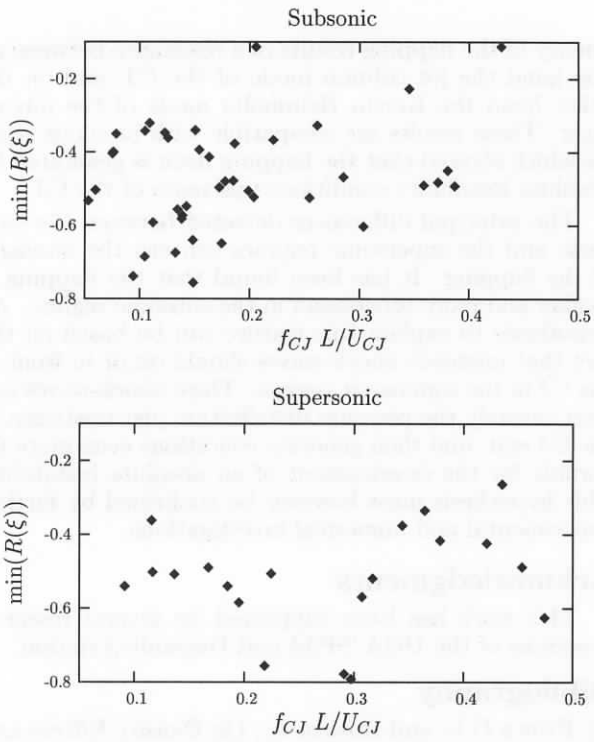

Figure 12: Characteristic frequencies of the flapping motion of the CJ plotted as a function of the minimal value of the auto-correlation $R(\xi)$ in the subsonic and supersonic regimes (frequencies are expressed as a Strouhal number of the CJ column mode based on the span length of the CJ nozzles)

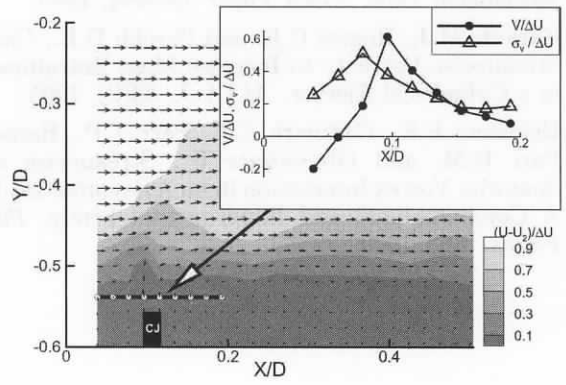

Figure 13: Close-up view of the mean velocity distribution for $Z = 0$, and extracted profile of vertical velocity in front of the CJ [14] (CJ type D, $M_1 = 1.4$, $NPR_{CJ}/NPR_1 = 0.85$)

5 Conclusion

A jet hypermixing device based on *a posteriori* pneumatic injector (control jet CJ) has been studied experimentally. A comparative analysis of the hypermixing efficiency and mechanisms has been performed in subsonic and supersonic regimes. Flow visualizations highlighted the presence of a strong flapping motion of the CJ for a range of flow conditions. A parametric study based on flow visualizations has been performed, involving advanced image processing tools. The parametric study put forward that the intensity and the characteristic fre-

quency of the flapping results of a resonance between on one hand the jet column mode of the CJ, and on the other hand the Kelvin Helmholtz mode of the mixing layer. These results are compatible with previous studies which showed that the flapping itself is generated by absolute instability conditions upstream of the CJ.

The principal differences detected between the subsonic and the supersonic regimes concern the intensity of the flapping. It has been found that the flapping is weaker and more broadband in the subsonic regime. An hypothesis to explain this feature can be based on the fact that unsteady shock-waves should occur in front of the CJ in the supersonic regime. These shock-waves can alter severely the pressure distribution just upstream of the CJ exit, and then generate conditions even more favorable for the development of an absolute instability. This hypothesis must however be confirmed by further experimental and numerical investigations.

Acknowledgments

This work has been supported by several research programs of the DGA/SPAé and Dassault-Aviation.

Bibliography

[1] Brown G.L. and Roshko A., On Density Effects and Large Structure in Turbulent Mixing layers, *J. Fluid Mech.*, 64(4), 1974.

[2] Papamoschou D. and Roshko A., The Turbulent Compressible Shear Layer: An Experimental Study, *J. Fluid Mech.*, 197, 1988.

[3] Bradbury L.J. and Khadem A.H., The Distortion of a Jet by Tabs, *J. Fluid Mech.*, 70, 1975.

[4] Ajuja K.K. and Brown W.H., Shear Flow Control by Mechanical Tabs, *AIAA Paper 89-0994*, 1989.

[5] Carletti M.J., Rogers C.B. and Parekh D.E., Use of Streamwise Vorticity to Increase Mass Entrainment in a Cylindrical Ejector, *AIAA J.*, 33(9), 1995.

[6] Grinstein F.F., Gutmark E.J., Parr T.P., Hanson-Parr D.M. and Obeysekare U., Streamwise and Spanwise Vortex Interaction in an Axisymmetric Jet. A Computational and Experimental Study, *Phys. Fluids*, 8(6), 1996.

[7] Zaman K.B., Axis Switching and Spreading of an Asymmetric Jet : the Role of Coherent Structure Dynamics, *J. Fluid Mech.*, 316, 1996.

[8] Foss J. and Zaman K.B., Large- and Small-Scale Vortical Motion in a Shear Layer perturbed by Tabs, *J. Fluid Mech.*, 382, 1999.

[9] Strykowski P.J., Krothapalli A. and Jendonbi S., The Effect of Counterflow on the Development of Compressible Shear Layers, *AIAA J.*, 37(2), 1999.

[10] Alvi F.S. and Strykowski P.J., Forward Flight Effects on Counterflow Thrust Vector Control of a Supersonic Jet, *AIAA J.*, 37(2), 1999.

[11] Davis M.R., Variable Control of Jet Decay, AIAA J., 20(5), 1982.

[12] Freund J.B. and Moin P., Jet Mixing Enhancement by High-Amplitude Fluidic Actuation, *AIAA J.*, 38(10), 2000.

[13] Delville J., Collin E., Lardeau S., Denis S., Lamballais E., Barre S., Bonnet J.P., Control of jets by radial fluid injection, in *Fluid Dynamics and Aeronautics New Challenges*, Priaux J., Champion M., Gagnepain J.J., Pironneau O., Stoufflet B., and Thomas Ph. (eds), International Center for Numerical Methods in Engineering (CIMNE), Barcelona, Spain, Sept. 2003.

[14] Collin E., Barre S. and Bonnet J.P., Experimental study of a supersonic jet-mixing layer interaction, *Physics of Fluids*, 16(3), 2004.

[15] Lardeau S., Collin E., Lamballais E., Bonnet J.P., Analysis of a jet-mixing layer interaction, ETMM5-10 - *IJHFF Special Issue*, 24, 2003.

[16] Perret L., Collin E., Delville J., Polynomial identification of POD based low-order dynamical system, *J. Turbulence*, 7(17), 2006.

[17] Huerre P. and Monkewitz P.A., Absolute and convective instabilities in free shear layers, *J. Fluid Mech.*, 159, 1985.

Introduction to Turbulent Combustion

Denis Veynante

Laboratoire E.M2.C.

CNRS et Ecole Centrale Paris

Grande Voie des Vignes, 92295 Châtenay-Malabry, France

denis.veynante@em2c.ecp.fr

1 Introduction

Combustion is involved in more of eighty percents of the primary energy conversion processes worldwide and is still an active research area to fit economical (reduced fuel consumption, increased efficiency) and environmental (reduced pollutant emissions, safety) requirements. A challenge is also to avoid combustion instabilities which are induced by a resonant coupling between hydrodynamics, heat release rate and pressure waves and may lead to burner destruction. One of the main objective, not yet achieved today, is to be able to design and optimize a practical system by numerical simulations to reduce development costs, building and testing a limited number of prototypes.

Combustion generally occurs in gaseous flows and may be characterized by a strong and irreversible heat release inducing strong temperature gradients (typical flame thicknesses are about 0.1 to 1 mm when temperature ratios between burnt and fresh gases are of the order of 5 to 7), linked to highly non-linear reaction rate (Arrhenius laws). Obviously, combustion strongly modifies the flow field (thermal expansion, viscosity changes with temperature, baroclinic effects due to density gradients,...). Combustion studies also involves various scientific fields: fluid mechanics, chemistry, mass and heat transfers, two- (liquid fuels) or three- (solid fuels) phase flows,...

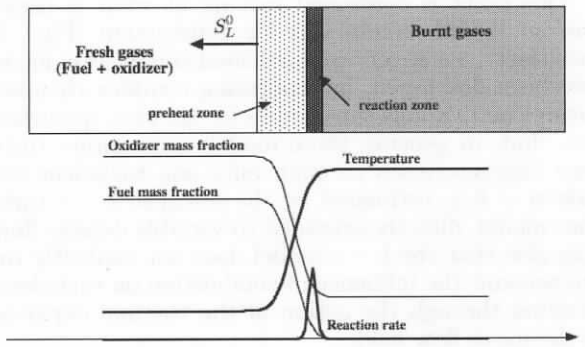

Figure 1: Sketch of a premixed laminar flame. Reactants are mixed prior to the combustion zone. The flame propagates at the laminar flame speed S_L^0 towards fresh gases. Typical values of S_L^0 are about tenths of m/s in deflagration waves, detonation waves propagating at supersonic speeds are not considered here.

Two ideal limiting cases are identified depending on the way to introduce reactants in the combustion zone. Reactants may be either mixed before the flame (*premixed flame*, Fig. 1) or introduced separately (*non-premixed flame*, Fig. 2). As reactants are mixed prior to combustion, premixed flames are more efficient but can propagate upstream of the combustion chamber, leading to safety problems. Reactant mixtures can react only in given proportions, between lean and rich extinction limits. On the other hand, non-premixed flames are simpler to build (a prototype non-premixed flame is a fuel jet discharging in ambient air), but are less efficient (reactants are bring to the reaction zone by molecular diffusion). Non-premixed flames have also a strong drawback: the maximum temperature found in the flame is the temperature of a stoichiometric premixed flames while premixed flames operate at lower temperatures when burning less (lean combustion) or more (rich combustion) fuel than in stoichiometric conditions. This point is of importance for pollutant formation as nitric oxydes (NO_x) are very sensitive to temperature. A way to decrease NO_x emissions is to burn at lower temperatures in lean premixed combustion regimes, promoting this type of burner despite of practical difficulties (ignition, flame stabilization, instabilities,...).

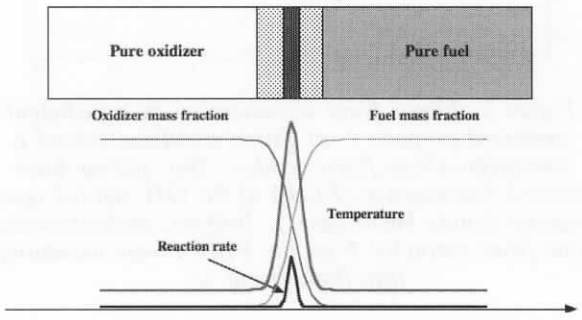

Figure 2: Sketch of a non-premixed laminar flame. Reactants are introduced separately in the combustion zone.

Turbulence is found to enhance combustion processes [1], mainly because turbulent motions wrinkle flame surfaces, increasing the overall reaction rates, at least below certain limits (too intense turbulence may quench the flame). For a given power, turbulent flames are more compact than laminar flames. Accordingly, most of the combustion applications deal with turbulent flows, combining two very complex phenomena. Laminar flames are limited to low power burners such as lighters, candles, domestic cookers and some domestic heaters.

In the following, numerical techniques for turbulent combustion are discussed (Section 2). Then, averaged balance equations and their closure schemes in combustion are briefly analyzed (Section 3). Section 4 describes the physical concepts underlying most of the models proposed in the literature for reaction rates. In Section 5,

the Bray-Moss-Libby (BML) analysis is developed to evidence some specificities of turbulent reacting flows. The last section gives two examples showing how large eddy simulations give access to very promising results (Section 6.2).

2 Numerical simulations in turbulent combustion

To discuss in details direct numerical simulation (DNS), large eddy simulation (LES) and Reynolds averaged Navier-Stokes equations (RANS) formalisms is beyond the scope of this paper but their implication in terms of modelling are simply illustrated here using experimental data extracted from a turbulent premixed propane/air flame stabilized behind a 50 % blockage ratio triangular shape obstacle [2, 3]. Planar laser-induced fluorescence on the OH radical visualizes the burnt gases (grey zones). Assuming an infinitely thin flame front, the progress variable θ (i.e. a reduced temperature or mass fraction) is extracted from the images by separating unburnt ($\theta = 0$) and burnt gases ($\theta = 1$), as shown in Fig. 3.

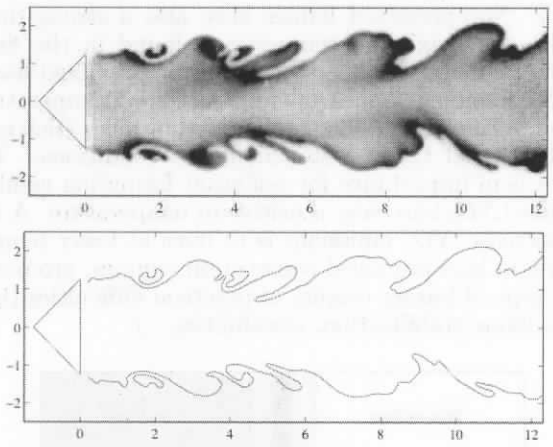

Figure 3: Flame front visualization in a turbulent premixed propane / air flame stabilized behind a triangular-shape flame holder. Top: planar laser induced fluorescence (PLIF) of the OH radical (grey regions denote burnt gases). Bottom: instantaneous flame front extracted from the PLIF image assuming a thin flame front [1].

Direct numerical simulations (DNS), where all the turbulent motions in the flow field are explicitly computed, will remain unreachable for simulations of practical combustion systems for a long time because of numerical requirements. Up to a recent period, computations where limited to the determination of the mean flow field by solving Reynolds averaged Navier-Stokes equations (RANS). Figure 4 displays a mean temperature field as expected to be predicted by RANS simulations but, in fact, at each spatial location, the instantaneous temperature may take only two values along time (telegraphic signal): fresh ($\theta = 0$) and fully burnt ($\theta = 1$) gas temperatures. Then, the mean θ-value only measures the probability to be in burnt gases, as shown in Section 5, and models should take into account this probability.

Since few years, large eddy simulations (LES), where the largest flow motions are explicitly computed while only the effects of the smaller ones are modelled [4], are strongly developing for reacting flows. LES computes a

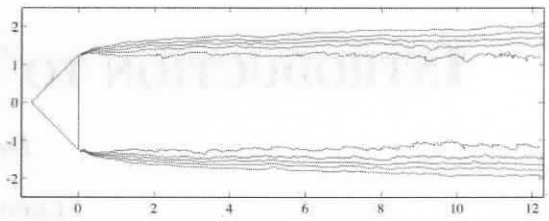

Figure 4: Mean progress variable field $\langle\theta\rangle$ obtained by averaging 200 instantaneous images similar to Fig. 3 [1].

filtered instantaneous flow field as displayed in Fig. 5. Each point in this figure corresponds to a weighted average over a small volume of the instantaneous progress variable θ. This approach, obviously more expensive than RANS in terms of computational costs, is found to be very well suited to combustion. First, reacting flows are generally controlled by large scale motions [5], especially when combustion instabilities occur. Also, locations of fresh and burnt gases are clearly identified at the resolved scale level making combustion modelling easier, as, for example, turbulence, radiative heat transfers or pollutant emissions strongly differ in fresh and burnt gases. This is the main reason why LES is so successful in combustion, even using quite simple turbulence and combustion subgrid scale models.

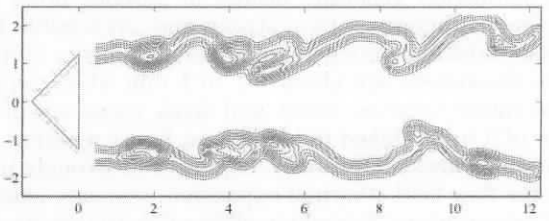

Figure 5: Filtered progress variable field $\overline{\theta}$ extracted from Fig. 3, using a Gaussian filter in the physical space [1].

This point is confirmed looking at what is usually done in RANS simulations for combustion (Fig. 6): since thirty years, very sophisticated combustion models have been developed, incorporating complex chemistry features and various sub-models for ignition, quenching, etc... but, in general, these models incorporate turbulence characteristics through only one turbulent time scale $\tau_t = k/\varepsilon$, estimated by the so-called $k - \varepsilon$ turbulence model, directly extended to variable density flows. Note also that the $k - \varepsilon$ model does not explicitly take into account the influence of combustion on turbulence, excepted through the action of the thermal expansion on the mean flow field.

3 Balance equations

3.1 Averaging

Balance equations for RANS or LES are derived by averaging or filtering instantaneous balance equations for mass, momentum, energy and species mass fractions. In the following, we will focus on some aspects of RANS balance equations (LES equations are formally similar, even their physical meaning differs). The reader will find details in usual textbooks [1, 6]. Averaging the instantaneous mass balance equation, written with usual notations:

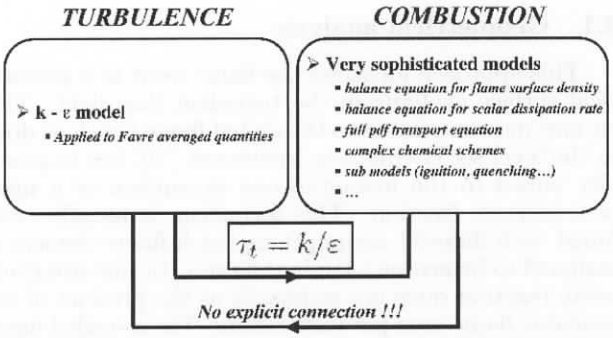

Figure 6: Usual RANS modelling scheme for turbulent combustion.

$$\frac{\partial \rho}{\partial t} + \frac{\partial \rho u_i}{\partial x_i} = 0 \tag{1}$$

gives, as derivation and averaging operators exchanges,

$$\frac{\partial \overline{\rho}}{\partial t} + \frac{\partial \overline{\rho} \overline{u}_i}{\partial x_i} = 0 \tag{2}$$

Decomposing any quantity Q into mean ($\overline{Q}$) and fluctuating (Q') part allow to split the mean mass fluxes $\overline{\rho u_i}$ as:

$$\overline{\rho u_i} = \overline{\rho} \overline{u}_i + \overline{\rho' u'}_i \tag{3}$$

where the second RHS term, corresponding to correlations between density and velocity fluctuations, is unclosed. In practice, the explicit modelling of these correlations, and of any correlation with density fluctuations, is avoided introducing a mass-weighted (or Favre) average as $\widetilde{Q} = \overline{\rho Q}/\overline{\rho}$, leading to the closed mass balance equation:

$$\frac{\partial \overline{\rho}}{\partial t} + \frac{\partial \overline{\rho} \widetilde{u}_i}{\partial x_i} = 0 \tag{4}$$

With this definition, balance equations are similar to usual Reynolds averaged equations for constant density flows. Unfortunately, mass-weighted averaging is only a mathematical formalism that may blur the physical understanding of numerical simulations:

- Usual and mass weighted averages are only linked through the definition $\overline{\rho}\widetilde{Q} = \overline{\rho}\overline{Q} + \overline{\rho' Q'}$, where the last term should be modelled. In fact, $\rho' Q'$ correlations remain hidden in Favre averages. Comparisons between numerical simulations, giving $\widetilde{Q}$, and experiments that generally provide $\overline{Q}$ are then made difficult as these quantities may strongly differ (see Section 5.2).

- Unresolved mass-weighted momentum ($\widetilde{u_i'' u_j''}$) and scalar ($\widetilde{u_i'' Y_k}$) turbulent fluxes have to be close to solve balance equations. Even they contain density fluctuations, there are generally described with usual models developed for constant density flows (turbulence $k - \varepsilon$ model, gradient assumptions). This approach is highly questionable (see Section 5).

3.2 Species mass fraction balance equations

Combustion mainly occurs in transport equations though reacting species mass fractions and energy (heat release rate). For a sake of clarity, we will focus here on the balance equation for the species k mean mass fraction ($\widetilde{Y}_k$):

$$\frac{\partial \overline{\rho} \widetilde{Y}_k}{\partial t} + \frac{\partial \overline{\rho} \widetilde{u}_i \widetilde{Y}_k}{\partial x_i} + \frac{\partial \overline{\rho} \widetilde{u_i'' Y''}_k}{\partial x_i} = -\frac{\partial \overline{V_{k,i} Y_k}}{\partial x_i} + \overline{\dot{\omega}}_k \tag{5}$$

where the last three terms, corresponding respectively to turbulent transport, molecular diffusion and reaction rate, are unclosed and require models. The turbulent transport is generally described under a gradient assumption, coming from mixing of non-reacting scalars in homogeneous flows:

$$\overline{\rho} \widetilde{u_i'' Y''}_k = -\frac{\mu_t}{\sigma_k^t} \frac{\partial \widetilde{Y}_k}{\partial x_i} \tag{6}$$

where μ_t is the turbulence viscosity, provided by the turbulence model, and the turbulent Schmidt number σ_k^t is a model parameter of order unity. This expression is numerically convenient as adding diffusion in the balance equation but may be wrong in some situations (countergradient transport, see § 5.3). Molecular diffusion is generally neglected assuming a large turbulence Reynolds number but may be taken into account by adding a laminar diffusivity into Eq. (6).

The main challenge is then to model the mean reaction rates $\overline{\dot{\omega}}_k$. As Arrhenius laws describing reaction rates are highly non-linear, including mass fraction products and exponential temperature dependence, the mean reaction rate cannot be estimated as the instantaneous reaction rate computed using Favre-averaged quantities:

$$\overline{\dot{\omega}\left(\Psi_1, \Psi_2, \cdots, \Psi_n,\right)} \neq \dot{\omega}\left(\widetilde{\Psi}_1, \widetilde{\Psi}_2, \cdots, \widetilde{\Psi}_n,\right) \tag{7}$$

where Ψ_i denotes thermochemical variables. A proper turbulent combustion model cannot be based on a simple Taylor expansion of reaction rates because this series contains unknown correlations and converges very slowly introducing large truncature errors (see, for example, [1]). This approach is not adapted to combustion problems but may be of interest for some applications such as atmospheric chemistry [7] or supersonic combustion [8]. Therefore, reaction rate closures are generally developed from physical analysis, comparing typical time and length scales for turbulence and combustion to determine whether combustion processes are controlled by turbulent transport or chemical reactions. This analysis leads to the so-called regime diagrams [1, 9, 10]. An example of such a diagram, due to Peters [10], is displayed in Fig. 7 for turbulent premixed flames. Three main regimes are identified: in the *wrinkled flamelet regime*, the flame locally keeps the inner structure of a laminar flame but is wrinkled by turbulence motions, all larger than the flame thickness; in the *thickened wrinkled flame regime*, turbulent motions become able to affect the flame preheat zone (Fig. 1) but the reaction zone remains unaffected; in the *thickened flame regime* no laminar flame structure can be identified any more and reaction zones are mixed by intense turbulence motions.

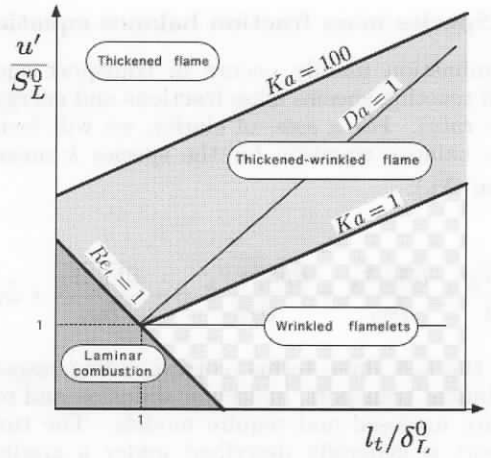

Figure 7: Turbulent premixed combustion diagram as proposed by Peters [10]. Combustion regimes are identified in terms of length (l_t/δ_L^0) and velocity (u'/S_L^0) ratios (log-log scale) where u' is the turbulence intensity, l_t the integral length scale. S_L^0 and δ_L^0 are respectively the laminar flame speed and thickness. The Damköhler number, Da, compares the turbulent integral (l_t/u') and the chemical (δ_L^0/S_L^0) time scales. The Karlovitz number Ka compares the chemical time scale to the Kolmogorov time scale [1].

Such diagrams are only based on qualitative arguments, give only orders of magnitudes and should be used with care. For example, practice shows that the wrinkled-flamelet regime probably extends over a larger zone [11, 12]. Similar diagrams are very difficult to derive for non-premixed combustion as such flames do not exhibit simple time and length scales (they do not have characteristic velocities or thicknesses). The next section is devoted to the physical approaches use to develop models for reaction rates.

4 Physical approaches for turbulent combustion models

According to Veynante and Vervisch [13], most combustion models are derived from one of the three following approaches summarized in Fig. 8.

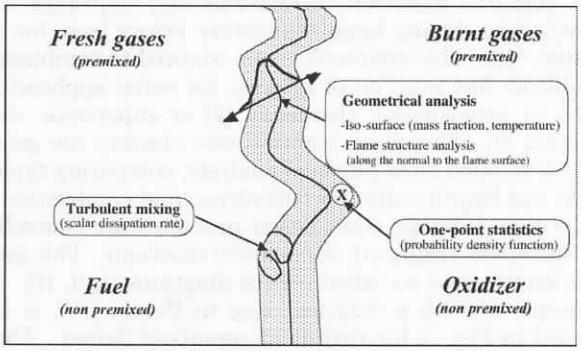

Figure 8: Modeling approaches for turbulent combustion: geometrical analysis (the flame front is identified to a surface), mixing description (the reaction rate is assumed to be controled by the mixing rate, i.e. the scalar dissipation rate) or pure statistical approach (probability density function formalism), following the analysis proposed by Veynante and Vervisch [13]. Extracted from [1].

4.1 Geometrical analysis

This approach identifies the flame front to a geometrical surface evolving in the turbulent flow field. This surface may be related to the global flame brush as done in the level set G-equation framework [10] but is generally linked to the instantaneous iso-surface of a mass or a mixture fraction. This formalism is usually combined with flamelet assumptions (each flame element is assumed to behave as a laminar flame). In this situation, mean reaction rates are estimated as the product of the available flame area per unit volume (the so-called flame surface density) multiplied by the mean reaction rate per unit of flame area. This reaction rate is generally estimated from laminar flame studies when the flame surface density may be either presumed as in the BML (Bray-Moss-Libby) model (Section 5.5, Eq. 25 [14]) or found as the solution of a balance equation [15, 16, 17].

4.2 Turbulent mixing

Under the assumption that chemical time scales are shorter than turbulent time scales (large Damköhler numbers), turbulent flame reaction rates are mainly limited by turbulent mixing rates. The challenge is then to model these turbulent mixing rates, generally expressed in terms of scalar dissipation rates. The simple popular models Eddy-Break-Up [18] for premixed flames and Eddy-Dissipation Concept [19] for non-premixed flames are derived from this point of view.

4.3 One-point statistics

Mean reaction rates are expressed combining instantaneous reaction rates given from Arrhenius laws or chemistry tables $\dot{\omega}_k(\Psi_1, \ldots \Psi_N)$ with the joint probability density function $p(\Psi_1, \Psi_2 \ldots, \Psi_N)$ to have given values of the thermochemical variables (i.e. species mass fractions, temperature...) $\Psi_1, \Psi_2, \ldots \Psi_N$:

$$\begin{aligned} \overline{\dot{\omega}}_k &= \int_{\Psi_1,\ldots\Psi_N} \dot{\omega}_k(\Psi_1, \ldots, \Psi_N) \\ &\times \; p(\Psi_1, \Psi_2 \ldots, \Psi_N)\, d\Psi_1\, \Psi_2 \ldots d\Psi_N \end{aligned} \quad (8)$$

In principle, this approach does not require assumptions on the flame structure such as a flamelet hypothesis or mixing-controlled combustion, even additional assumptions are required in practice to determine unknown quantities. The probability density function may be either presumed, in general as beta-functions [1], or found as a solution of a balance equation [20, 21]. In this last case, reaction rate terms are closed as dependent only on thermochemical variables and do not require any model. Then, this approach can theoretically handle complex chemical schemes. Unfortunately, the molecular transport, involving spatial gradients in the physical space, needs modelling.

4.4 Comments

Even though the previous approaches are based on different physical concepts, they are closely related. To derive the mathematical relations between modeling tools is beyond the scope of such a paper and the reader is referred to reference [13]. These relations are useful to understand the exact implications of the physical hypothesis underlying model developments. According

to this analysis, no approach displays a decisive advantage among others and results will mainly depend on the ability to close unknown quantities.

5 The Bray-Moss-Libby analysis

5.1 Introduction

A very interesting analysis of premixed turbulent flames has been proposed by Bray, Moss and Libby under the assumption of infinitely thin flame fronts [22]. In this situation, the reduced temperature $\theta = (T - T_u)/(T_b - T_u)$, where T_u and T_b correspond to fresh and burnt gases temperatures respectively, may only have two values: $\theta = 0$ in fresh gases and $\theta = 1$ in fully burnt ones. The probability density function $p(\theta)$ of the reduced temperature θ has two peaks and may be written:

$$p(\theta) = \alpha\delta(\theta) + \beta\delta(1-\theta) \tag{9}$$

where δ is the Dirac δ-function and α and β respectively denote the probability to have fresh and burnt gases at a given location ($\alpha + \beta = 1$). The mean value of any quantity Q is given by:

$$\overline{Q} = \int_0^1 Q(\theta)\, p(\theta)\, d\theta = \alpha\overline{Q}^u + \beta\overline{Q}^b \tag{10}$$

where $\overline{Q}^u$ and $\overline{Q}^b$ denote the conditional averages of Q in fresh and burnt gases respectively. Then:

$$\overline{\theta} = \int_0^1 \theta p(\theta)\, d\theta = \beta \tag{11}$$

showing that the averaged temperature $\overline{\theta}$ is the probability to be in burnt gases. The Favre (mass-weighted) average temperature $\widetilde{\theta}$ is directly linked to $\overline{\theta}$ through:

$$\overline{\rho}\widetilde{\theta} = \overline{\rho\theta} = \rho_b\beta = \rho_b\overline{\theta} \tag{12}$$

where ρ_b is the density in burnt gases. The mean density is given by:

$$\overline{\rho} = \alpha\rho_u + \beta\rho_b = (1-\beta)\rho_u + \beta\rho_b \tag{13}$$

where ρ_u is the density in fresh gases. The previous relation is easily recast as:

$$\overline{\rho}(1 + \theta\widetilde{\tau}) = \rho_u = \rho_b(1+\tau) \tag{14}$$

where $\tau = \rho_u/\rho_b - 1 = T_b/T_u - 1$ is the heat release factor. Combining the previous relations gives:

$$\alpha = \frac{1-\widetilde{\theta}}{1+\tau\widetilde{\theta}} \quad \text{and} \quad \beta = \frac{(1+\tau)\widetilde{\theta}}{1+\tau\widetilde{\theta}} \tag{15}$$

providing the probability to be in fresh and burnt gases repectively. An other interesting relation is:

$$\widetilde{Q} = \alpha\frac{\rho_u}{\overline{\rho}}\overline{Q}^u + \beta\frac{\rho_b}{\overline{\rho}}\overline{Q}^b = \left(1-\widetilde{\theta}\right)\overline{Q}^u + \widetilde{\theta}Q^b \tag{16}$$

The Favre average value of any quantity Q is the average of mean values in fresh and burnt gases weighted by the reduced temperature $\widetilde{\theta}$. This analysis has various consequences briefly described in the following sections.

5.2 Relations between Favre and Reynolds averages

Equations (11) and (15) provide a direct relation between Reynolds ($\overline{\theta}$) and Favre ($\widetilde{\theta}$) of the reduced temperature θ:

$$\overline{\theta} = \frac{(1+\tau)\widetilde{\theta}}{1+\tau\widetilde{\theta}} \tag{17}$$

In fact, to assume intermittency between fresh and fully burnt gases implicitly models the density / temperature correlations $\overline{\rho'\theta'}$ linking unweighted and mass-weighted temperature averages. As shown in Fig. 9, $\overline{\theta}$ and $\widetilde{\theta}$ may strongly differ and discrepancies are, as expected, enhanced by high values of the heat release factor. Such discrepancies should be taken into account when comparing numerical results and experimental data.

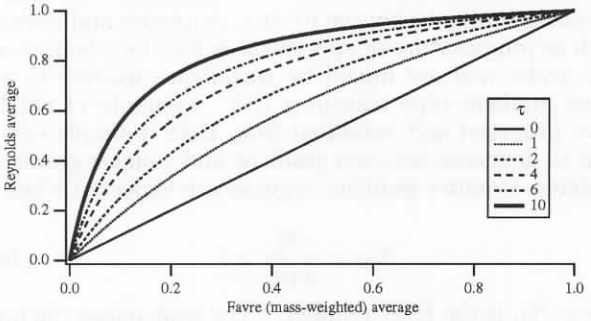

Figure 9: Reynolds averaged temperature $\overline{\theta}$ as a function of the Favre averaged temperature $\widetilde{\theta}$ for various values of the heat release factor τ, assuming a bimodal distribution ($\theta = 0$ or $\theta = 1$) of the reduced temperature θ (Eq. 17) [1].

5.3 Scalar turbulent transport

An exact expression for the turbulent temperature fluxes $\widetilde{u_i''c''}$, to be modeled in RANS, is easily derived from Eq; (16):

$$\overline{\rho}\widetilde{u_i''\theta''} = \overline{\rho}\left(\widetilde{u_i\theta} - \widetilde{u}_i\widetilde{\theta}\right) = \overline{\rho}\widetilde{\theta}(1-\widetilde{\theta})\left(\overline{u}_i^b - \overline{u}_i^u\right) \tag{18}$$

where $\overline{u}_i^u$ and $\overline{u}_i^b$ are the mean conditional i-components of the velocity in fresh and burnt gases respectively. Such fluxes are usually modelled under a gradient assumption (Eq. 6). One may assume, without lost of generality, that the coordinate axis is oriented from fresh to burnt gases (increasing reduced mean temperature $\widetilde{\theta}$. The turbulent flux modelled by the gradient expression (6) is negative. On the other hand, because of thermal expansion, $\overline{u}_i^b - \overline{u}_i^u$ and $\widetilde{u_i''\theta''}$ are expected to be positive in Eq. (18). In fact, to analyse conditional velocities is not so simple and Eq. (18) may lead to both positive or negative values depending on turbulence intensity as shown by DNS [23]. Turbulent transport in the opposite direction than predicted by the gradient assumption (6) is known as *counter-gradient transport*, is observed in experiments [24, 25] and is explained by differential buoyancy effects acting on heavy cold fresh gases and on light hot burnt gases (see a rough scheme in Fig. 10).

For low turbulence levels, the flow field is mainly dominated by the thermal expansion induced by the

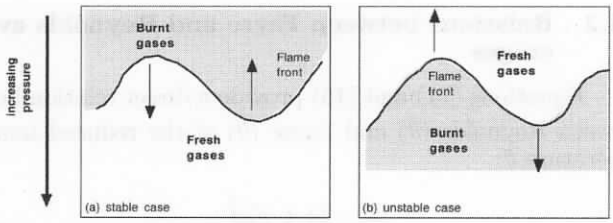

Figure 10: Rough scheme to illustrate differential buoyancy effects acting on heavy fresh and light burnt gases. Left: stable situation, leading to counter-gradient turbulent transport. Right: unstable situation, promoting gradient turbulent transport.

heat release and the transport is of counter-gradient type (the conditional velocity in burnt gases is higher than the conditional velocity in fresh gases). On the other hand, for high turbulence intensities, the flame becomes unable to impose its own dynamics and scalars such as temperature or species mass fractions behave as any scalar and are mixed by turbulence leading to an usual gradient-type transport [23]. Veynante *et al.*[23] have proposed and validated from DNS a simple criterion to delineate between gradient and counter gradient regimes. Counter-gradient regimes are expected when:

$$N_B = \frac{\tau S_L^0}{2\alpha u'} \geq 1 \tag{19}$$

where N_B is the Bray number, τ the heat release factor, S_L^0 the laminar flame speed, u' the turbulence intensity and α a factor measuring the ability of turbulent motions to wrinkle the flame front ($0 \leq \alpha \leq 1$, its maximum value $\alpha = 1$ is reached when the turbulence length scale l_t is larger than about five times the laminar flame thickness δ_L^0).

Favorable pressure gradients also enhance counter-gradient transport [26]. To take into account counter-gradient transport phenomena requires to use (at least) second order turbulence models [27], closing solving 9 additional balance equations in three-dimensional simulations (3 for the turbulent scalar fluxes $\widetilde{u_i''c''}$, 6 for the Reynolds stresses $\widetilde{u_i''u_j''}$, found in $\widetilde{u_i''c''}$-balance equations). Note that the contribution of resolved turbulence motions to counter-gradient transport is directly predicted in large eddy simulations without ad hoc models (Section 6.1, [1, 28]).

5.4 Turbulent stresses and turbulent kinetic energy

Relation (16) may also be applied to Reynolds stresses leading to:

$$\widetilde{u_i''u_j''} = \underbrace{(1-\widetilde{\theta})\overline{u_i'u_j'}^{u}}_{\text{fresh gases}} + \underbrace{\widetilde{\theta}\overline{u_i'u_j'}^{b}}_{\text{burnt gases}} + \underbrace{\widetilde{\theta}(1-\widetilde{\theta})\left(\overline{u}_i^b - \overline{u}_i^u\right)\left(\overline{u}_j^b - \overline{u}_j^u\right)}_{\text{intermittency}} \tag{20}$$

$\widetilde{u_i''u_j''}$ then appear as a weighted average of fresh and burnt gases Reynolds stresses, corresponding to real turbulence, and to an additional term due to the intermittency between fresh and burnt gases. This last term is not related to turbulent motions and appears because the velocities fluctuations u_i'' and u_j'' have no physical meaning in terms of turbulence. They are referred to Favre averaged velocities $\widetilde{u}_i$ and $\widetilde{u}_j$ when turbulence in the fresh gases should be referred to $\overline{u}_i^u$ and $\overline{u}_j^u$ and turbulence in the burnt gases to $\overline{u}_i^b$ and $\overline{u}_j^b$. Note that the intermittency term involves the differences between conditional mean velocity in fresh and burnt gases, $\overline{u}_i^b - \overline{u}_i^u$ and $\overline{u}_j^b - \overline{u}_j^u$. This point is illustrated in Fig. 11, where laser Doppler velocity measurements have been performed in a V-shape turbulent premixed flame stabilized behind a small rod [29]. As expected, gaussian-type probability density function are observed in fresh gases (a) and in fully burnt ones (c). But, in the mean reaction zone (b), a two-peak histogram reveals the intermittency between fresh and burnt gases. Note that in this situation, as the conditional averaged velocity is higher in burnt gases than in fresh gases, the scalar turbulent transport is of counter-gradient type. Such a two-peak histogram is not taken into account in widely used turbulence models.

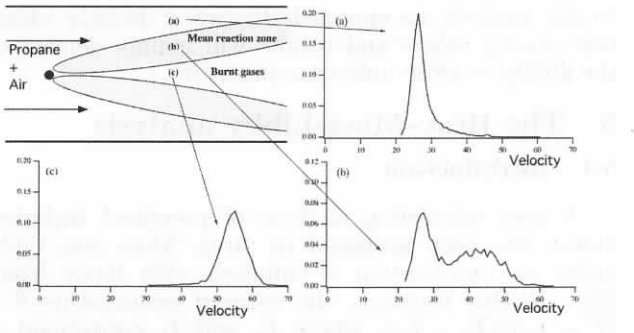

Figure 11: Velocity measurements in a V-shape turbulent premixed flame stabilized behind a small rod (top). Velocity probabilities are displayed in fresh gases (location a), in the mean reaction zone (b) and in burnt gases (c) [1, 29].

5.5 Mean reaction rate

As the flame is assumed to be infinitely thin in the framework of the BML analysis, the mean reaction rate cannot be estimated from the probability density function (Eq. 9) because reacting gases are neglected. Starting from the instantaneous progress variable θ balance equation:

$$\frac{\partial \rho\theta}{\partial t} + \frac{\partial \rho u_i \theta}{\partial x_i} = -\frac{\partial}{\partial x_i}\left(\rho D \frac{\partial \theta}{\partial x_i}\right) + \dot{\omega}_\theta \tag{21}$$

where the molecular diffusion has been modelled by a Fick's law, a balance equation for $\theta(1-\theta)$ is derived:

$$\frac{\partial}{\partial t}\left[\rho\theta\left(1-\theta\right)\right] + \frac{\partial}{\partial x_i}\left[\rho u_i \theta\left(1-\theta\right)\right] = -\frac{\partial}{\partial x_i}\left(\rho D \frac{\partial}{\partial x_i}\left[\theta\left(1-\theta\right)\right]\right) + 2\rho D \frac{\partial\theta}{\partial x_i}\frac{\partial\theta}{\partial x_i} - 2\theta\dot{\omega}_\theta + \dot{\omega}_\theta \tag{22}$$

Averaging this equation, taking into account that under the BML assumption $\theta = 0$ or $\theta = 1$ (i.e. $\theta(1-\theta) = 0$) gives:

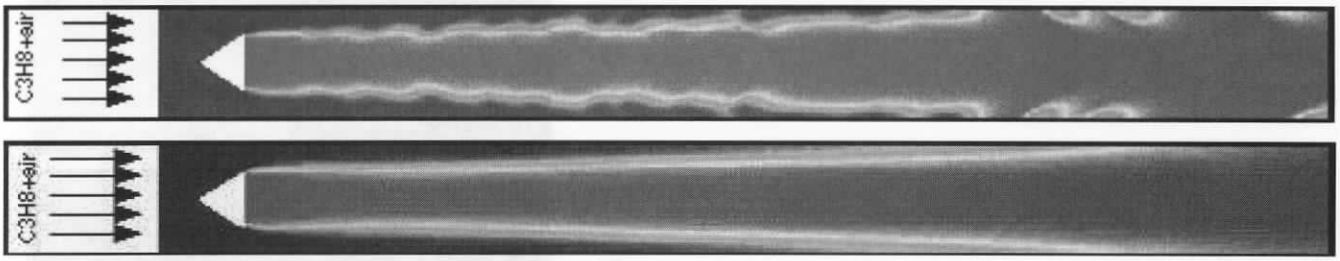

Figure 12: Large eddy simulations of a turbulent premixed propane/air flame stabilized behind a triangular shape flame-holder [28]. Top: instantaneous filtered progress variable $\widetilde{\theta}$ ($\theta = 0$ in fresh gases and $\theta = 1$ in fully burnt ones); bottom: time-averaged filtered progress variable field ($\{\widetilde{\theta}\}$).

$$\overline{\dot{\omega}}_\theta = \frac{1}{2\theta_m - 1}\left(\overline{2\rho D \frac{\partial\theta}{\partial x_i}\frac{\partial\theta}{\partial x_i}}\right) = \frac{\overline{\rho}\widetilde{\chi}_\theta}{2\theta_m - 1} \tag{23}$$

where $\theta_m = \overline{\theta\dot{\omega}}_\theta/\overline{\dot{\omega}}_\theta$ may be estimated from the structure of a laminar flame (flamelet assumption) and the scalar dissipation rate $\widetilde{\chi}_\theta$ measures the turbulent mixing speed of the reduced temperature θ. $\widetilde{\chi}_\theta$ may be determined as a solution of a balance equation or simply modelled as:

$$\widetilde{\chi}_\theta \approx \frac{\widetilde{\theta''^2}}{\tau_t} = \frac{\widetilde{\theta}\left(1-\widetilde{\theta}\right)}{\tau_t} \tag{24}$$

where τ_t is a turbulent time, for example given by the $k-\varepsilon$ model as $\tau_t = k/\varepsilon$. This last expression corresponds to a mathematical derivation of the well-known Eddy-Break-Up model [18], initially based on phenomenological arguments.

The BML model has been then recast in terms of flame crossing frequencies [30, 31] and in terms of flame surface densities [14]. In this last version, the flame surface density (i.e. the available flame surface density per unit volume) is expressed as:

$$\Sigma = \frac{g}{\sigma_y}\frac{\overline{\theta}\left(1-\overline{\theta}\right)}{L_y} \tag{25}$$

where g is a model parameter, σ_y an orientation factor supposed to be constant ($\sigma_y \approx 0.6$) and L_y the wrinkling length scale (in fact, the mean spatial period of flame wrinkling), modelled as a function of the turbulence integral length scale l_t according to:

$$L_y = C_l l_t \left(\frac{S_L^0}{u'}\right)^n \tag{26}$$

where C_l and n are two model parameters of order unity.

The Bray-Moss-Libby analysis starts with a statistical analysis based on a presumed probability density function (Eq. 9), expresses the reaction rate in terms of mixing (scalar dissipation rate, Eq. 23) and may be recast in terms of flame surface (Eq. 25), illustrating the strong links between various modelling approaches (Section 4).

6 Examples of large eddy simulations

Large eddy simulations have already proved its ability to provide very relevant description for turbulent combustion even in complex industrial configurations (see, for example, [32, 33, 34, 35] among a large number of references) and would deserve a review paper. Our objective here is just, through two simple examples, to evidence some advantages of LES compared to RANS simulations.

6.1 Turbulent scalar transport

Figure 12 displays an example of large eddy simulation of a V-shape turbulent premixed propane / air flame [28]. In this simulation, the unresolved scalar transport (i.e. the scalar transport due to subgrid scale motions) is modelled with an usual gradient assumption. This assumption may be wrong (Section 5.3) but, as unresolved LES fluxes are lower than in RANS, model uncertainties have less dramatic consequences. The contribution of the turbulent transport due to resolved motions is explicitly computed in LES and may be extracted from simulations by evaluating $\{\widetilde{u}_i\widetilde{\theta}\} - \{\widetilde{u}_i\}\{\widetilde{\theta}\}$.[1] Three transverse profiles of this quantity, to be modelled in RANS simulations, are displayed on Fig. 13. Close to the flame-holder, the transport due to resolved motions is of gradient type but becomes counter-gradient further downstream because of thermal expansion and the velocity increase in burnt gases, according to experiments [25, 29]. These results show that countergradient turbulent transport, at least at the resolved level, is easily recovered in LES even using a simple gradient subgrid scale model because LES provides a better turbulence description as the different dynamics of resolved fresh and burnt gases is directly taken into account.

6.2 LES of combustion including radiative heat transfers

Radiative heat transfers are strongly controlled by burnt gas zones: high temperatures, species such as water (H_2O), carbon monoxide (CO) or carbon dioxide (CO_2). A better prediction of these transfers is then expected using LES, even neglecting the contribution of unresolved turbulent motions.

Fig. 14 displays an example of preliminary results in a configuration similar to the one in Fig. 12. These simulations have evidenced a strong influence of radiative heat transfers on the flame dynamics (see [36] for details). Similar conclusions have been achieved by Schmitt et al. [37] using a simpler radiation model. Note that the computation displayed in Fig. 14 has been performed by coupling two codes running asynchronously,

[1] In this section, $\overline{Q}$ and $\widetilde{Q}$ denote filtered and mass-weighted filtered LES quantities respectively while $\langle Q\rangle$ and $\{Q\}$ corresponds to time and mass-weighted time averages.

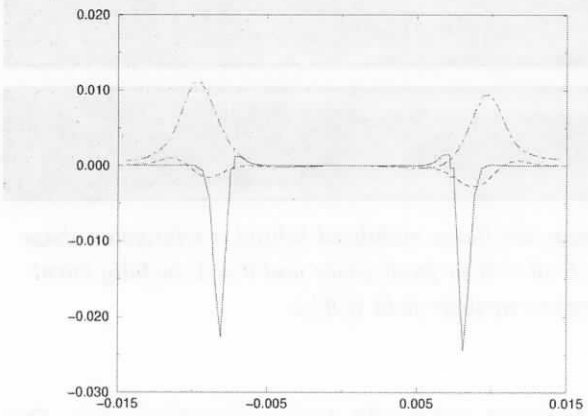

Figure 13: Transverse profiles of the resolved turbulent fluxes $\{\widetilde{u}_i\widetilde{\theta}\} - \{\widetilde{u}_i\}\{\widetilde{\theta}\}$ extracted from the computation of Fig. 12 for three locations: 2 cm (——), 6 cm (- - - -) and 10 cm (— · —) downstream of the flame holder. Positive values indicate counter-gradient transport [28].

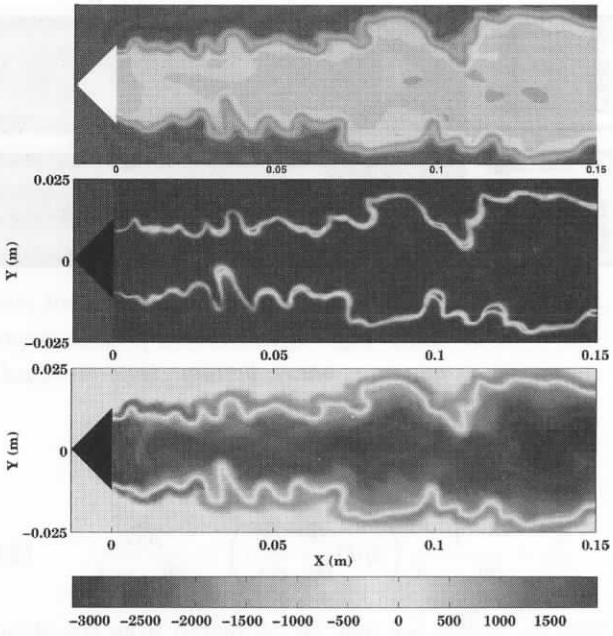

Figure 14: Resolved instantaneous fields of temperature (top), heat release rate (middle) and radiative power (bottom) from a coupled combustion / radiative heat transfer computation of a turbulent premixed propane / air flame stabilized downstream of a flame-holder [39, 36]. Negative radiative power (in kW/m^3) are lost by hot gases.

a combustion code (AVBP from CERFACS) and a heat transfer code (Rayon, from EM2C), using a specialised language (CORBA [38]) developed for communications between computers through networks. This approach has several advantages:

- Combustion and radiative heat transfer codes have very different structures. In general, as combustion codes are based on small volume balances (finite volume framework), they are parallelized by domain splitting. On the other hand, parallelization by wavelength ranges or/and radiation directions is more relevant for radiative heat transfers.
- Codes exchange data (temperature and species mass fractions fields from the combustion code to radiative transfer code, radiative power field and wall fluxes in the opposite way) only through the CORBA interface, ensuring the portability of the coupling over networks and between different machines.
- The combustion code is here compressible and explicit and, accordingly, limited by acoustic waves propagation. Radiative heat transfers are infinitely fast phenomena but evolve with the convection of resolved scale structures. Accordingly, the update of radiation data is not required at each iteration of the combustion code, saving computational resources.

7 Conclusions

Turbulent combustion is of strong practical interests but combines two very complex phenomena. Turbulence is known to enhance combustion and corresponding reaction rates leading to more compact flames. Combustion may either damp (high viscosities and reduced Reynolds numbers because of temperature increases) or promote (thermal expansion, baroclinic effects) turbulence depending on the situation. Reacting species do not behave as passive scalars and flames may become able to impose their own dynamics to the flow field, leading to a priori surprising effects such as counter-gradient turbulent transport.

Turbulence may be quite different in fresh and in burnt gases and probably cannot be correctly predicted by simple models, such as the widely-used $k-\varepsilon$ model, that do not take into account intermittency between fresh and burnt gases. In fact, very sophisticated combustion models have been developed for RANS simulations, including complex chemistry features, but are based on only one input from turbulence characteristics: the integral time scale. To improve RANS description would require improved turbulence models including combustion phenomena. An other alternative is large eddy simulations providing very promising results even with quite simple models mainly because of the better description of the flow dynamics and of the identification, at the resolved scale level, of the instantaneous fresh and burnt gas locations.

Bibliography

[1] Poinsot T. and Veynante D., *Theoretical and Numerical Combustion*, Edwards Inc., Philadelphia, PA, U.S.A, 2nd edition, 2005.

[2] Nottin C., Knikker R., Boger M. and Veynante D., Large eddy simulations of an acoustically excited turbulent premixed flame, *Proc. Comb. Institute*, 28:67 – 73, 2000.

[3] Knikker R., Veynante D. and Meneveau C., A priori testing of a similarity model for large eddy simulations of turbulent premixed combustion, *Proc. Combust. Inst.*, 29:2105 – 2111, 2000.

[4] Sagaut P., *Large Eddy Simulation for incompressible flows*, Scientific computation series, Springer-Verlag, 2000.

[5] Coats C.M., Coherent structures in combustion, *Progress in Energy and Combustion Science*, 22:427 – 509, 1996.

[6] Kuo K.K., *Principles of Combustion*, John Wiley, New York, 1986.

[7] Nieuwstadt F.T.M. and Meeder J.P., Large-eddy simulation of air pollution dispersion: a review, in *New tools in turbulence modelling*, Les Editions de Physique, Springer Verlag, pages 264 – 280,1997.

[8] Villasenor R., Chen J.Y. and Pitz R.W., Modeling ideally expanded supersonic turbulent jet flows with nonpremixed H2-air combustion, *AIAA J.*, 30(2):395–402, 1992.

[9] Borghi R. and Destriau M., *Combustion and flames, chemical and physical principles*, Editions TECHNIP, 1998.

[10] Peters N., *Turbulent combustion*, Cambridge University Press, 2000.

[11] Roberts W.L., Driscoll J.F., Drake M.C. and Goss L.P., Images of the quenching of a flame by a vortex: to quantify regimes of turbulent combustion, *Combust. Flame*, 94:58–69, 1993.

[12] Poinsot T., Veynante D., and Candel S., Quenching processes and premixed turbulent combustion diagrams, *J. Fluid Mech.*, 228:561–606, 1991.

[13] Veynante D. and Vervisch L., Turbulent combustion modeling, *Proc. Energy and Comb. Science*, 28(3):193 301, 2002.

[14] Bray K.N.C, Champion M., and Libby P.A., The interaction between turbulence and chemistry in premixed turbulent flames, in R. Borghi and S.N. Murphy, editors, *Turbulent Reacting Flows*, volume 40 of *Lecture Notes in Engineering*, Springer, pages 541 – 563, 1989.

[15] Marble F.E. and Broadwell J.E., The coherent flame model of non-premixed turbulent combustion, Project Squid TRW-9-PU, Project Squid Headquarters, Chaffee Hall, Purdue University, 1977.

[16] Pope S.B., The evolution of surfaces in turbulence, *Int. J. Eng. Sci.*, 26(5):445–469, 1988.

[17] Trouvé A. and Poinsot T., The evolution equation for the flame surface density, *J. Fluid Mech.*, 278:1–31, 1994.

[18] Spalding D.B., Mixing and chemical reaction in steady confined turbulent flames, in *13th Symposium (International) on Combustion*, The Combustion Institute, Pittsburgh, pages 649–657, 1971.

[19] Magnussen B.F. and Mjertager B.H., On mathematical modeling of turbulent combustion, in *16th Symposium (International) on Combustion*, The Combustion Institute, Pittsburgh, pages 719–727, 1976.

[20] Pope S.B., Pdf methods for turbulent reactive flows, *Progress in Energy and Combustion Science*, 11:119 – 192, 1985.

[21] Dopazo C., Recent developments in pdf methods, in P.A. Libby and F.A. Williams, editors, *Turbulent Reacting Flows*, Academic, London, pages 375 – 474, 1994.

[22] Bray K.N.C. and Moss J.B., A unified statistical model of the premixed turbulent flame, *Acta Astronautica*, 4:291 – 319, 1977.

[23] Veynante D., Trouvé A., Bray K.N.C. and Mantel T., Gradient and counter-gradient scalar transport in turbulent premixed flames, *J. Fluid Mech.*, 332:263 – 293, 1997.

[24] Bray K.N.C., Libby P.A., Masuya G. and Moss J.B., Turbulence production in premixed turbulent flames, *Combust. Sci. Technol.*, 25:pp 127 – 140, 1981.

[25] Shepherd I.G., Moss J.B. and BrayK.N.C., Turbulent transport in confined premixed flame, in *19th Symposium (International) on Combustion*, The Combustion Institute, Pittsburgh, pages 423 – 431, 1982.

[26] Veynante D. and Poinsot T., Effects of pressure gradients on turbulent premixed flames, *J. Fluid Mech.*, 353:83–114, 1997.

[27] Bailly P., *Contribution à l'étude de l'interaction turbulence - combustion dans les flammes turbulentes de prémélange à l'aide de modèles du second ordre*, PhD thesis, Université de Poitiers, 21 Mars 1996.

[28] Boger M. and Veynante D., Large eddy simulations of a turbulent premixed v-shape flame, in *Eighth European Turbulence Conference*, Barcelona, Spain, 2000.

[29] Veynante D., Piana J., Duclos J.M. and Martel C., Experimental analysis of flame surface density model for premixed turbulent combustion, in *Twenty-sixth Symposium (International) on Combustion*, The Combustion Institute, pages 413 – 420, 1996.

[30] Bray K.N.C., Libby P.A. and Moss J.B., Flamelet crossing frequencies and mean reaction rates in premixed turbulent combustion, *Combust. Sci. Technol.*, 41:143–172, 1984.

[31] Bray K.N.C. and Libby P., Passage times and flamelet crossing frequencies in premixed turbulent combustion, *Combust. Sci. Technol.*, 47:253, 1986.

[32] Selle L., Lartigue G., Poinsot T., Koch R., Schildmacher K.U, Krebs W., Prade B., Kaufmann P. and Veynante D., Compressible large eddy simulation of turbulent combustion in complex geometry on unstructured meshes, *Combustion and Flame*, 137:489 – 505, 2004.

[33] Roux S., Lartigue G., Poinsot T., Meier U. and Bérat C., Studies of mean and unsteady flow in a swirled combustor using experiments, acoustic analysis and large eddy simulations, *Combustion and Flame*, 141(1-2): 40 – 54, 2005.

[34] Staffelbach G., Gicquel L.Y.M. and Poinsot T., Highly parallel large eddy simulations of multiburner configurations in industrial gas turbines, in *The Cyprus International Symposium on Complex Effects in Large Eddy Simulations*, 2005.

[35] Pitsch H., Large-eddy simulation of turbulent combustion, *Annu. Rev. Fluid Mach.*, 38:453 – 482, 2006.

[36] Goncalves dos Santos R., Lecanu M., Ducruix S., Gicquel O., Iacona E. and Veynante D., Large eddy simulations of combustion / radiative heat transfers coupling using the specialised communication language corba, in *The Cyprus International Symposium on Complex Effects in Large Eddy Simulations*, Limassol, Cyprus, 2005.

[37] Schmitt P., Schuermans B., Geigle K. and Poinsot T., Effects of radiation, wall heat loss and effusion cooling on flame stabilisation and pollutant prediction in les of gas turbine combustion, in *ECCOMAS thematic conference on computational combustion*, Lisbon, Portugal, 2005.

[38] Henning M. and Vinoski S., *Advanced CORBA Programming with C++*, Addison-Wesley, 1999.

[39] Lecanu M., *Couplage muti-physique combustion turbulente - rayonnement - cinétique chimique*, Phd thesis, Ecole Centrale Paris, 2005.

Leonardo Da Vinci Colloquium and Competition

Greek Pilot Centre, Athens, 27th October 2006

ERCOFTAC's Scientific Programme Committee resolved, at its meeting in Vienna in Nov. 2005, to organise a competition for the best PhD study in Flow, Turbulence & Combustion in the period 1st January 2005 to 31st June 2006. The winner will be awarded the Leonardo Da Vinci Prize (with a monetary value of € 1000). The whole-day event will consist of two invited presentations, followed by five PhD presentations selected from entries made through national Pilot Centres.

Each and every PC has been asked to nominate up to three candidates for the competition. Candidates may be PhD students or PhD graduates who have submitted their theses no earlier than 1st January 2005. A Jury (see below) will select five entries on the basis of 3-page abstracts submitted by 1st July 2006. The selected candidates will be invited to make related presentations in Athens, with all costs covered from ERCOFTAC resources.

Members of the Jury are: Prof. Stan Drobniak, Dr. Rene Duursma, Prof. Tony Hutton, Prof. Michael Leschziner, Prof. René Oliemans, Prof. Jose Redondo, Prof. Wolfgang Rodi, Prof. Anton van Steenhoven, Prof. Nicholas Vlachos.

All ERCOFTAC members are most welcome to attend. Queries should be addressed to
mike.leschziner@imperial.ac.uk.

ASPECTS OF TURBULENCE IN ASTROPHYSICS

R. Walder [1,2], D. Folini [2], J. Favre [3]

[1] Observatoire de Strasbourg, rue de l'université, 67000 Strasbourg, France

[2] Institute of Astronomy, ETH Zentrum, 8092 Zurich, Switzerland

[3] Swiss National Supercomputing Center CSCS, via Cantonale, 6928 Manno, Switzerland

walder@astro.phys.ethz.ch, folini@astro.phys.ethz.ch, jfavre@cscs.ch

Abstract

Turbulence in astrophysics is a key ingredient for the dynamical understanding of many objects. Birth, life, and death of stars, as only one example, crucially depend on it. We give a short overview of the different turbulent regimes encountered in different astrophysical objects. We describe some aspects of supersonic turbulence, i.e. turbulence with root mean square Mach number clearly above 1 and dissipation is mostly due to shocks. Finally, we discuss some issues related to numerical realization.

1 Introduction

Turbulence is ubiquitous in astrophysics. It has its peculiarities, however, bringing new, interesting facets into the field of research. The first peculiarity is its dynamical interaction with other physical processes under nearly all circumstances. Magnetic and radiative fields, gravity, nuclear, and chemical reactions substantially contribute to the momentum and energy balance. The second peculiarity is the eminent dynamical role turbulence plays for the evolution of many astrophysical objects. A third peculiarity results from the fact that theoretical or numerical results are hard to confront with laboratory measurements due to the extreme, nonterrestrial conditions under which the physical and chemical processes take place. Indeed, the essentially single source of information astrophysicists have on turbulence in outer space is the light from the object, either as a picture or merely as a spectrum. Abundant as such data are, they contain only indirect information (like the width of spectral lines) integrated along the entire line of sight. Consequently, the analysis of this data with regard to turbulence is a research field in its own right [1,2].

2 Turbulence in astrophysics: an overview

A nice overview of different aspects of turbulence in astrophysics provides the conference proceedings [3, 4, 5].

2.1 Stellar structure and evolution

To understand the chemical evolution of the universe stellar evolution must be understood, as essentially all chemical elements beyond Beryllium are produced by nuclear reactions in stars [6]. Essential for the understanding of stellar evolution is the transport of energy and angular momentum within stars. Energy produced by nuclear fusion is transported outwards in essentially two ways: convection and radiation. Angular momentum is also transported by turbulent convection, losses (by stellar winds) or gains (by accretion from a binary companion) at the stellar surface thus affect the rotation profile throughout the star. Magnetic fields can substantially enhance the efficiency of the transport. Turbulence also plays a crucial role for the production of magnetic fields in a stellar dynamo [5]. Turbulence also transports newly produced chemical elements from the central region of the star to its outer layers [7]. The associated change in chemical composition of the outer layers can affect the mass loss and thus the further evolution of the star. The mutual interactions of the different processes, which happen on different scales and in different locations within the star, have not yet emerged into a unique, complete picture. A lot of progress has, however, been achieved in the last few years. The far reaching consequences sketched at the beginning of the paragraph make the proper treatment of turbulence, turbulent mixing, and the interaction of the turbulence with the radiation- and/or magnetic field of the star a key topic in astrophysics.

2.2 Star formation

Star formation today takes place only in molecular clouds: cold (10K), high density (10^2-10^4 part./cm^3) regions of interstellar space (2–20 pc, 1 pc = $3*10^{18}$ cm) that are molecular in nature and contain 10^2 - 10^4 solar masses. From observations it is further known that these clouds are turbulent. Compressible turbulence is thought to regulate the efficiency at which stars form in such clouds. Turbulent pressure prevents global collapse of the cloud, which would result in a much higher star formation efficiency than what is observed. Locally, turbulence leads to density enhancements from which individual stars or small groups of stars can form by cooling and subsequent gravitational collapse. Whether the mass distribution of the newly formed stars (the initial mass function or IMF) is directly set by the turbulence is not clear. The question is of fundamental importance as the initial mass of a star is crucial for its evolution (e.g. life time and synthesis of chemical elements). Another important question is the driving of the turbulence, the energy source and injection scale. For reviews and further references we refer to [8-10].

2.3 Accretion, winds, and jets

Accretion of mass and angular momentum onto a star or a black hole is one of the crucial processes in astrophysics. Turbulence plays a decisive role in this process. Conservation of angular momentum hinders direct infall of matter onto accreting objects. Accretion-disks form in which the fluid parcels have nearly Keplerian orbits. The orbital velocity is highly supersonic (up to Mach 100). Mass is brought inwards by the

transport of angular momentum outwards. One mechanism for this is viscous dissipation provided by turbulence. Commonly it is believed that magnetic shear provides the mechanism that excites and drives the turbulence [11-13]. Strong magnetic fields can be generated in an effective dynamo [5] at the same time. Spiral shocks and disk winds provide an additional source of angular momentum transport.

Outflows or mass ejections are not only essential for stellar evolution but also for the chemical enrichment of the universe. Moreover, they are principally linked to high-energy events such as supernova, γ-ray-bursts and quasars. Often, they are driven by external forces: momentum transfer from photons by scattering in spectral lines or on dust grains. Another important mechanism is centrifugal acceleration along magnetic field lines which fixes the matter to rigid rotation (e.g. winds and jets from accretion disks). Turbulence in outflows presumably originates from unstable driving [14]. Most likely this process leads to a highly fragmented medium, high density knots, some kind of supersonic turbulence described in section 3.

2.4 Supernovae

We distinguish between two different classes of supernovae which both provide 10^{51} ergs explosion energy and 10^{49} ergs in light emission. In both classes, turbulence seems to play a principal role.

The first class is a thermonuclear runaway (type Ia in the phenomenological classification), which burns within less than a second about 1.4 solar masses of oxygen and carbon to iron. The turbulent reactive burning front probably develops from a combustion to a detonation regime (see e.g. Röpke and Hillebrandt in [4]).

The second class results from the gravitational collapse of the iron core of a massive star at the very end of its evolution. Most of the released gravitational energy is stored in neutrini. Only about 1 per mille of the energy is initially in the flow. Within less than a second after collapse and subsequent stabilization of the core in a neutron star, the neutrini start to dump energy into the gas, leading to strong convection. The still falling rest of the star gets shocked. As pointed out by [15] and [16], this can trigger a rapidly growing vortical-acoustic cycle: vorticity is generated at the kinked accretion shock, transported into the core, where it is scattered. The scattering produces strong sound waves which kink the shock even more when interacting with it. Moreover, the sound-waves strongly influence the energy dumping into the gas since the heating/cooling by the neutrini is proportional to T^6 (T: Temperature). All these processes combine to a so far very poorly understood gravo-neutrino-magnetohydrodynamical turbulence which eventually triggers the explosion of the entire star.

3 Aspects of supersonic turbulence

We use the term 'supersonic turbulence' for turbulence with root mean square Mach number larger than one, $M_{rms} > 1$. Turbulence in this regime clearly deviates from the incompressible picture and is also much less understood. Most progress has been made for isothermal conditions (γ=1) on which we focus in the following. The results we are going to summarize are based on numerical simulations for the most part. Isothermal supersonic turbulence is thought to be a good first order model for the interstellar medium (ISM, Section 2.3) and, partly, stellar winds and jets (Section 2.4). An important aspect of the driving of this turbulence is the collision of two flows (e.g. faster and slower parts of radiatively driven stellar winds, wind-wind, supernova ejecta-ISM). We discuss a very simple model of such collision zones in Section 3.2.

3.1 Isothermal supersonic turbulence

Isothermal supersonic turbulence is characterised by the presence of shocks, strong density and velocity contrasts, and a patchy appearance of the flow (figure 1). Density has a log-normal distribution (figure 2; here γ=1 is crucial [17, 18]), correlation with velocity is essentially zero. Shocks account for at least 70% of the total energy loss [19, 20]. In driven turbulence, the strongest shocks dissipate most of the energy, while in decaying turbulence energy is dissipated by a large number of weak shocks. In the later case, the kinetic energy decays as $t^{-\eta}$, with $0.85 < \eta < 1.2$ [21]. The patchy spatial pattern formed by the shocks scales with the energy injection scale [8]. For the velocity structure functions of driven isothermal turbulence, a unifying description from subsonic to supersonic has been proposed [22, 23]. Only one parameter, the Hausdorff dimension D of the most dissipative structure, has to be adapted as a function of M_{rms}, from D=1 (filaments) in the subsonic case to D=2 (sheets) in the supersonic case (M_{rms} = 10). Under non-isothermal conditions, values up to D=2.3 have been reported [24].

3.2 An example: the 2D slab

Whereas most studies of supersonic turbulence so far are based on computations in a periodic cubic box with artificial driving, we report now on a first systematic investigation of supersonic isothermal turbulence driven by colliding hypersonic flows [25]. Such a scenario is both realistic and relevant. Stellar winds and stellar debris from exploded stars are among the most significant sources of energy for the ISM. Preliminary results of turbulence in colliding hypersonic flows which include strong (radiative) cooling can be found in [26-29].

Figure 1 shows the turbulent interaction zones from several simulations. Such zones are shown to be non-linearly unstable [30]. In each simulation, the flows are anti-parallel but otherwise identical. The solution only depends on one single parameter, the upstream Mach number M_u, ranging from 5.5 to 87. The interaction zone is supersonically turbulent with characteristics as discussed in the last paragraph: $1 < M_{rms} < 16$, log-normal density distribution (figure 2), patchy appearance.

Assuming self-similarity in infinite space and no correlation between density and velocity, [25] performed a dimensional analysis within the frame of isothermal Euler equations. The analysis reveals the mean density in the turbulent interaction zone to be independent of M_u while M_{rms} scales linearly with M_u. Numerically – including viscous dissipation implicitly (see section 4) – this result is confirmed and $\langle\rho\rangle \sim 30\rho_u$, $M_{rms} \sim 0.2\, M_u$. This is in sharp contrast to the situation in 1D, where it can be shown that $\langle\rho\rangle \sim \rho_u M_u^2$ and $M_{rms} = 0$.

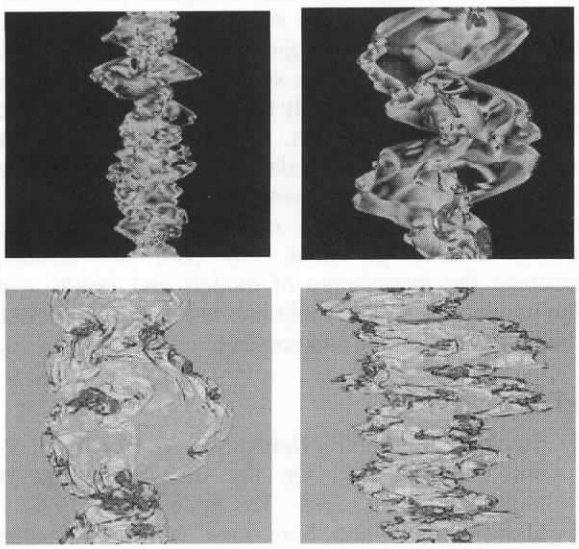

Figure 1: Supersonically turbulent interaction zone of head on colliding flows. Upper row: density for the case of $M_u = 20$ at an early time (left) and a late time (right). Lower row: velocity divergence for $M_u = 10$ flows (left and for $M_u = 30$ (right). The size of the patches and the wiggeling of the bounding shocks are closely linked and depend on M_{rms} and the width of the slab.

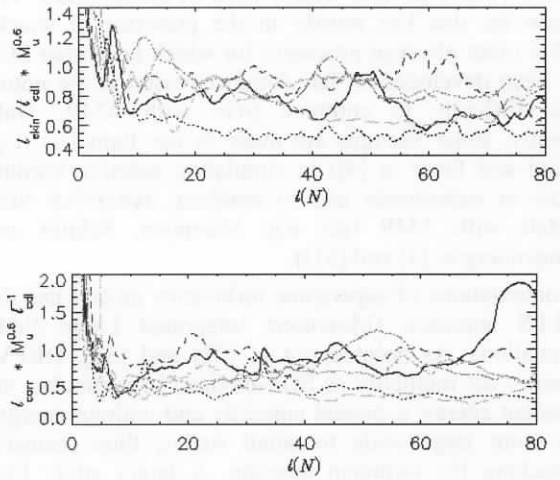

Figure 3: The length scale characterizing the dissipation, l_{ekin} (l_{diss} in the text) and the spatial scale of the wiggeling of the bounding shocks (l_{corr}) scale linearly with the width of the slab (l_{cdl}) and $M_u^{-0.6}$. Shown are the scalings against the mass accumulated in the slab (l(N)) for all runs of our sample. Inprints of the initial conditions die out at approximately l(N)~15, the finite size of the computational box start to affect the results at approximately l(N)=70.

The analysis also brings a deeper insight into the nature of the turbulence. On dimensional grounds, the dissipated energy per unit volume and time must be proportional to $\rho_{diss} v_{diss}^3 l_{diss}^{-1}$. For the average column integrated value (average width of the slab: $l_{cdl.}$) this results in $\varepsilon_{diss} \sim \rho_{diss} v_{diss}^3 l_{diss}^{-1} l_{cdl}$. With no other spatial scale and velocity scale present, it is then naturally to assume $l_{diss} \sim l_{slab}$, and $v_{diss} \sim v_{rms,}$ leading to $\varepsilon_{diss} \sim \rho_{diss} v_{rms}^3$, or $\varepsilon_{diss} \sim \rho_{diss} M_u^3$. A closer analysis given in [18] reveals a very weak Mach-number dependence of ρ_{diss}.

The numerical results coincide with this analysis (figures 1, 3). The dissipation scale l_{diss} and the auto-correlation length of the shock wiggeling l_{corr} nicely scale linearly among each other and with the averaged width of the slab, l_{cdl} . All lengths scale with $M_u^{-0.6}$ (figure 3). This also confirms the eye-catching distribution of the patches and the shock-wiggeling which can be taken from figure 1. The patches and the shock-wiggles are big for large slabs and low Mach-numbers and small for small slabs and high Mach-numbers. The dissipation scale in this supersonically turbulent regime is clearly related to the mean distance between shocks and not to a viscous dissipation length. The good coincidence of the dimensional analysis based on the Euler equations with the numerical results which include implicitly viscous dissipation indeed proves the 'Euler-like' character of the turbulence in this regime.

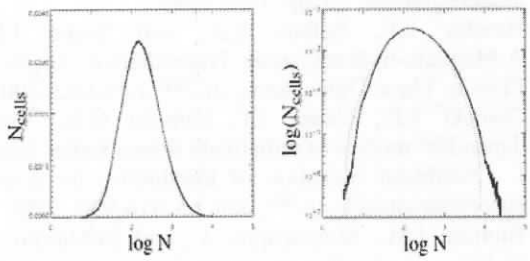

Figure 2: Log-normal density distribution of turbulent flow field shown in Figure 1. The slight deviation indicates probably a slight decay of the turbulence.

4 Aspects of the numerical realization

In astrophysical hydrodynamical simulations, both high resolution finite volume shock capturing schemes (HRFV) such as PPM and statistical methods (so called 'smoothed particle hydrodynamics', SPH, see e.g. [8] for a review) are widely used. Other processes like gravity, radiation, and magnetic fields are mostly included using fractional step methods. Validating self-gravitating magneto-radiation-hydrodynamical simulations is difficult and most of the codes so far are not validated in a scientifically proper way.

In astrophysical simulations, Adaptive Mesh Refinement (AMR) has proven to be very useful. AMR helps, for example, to resolve turbulent burning layers in stars, which are – although geometrically thin – often the source of a convective overturn of large parts of the star. A turbulent molecular cloud starts to collapse due to gravity and cooling at an arbitrary moment of time at an arbitrary location in space, and one would like to follow that collapse over 3-4 orders of magnitude in space in a computationally well resolved manner. However, in connection with turbulence, AMR may also be a nuisance.

Compared to engineering, dynamical subgrid scale models (SGS) are less widely used in astrophysics. The reason for this lies mostly in the presence of shocks and/or other physical processes for which no proper SGS has been developed so far. Another reason is the notorious difficulty to combine SGS with AMR. Only recently, some attempts are made to use flamelets (e.g. Ewald and Peter in [4]) in simulating reactive burning fronts in supernovae and to combine dynamical SGS models with AMR (see e.g. Niemeyer, Schmit and Klingenberg in [4] and [31]).

Computations of supersonic turbulence mostly use the MILES approach (Monotone Integrated Large Eddy Simulation). As pointed out in [32] and [33], HRFV-schemes act implicitly as SGS-models. In particular, the turbulent energy is passed correctly and without energy-jam from large scale to small scales, thus correctly mimicking the turbulent cascade. A larger study [34] confirms this for a large variety of schemes, such as MUSCL, (W)ENO, and Jameson. It also shows, however, the clear limitation of this approach. Many small scale flow features are suppressed by the large diffusivity of these schemes. The further use of an explicit dynamical SGS-model even makes the situation more worse. Having no other tools at hand, all the simulations discussed in Section 3 nevertheless used this approach. However, none of the only very few grid studies have shown convergence. Figure 4 shows the ratio of M_{rms} as computed on a fine and coarse grid for set of simulations used in section 3.2. Although 1280 and 2560 cells are used, the two M_{rms} differ by about 15 percent. Remarkably, the finer discretization shows more dissipation. In our view, this results from the better resolution of shocks, the main source of dissipation, on a finer grid.

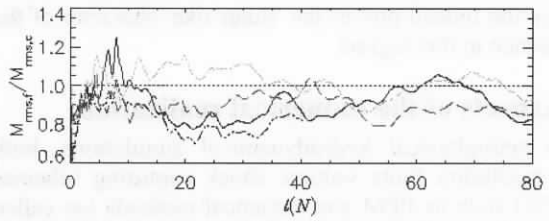

Figure 4: Difference in M_{rms} as computed on a fine and a coarse grid for our set of runs.

Clearly, the situation demands remedy. The authors make currently an attempt to develop appropriate methods which hopefully help to overcome the sketched problems in computation and validation.

5 Conclusions

Observations and theoretical arguments strongly support the view that turbulence is a key-process in astrophysics. The properties and evolution of a wide variety of astrophysical objects can only be understood if turbulence is taken properly into account. 'Properly' in astrophysics signifies that the turbulence is mostly compressible, even supersonic, and usually interwoven with other physical processes. Attempts to model these facets of turbulence have started only recently, in the wake of the steadily increasing computer power. More appropriate numerical tools still have to be developed. They must be able to cope with both, the chaotic dynamics of shocks and the subsonic turbulent cascade. Moreover, they must properly take into account the effect of external fields (radiation, magnetic, gravity) on the momentum and energy balance. Astrophysics is an excellent lab for studying many facets of turbulence and we predict a 'golden age' of turbulence research in astrophysics. To go along this path, we strongly encourage the interchange of models and results with other communities. We would like to thank ERCOFTAC to make this happening and possible.

References

[1] Stutzki J., Bensch F., Heithausen A., Ossenkopf V., and Zielinsky M., On the fractal structure of molecular clouds, *A&A**, 336, pp. 697-720, 1998.

[2] Ossenkopf V. and Mac Low M.-M., Turbulent velocity structure in molecular clouds, *A&A**, 390, pp. 307-326, 2002.

[3] Falgarone E. and Passot T., Turbulence and magnetic fields in astrophysics, Lecture Notes in Physics 614, Springer-Verlag Berlin, 2003.

[4] Kupka F. and Hillebrandt W., Inter-disciplinary aspects of turbulence, conference proceedings (/www.mpa-garching.mpg.de/mpa/publications/proceedings/proceedings-en.html), 2005.

[5] Proctor M.R.E. et al., Solar and Planetary Dynamos, Publications of the Newton Institute, 1995.

[6] Woosley S.E., Heger A., and Weaver T.A., The evolution and explosion of massive stars, *Reviews of modern physics*, 74, pp. 1015-1072, 2002.

[7] Meynet G. and Maeder A., Rotation and mixing in massive stars: principles and uncertainties, ASP Conference Series, 337, pp. 15-27, 2005.

[8] Mac Low M.-M. and Klessen R. S., Control of star formation by supersonic turbulence, *Reviews of modern physics*, 76, pp. 126-194, 2004.

[9] Elmegren B. G. and Scalo J., Interstellar turbulence I: observations and processes, *Ann. Rev. of Astronomy and Astrophysics*, 42, pp. 211-273, 2004.

[10] Scalo J. and Elmegren B.G., Interstellar turbulence II: implications and effects, *Ann. Rev. of Astronomy and Astrophysics*, 42, pp. 274-316, 2004.

[11] Shakura N.I. and Sunyaev R.A., Black holes in binary systems. Observational appearance, *A&A**, 24, pp. 337-355, 1973.

[12] Balbus S.A. and Hawley J.F., Instability, turbulence, and enhanced transport in accretion disks, *Reviews of modern physics*, 70, pp. 1-53, 1998.

[13] Hawley J.F, Balbus S.A. and Stone J.M., A Magneto-hydrodynamic Nonradiative Accretion Flow in Three Dimensions, *ApJ***, L49-L52, 2001.

[14] Owocki S.P., Castor J.I., Rybicki G.B., Time-dependent models of radiatively driven stellar winds. I - Nonlinear evolution of instabilities for a pure absorption model, *ApJ***, 335, pp. 914-930, 1988.

[15] Blondin J.M., Mezzacappa A., and DeMarino C., Stability of standing accretion shocks, with an eye toward core-collapse supernovae, *ApJ***, 584, pp. 971-980, 2003.

[16] Foglizzo T., Scheck L., Janka H.-T., Neutrino-driven convection versus advection in core collapse supernovae, *ApJ***, in press, astro-ph/0507636 (http://fr.arxiv.org/), 2005.
[17] Passot T. and Vázquez-Semadeni E., Density probability distribution in 1-dimensional polytropic gas dynamics, *Phys. Rev.*, E 58, pp. 4501-45001, 1998.
[18] Scalo J., Vázquez-Semadeni E., Chappell D., and Passot T., On the probability density function of galactic gas. I. Numerical simulations and the significance of the polytropic index, *ApJ***, 504, pp. 835-853, 1998.
[19] Smith M.D., Mac Low M.-M. and Zuev J.M., The shock waves in decaying supersonic turbulence, *A&A**, 356, pp. 287-300, 2000.
[20] Smith M.D., Mac Low M.-M. and Heitsch F., The distribution of shock waves in driven supersonic turbulence, *A&A**, 362, pp. 333-341, 2000.
[21] Mac Low M.-M., Klessen R.S., Burkert A. and Smith M.D., Kinetic energy decay rates of supersonic and super-Alfvenic turbulence in star-forming clouds, *Phys. Rev. Lett.*, 80, pp. 2754-2757, 1998.
[22] Boldyrev S., Kolmogorov-Burgers model for star-forming turbulence, *ApJ***, 569, pp. 841-845, 2002.
[23] Padoan P., Jimenez R., Nordlund Å. and Boldyrev S., Structure function scaling in compressible super-Alfvenic MHD turbulence, *Phys. Rev. Lett.*, 92, 19, 2004.
[24] Kritsuk A.G. and Norman M.L., Scaling relations for turbulence in the multiphase interstellar medium, *ApJ***, 601, L55-L88, 2004.
[25] Folini D. and Walder R., Supersonic turbulence in shock-bound interaction zones I: symmetric settings, *ApJ***, in press, astro-ph/0606753, (http://fr.arxiv.org/), 2006.
[26] Walder R. and Folini D., On the stability of colliding flows: radiative shocks, thin shells, and supersonic turbulence, *Astrophysics and Space Science*, 274, pp. 343-352, 2000.
[27] Walder R. and Folini D., Knots, filaments and turbulence in radiative shocks, *A&A**, 330, L21, 1998.
[28] Heitsch F., Burkert A., Lee W., Slyz A.D. and Devriendt J.E.G., Formation of Structure in Molecular Clouds: A Case Study, *ApJ***, 633, L113-L116, 2005.
[29] Vázquez-Semadeni E., Ryu D., Passot T., González R., and Gazol A., Molecular Cloud Evolution. I. Molecular Cloud and Thin Cold Neutral Medium Sheet Formation, *ApJ***, 643, pp. 245-259, 2006.
[30] Vishniac E.T., Non-linear instabilities in shock-bounded slabs, *ApJ***, 428, pp. 186-208, 1994.
[31] Kritsuk A.G., Norman M.L., Padoan P., Adaptive mesh refinement for supersonic molecular cloud turbulence, *ApJ***, 638, L25-L28, 2006.
[32] Boris J.P, Grinstein F.F, Oran E.S. and Kolbe R.L., New insights into large eddy simulation, *Fluid. Dynam. Res.*, 10, pp. 199-228, 1992.
[33] Porter D.H., Pouquet A. and Woodward P.R., Kolmogorov-like spectra in decaying three-dimensional supersonic flows, *Phys. Fluids*, 6, pp. 2133-2142, 1994.
[34] Garnier E., Mossi M., Sagaut P., Comte P. and Deville M., On the use of shock-capturing schemes for large eddy simulation, *Journal of Computational Physics*, 153, pp. 273-311, 1999.

* *A&A = Astronomy and Astrophysics*
** *ApJ = Astrophysical Journal*

The ERCOFTAC Best Practice Guidelines for Industrial Computational Fluid Dynamics are

Available in Electronic Form!

The Best Practice Guidelines can now be provided in electronic form.

- For a one-off payment of 2500 Euro, organisations can provide access to all members of staff by placing the Guidelines on their corporate intranet. (Security of the network must be guaranteed)
- Original, fee-paying members of the Quality and Trust Special Interest Group can receive an electronic copy, without charge, from which they are free to make paper copies.

Please contact:

A.G. Hutton
G26/X80
QinetiQ Ltd.
Cody Technology Park
Ively Road
Hants. GU14 0LX, U.K.

Tel.: +44 1252 395568
Fax: +44 1252 395275
Email: aghutton@qinetiq.com

Second Symposium on "Hybrid RANS-LES Methods" Chandris Hotel, Corfu, Greece, 17-18 June 2007

Organised by EADS Military Air Systems, Germany and
Swedish Defence Research Agency (FOI), Sweden, in association with ECOFTAC

Summary

Hybrid simulation methods, combining RANS and LES techniques, have received increasing attention over the past few years from the turbulence-research community, CFD code developers and industrial CFD engineers. In particular, the Detached Eddy Simulation (DES) method, first introduced in 1997, has acquired a predominant profile and has been the subject of much interest and study.

The fundamentals of DES and other hybrid RANS-LES methods, as well as the recent Scale-Adaptive Simulation (SAS) approach, together with their applications to industrial flow problems, constitute the main focus of the EU-funded project DESider. The present Symposium, which is closely associated with the DESider project, thus addresses the general objective of the project, i.e. to improve CFD-aided design procedures, flow control and analysis of unsteady turbulent aerodynamic flows for the purpose of making DES and hybrid RANS-LES techniques available to the European Aeronautic community.

As with the First Symposium held in Stockholm, 14/15 July 2005, at FOI, the aim of the Second Symposium is to provide a forum for researchers and industrial engineers to exchange their knowledge and experience, to discuss current problems and results and to present recent achievements in the development and applications of hybrid RANS-LES methods - including physical models and related numerical issues. It is expected that the Symposium will encourage an emergence of new ideas and inspire participants to pursue and intensify efforts towards future developments and applications of hybrid RANS-LES methods.

During the symposium, an Exhibition of commercial CFD software will be held. Thus, commercial software vendors are invited to participate. For further details, please contact the Symposium organisers.

Main Topics

Unsteady RANS, LES versus DES
Improved DES
Hybrid URANS-LES
Embedded LES
DES-related numerical issues
SAS model and variants
Industrial applications of DES
Commercial CFD software exhibition

Abstracts, Presentation, Full Papers

Authors should submit an abstract of approx. 1 page.

Full papers (10/15 pages for distributed/invited papers) should be submitted according to the "Important Dates" (please see below).

Following a peer review, revised full papers will be published in the Springer Book Series "Notes on Numerical Fluid Mechanics" including a "Technology Review" by Dr P. Spalart.

Invited Speakers

B. Geurts, University of Twente, Netherlands
M. Mallet, Dassault Aviation, France
U. Piomelli, University of Maryland, USA
P. Sagaut, Lab. de Modélisation en Mécanique, France

Important Dates

01 March 2007	Abstract submission
24 March 2007	Paper acceptance
15 April 2007	Hotel booking deadline
15 May 2007	Deadline for registration
01 June 2007	"Draft" of full papers
17/18 June 2007	DESider Symposium
18-22 June 2007	IUTAM Symposium
16 July 2007	Revised full papers

Organisational Information

The 'Hybrid RANS-LES' Symposium is hosted by the EU-funded project "DESider", which forms part of the final review and is associated to the dissemination and exploitation activities of the project. For information about the DESider project and the project consortium, please visit http://cfd.me.umist.ac.uk/desider.

The symposium is open to academic researchers, graduate students, industrial engineers, industrial R&D managers and consultants with an active interest in the fields of turbulent-flow modelling, simulations and measurements and multidisciplinary CFD applications, such as flow control, aero-acoustics and aero-elasticity.

To receive detailed and forthcoming information of the Symposium, please send your name, affiliation and e-mail address to the organisers (Werner Haase, EADS-MAS, and Shia-Hui Peng, FOI), via e-mail to:

werner.haase@eads.com or peng@foi.se

Please note that the Symposium on Hybrid RANS-LES Methods is preceding the IUTAM Symposium on UNSTEADY SEPARATED FLOWS and their CONTROL, 18-22 June 2007, at the same venue.

NEXT ERCOFTAC EXECUTIVE MEETINGS

The ERCOFTAC Executive meetings will be held on the following dates:

SCIENTIFIC PROGRAMME COMMITTEE AND INDUSTRIAL ADVISORY COMMITTEES:

October 26, 2006
Athens, Greece

May 3, 2007
Berlin, Germany

EXECUTIVE COMMITTEE MEETING:

May 4, 2007
Berlin, Germany

MANAGING BOARD AND GENERAL ASSEMBLY MEETING:

October 26, 2006
Athens, Greece

Please note that the meetings in **Athens** are on Thursday (Leonardo Da Vinci Awards on Friday Oct 27, 2006).

For further information contact Dr. Thierry Ursenbacher at the ERCOFTAC Coordination Centre (contact details inside the back page of the Bulletin).

BULLETIN THEMES AND PC REPORTS

PAST AND FUTURE

The ERCOFTAC Bulletin aims to publish news of, and of interest to, the ERCOFTAC Community every 3 months. Every second issue (March and September) is dedicated to a scientific theme. Pilot Centres are supposed to report occasionally on their activities, and the non-theme issues (June and December) since March 1996 should contain two Pilot Centre reports.

We list below the Themes and PC reports of past and planned future issues from 2003 to 2006. PC chairmen are asked to note when their report is due. A complete list of Bulletin themes can be found in the Bulletin section of the ERCOFTAC web server.Those interested in organising a theme issue or in contributing to planned theme issues are invited to contact the Coordination Centre.

2003

March	*Theme:*	Complex Flow Problems (I. Eames)
June	*PC reports:*	Germany South Nordic Spain (R. Castilla)
September	*Theme:*	Aeroacoustics (B. Boersma)
December	*PC reports:*	France South PC FranceWest PC Germany North PC

2004

March	*Theme:*	Geophysical and Environmental Turbulence Modeling (J. Redondo)
June	*PC reports:*	France PEPIT PC (delayed) Netherlands PC
September	*Theme:*	New Developments in Numerical Methods for CFD (D. Laurence & Ch. Hirsch)
December	*PC reports:*	Belgium PC Switzerland PC France PEPIT PC

2005

March	*Theme:*	Combustion (A. Turan)
June	*PC reports:*	Polish PC
September	*Theme:*	Design Optimisation (W. Haase, F. Menter)
December	*PC reports:*	Czech Republic PC Greek PC Italian PC (short report)

2006

March	*Theme:*	Bio Fluids (A. Van Steenhoven)
June	*PC reports:*	Germany West PC (delayed) Italian PC UK PC
September	*Theme:*	Turbulence and Compressible Flow (P. Comte)
December	*PC reports:*	German South PC Nordic PC

Special Interest Groups

1. Large Eddy Simulation (LESig)
B.J. Geurts, University of Twente, NL
☎ 31.53.489.4125
Fax 31.53.489.4888
b.j.geurts@math.utwente.nl

2. Turbulent Boundary Layers
J. Morrison, Imperial College London, UK
☎ 44.171.594.5067
Fax 44.171.184.8120
j.morrison@ic.ac.uk

4. Turbulence in Compressible Flows
P. Comte, ULP, Strasbourg, F
IMFS
☎ 33.3.90.242.894
Fax 33.3.88.614.300
comte@imfs.u-strasbg.fr

5. Environmental CFD
H. Morvan, University of Nottingham, UK
☎ 44.115.846.6374
Fax 44.115.951.3898
Herve.Morvan@nottingham.ac.uk

8. Turbomachinery
M. Casey,
Universität Stuttgart, D
☎ 49.711.685.3516
Fax 49.711.685.3280
casey@itsm.uni-stuttgart.de

10. Transition Modelling
E. Dick,
Universiteit Gent
Gent, B
☎ 32.9.264.3301
Fax 32.9.264.3586
erik.dick@ugent.be

12. Dispersed Turbulent Two Phase Flow
M. Sommerfeld, Martin-Luther Universität, Halle-Wittenberg, D
☎ 49.3461.462.879
Fax 49.3461.462.878
Martin.Sommerfeld@iw.uni-halle.de

14. Stably Stratified and Rotating Turbulence
J.M. Redondo, UPC, Barcelona, E
☎ 34.93.401.7984
Fax 34.93.401.6090
redondo@fa.upc.es

15. Turbulence Modelling
K. Hanjalic, University of Technology, Delft, NL
☎ 31.15.278.1735
Fax 31.15.278.1204
hanjalic@wt.tn.tudelft.nl

20. Drag Reduction and Flow Control
K.S.Choi, Nottingham University, UK
☎ 44.115.9513.792
Fax 44.115.9513.800
Kwing-So.Choi@nottingham.ac.uk

24. Variable Density Turbulent Flows
F. Anselmet, IMST, Marseille, F
☎ 33.4.91.505.439
Fax 33.4.91.081.637
Fabian.Anselmet@irphe.univ-mrs.fr

28. Reactive Flows
A. Tomboulides
Aristotle Univ. of Thessaloniki
Thessaloniki, GR
☎ 30.2310.991.306
Fax 30.2310.991.304
ananiast@enman.auth.gr

32. Particle Image Velocimetry
M. Stanislas, Ecole Centrale de Lille, Villeneuve d'Asq, F
☎ 33.3.20.337.170
Fax 33.3.20.337.169
stanislas@ec-lille.fr

33. Transition Mechanisms, Prediction and Control
A. Hanifi, FOI, Stockholm, S
☎ 46.8.5550.4334
Fax 46.8.5550.3481
ardeshir.hanifi@foi.se

34. Design Optimisation
R. Schilling, TU München, D
☎ 49.89.289.16295
Fax 49.89.289.16297
schilling@lhm.mw.tum.de

35. Multipoint Turbulence Structure and Modelling
C. Cambon, ECL Ecully, F
☎ 33.4.72.186.161
Fax 33.4.78.647.145
cambon@mecaflu.ec-lyon.fr

36. Swirling Flows
M. Braza, IMFT, Toulouse, F
☎ 33.5.61.285.839
Fax 33.5.61.285.899
braza@imft.fr

37. Bio-Fluid Mechanics
A.A. van Steenhoven
Eindhoven Univ. of Technology, NL
☎ 31.40.2472.722
Fax: 31.40.2433.445
a.a.v.steenhoven@wtb.tue.nl

38. Microfluids and micro heat transfer (MicroSIG)
M. Favre-Marinet, LEGI, Institut National Polytechnique de Grenoble, Grenoble, F
☎ 33.4.76.825.049
Fax 33.4.76.825.271
michel.favre-marinet@inpg.fr

39. Aeroacoustics
B.J. Boersma, University of Technology, Delft, NL
☎ 31.1.5278.7979
Fax 31.1.5278.2947
b.j.boersma@wbmt.tudelft.nl

40. Smoothed Particle Hydrodynamics (SPH)
D. Violeau, EDF
Chatou, F
☎ 33.1.30.87.78.31
Fax 33.1. xxx
damien.violeau@edf.fr

101. Quality and Trust in Industrial CFD (IAC SIG)
A.G. Hutton, QinetiQ,
Farnborough, UK
☎ 44.1252.395.568
Fax 44.1252.395.322
ahutton@QinetiQ.com

102. ERCOFTAC Database Interest Group (Dbig)
ad interim
D. Laurence, UMIST,
Manchester, UK
☎ 44.161.200.3704
dominique.laurence@manchester.ac.uk

The following activities have ceased: 3, 6, 7, 9, 11, 13, 16, 17, 19, 18, 21, 22, 23, 25, 26, 27, 29, 30 and 31.

This page lists the Special Interest Groups currently believed to be active and gives one contact person for each one.

Please notify any corrections to the Coordination Centre in Lausanne.

ERCOFTAC PILOT CENTRES

Austria-Hungary-Slovenia
Prof. H. KUHLMANN
Institute of Fluid Mechanics and Heat Transfer
Vienna University of Technology
Resselgasse 3/1/2
A - 1040 VIENNA
☎ 43.1.58801.32212
Fax 43.1.58801.32298
h.kuhlmann@fluid.tuwien.ac.at

Belgium
Prof. E. DICK
Universiteit Gent
Department of Flow, Heat and Combustion Mechanics
Sint Pietersnieuwstraat 41
B - 9000 GENT
☎ 32.9.264.3301
Fax 32.9.264.3586
erik.dick@ugent.be

Czech Republic
Prof. J. PRIHODA
Institute of Thermomechanics AS CR
5 Dolejskova
CZ - 18200 PRAHA 8
☎ 420.286.890.383
Fax 420.286.584.695
prihoda@it.cas.cz

France - Centre Henri Bénard
Dr. C. CAMBON
Ecole Centrale de Lyon
L.M.F.A. - B.P. 163
F - 69131 ECULLY Cedex
☎ 33.4.72.18.6161
Fax 33.4.78.64.7145
cambon@ mecaflu.ec-lyon.fr

France South
Dr. M. BRAZA
IMF Toulouse
UMR CNRS/INPT-N° 5502
Av. du Prof. Camille Soula
F - 31400 TOULOUSE
☎ 33.5.61.28.5839
Fax 33.5.61.28.5899
braza@imft.fr

France West
Dr. J.-P. BONNET
LEANP, CNRS
BP 30179
F - 86962 Futuroscope - Chasseneuil
☎ 33.5.49.36.6031
Fax 33.5.49.53.6001
jean-paul.bonnet@univ-poitiers.fr

Germany North
Dr. C. WAGNER
DLR
Inst. für Strömungsmechanik
Bunsenstrasse 10
D-37073 GÖTTINGEN
☎ 49.551.709.2261
Fax 49.551.709.2404
claus.wagner@dlr.de

Germany South
Dr. F. MENTER
ANSYS Germany
Staudenfeldweg 12
D - 83624 OTTERFING
☎ 49.8024.905.415
Fax 49.8024.905.417
florian.menter@ansys.com

Germany West
Prof. N. PETERS
RWTH-Aachen
Templergraben 64
D - 52056 AACHEN
☎ 49.241.809.4609
Fax 49.241.809.2923
n.peters@itm.rwth-aachen.de

Greece
Prof. N. VLACHOS
Dept. of Mechanical & Industrial Engineering
Univ. of Thessaly,
Athens Ave. - Pedion Areas
GR-38334 VOLOS
☎ 30.24.210.74094
Fax 30.24.210.74085
vlachos@uth.gr

Italy
Prof. F. MARTELLI
University of Florence
Dept. of Energy
Via Santa Marta 3
I - 50139 FIRENZE
☎ 39.055.479.6237
Fax 39.055.479.6342
martelli@ing.unifi.it

Nordic
Dr. S. WALLIN
Dept. of Mechanics
KTH
S - 10044 STOCKHOLM
☎ 46.8.790.7172
Fax 46.8.796.9850
stefan.wallin@foi.se

Poland
Prof. S. DROBNIAK
Tech. Univ. of Czestochowa
Thermal Machinery Inst.
al. A. Krajowej 21
PL - 42 200 CZESTOCHOWA
☎ 48.34.3250.507
Fax 48.34.3250.555
imc@imc.pcz.czest.pl

Spain
Prof. E. ONATE
Universitat Politecnica de Catalunya - C.I.M.N.E.
Edificio C-1- Campus Norte
Gran Capitan s/n.
E - 08034 BARCELONA
☎ 34.93.401.6035
Fax 34.93.401.6517
onate@cimne.upc.es

Switzerland
Prof. P. MONKEWITZ
EPFL - STI - ISE - LMF
ME B2 485, Station 9
CH - 1015 LAUSANNE
☎ 41.21.693.5322
Fax 41.21.693.5307
peter.monkewitz@epfl.ch

The Netherlands
Prof. G. OOMS
J.M. Burgerscentrum
Mekelweg 2
NL - 2628 CD DELFT
☎ 31.15.278.3216
Fax 31.15.278.2979
g.ooms@wbmt.tudelft.nl

United Kingdom
Prof. A.B. CROWLEY
Cranfield University (RMCS)
Shrivenham, Swindon
UK - Wilts, SN6 8LA
☎ 44.1793.78.5277
Fax 44.1793.78.4196
a.b.crowley@cranfield.ac.uk

Chairman

Prof. R.V.A. OLIEMANS
Multiphase Flow B.V.
Noord Houdringelaan 30
NL - 3722 BR Bilthoven, The Netherlands
☎ +31.30.229.1719
Fax +31.15.278.2838
oliemans@globalxs.nl

Seat, Administration and Development Office

Prof. Ch. HIRSCH
ERCOFTAC
Av. Franklin Roosevelt 5
B - 1050 - Brussels / Belgium
☎ +32.2.643.3572
Fax +32.2.647.9398
ado@ercoftac.be

Coordination Centre

Dr. T. URSENBACHER
ERCOFTAC - Coordination Centre
EPFL STI ISE ERCOFTAC
ME B2 495, Station 9
CH - 1015 Lausanne / Switzerland
☎ +41.21.693.5305
Fax +41.21.693.5307
ercoftac@epfl.ch

The ERCOFTAC Best Practice Guidelines for Industrial Computational Fluid Dynamics

The Best Practice Guidelines (BPG) were commissioned by ERCOFTAC following an extensive consultation with European industry which revealed an urgent demand for such a document. The first edition was completed in January 2000 and constitutes generic advice on how to carry out quality CFD calculations. The BPG therefore address mesh design; construction of numerical boundary conditions where problem data is uncertain; mesh and model sensitivity checks; distinction between numerical and turbulence model inadequacy; preliminary information regarding the limitations of turbulence models etc. The aim is to encourage a common best practice by virtue of which separate analyses of the same problem, using the same model physics, should produce consistent results. Input and advice was sought from a wide cross-section of CFD specialists, eminent academics, end-users and, (particularly important) the leading commercial code vendors established in Europe. Thus, the final document can be considered to represent the consensus view of the European CFD community.

Inevitably, the Guidelines cannot cover every aspect of CFD in detail. They are intended to offer roughly those 20% of the most important general rules of advice that cover roughly 80% of the problems likely to be encountered. As such, they constitute essential information for the novice user and provide a basis for quality management and regulation of safety submissions which rely on CFD. Experience has also shown that they can often provide useful advice for the more experienced user. The technical content is limited to single-phase, compressible and incompressible, steady and unsteady, turbulent and laminar flow with and without heat transfer. Versions which are customised to other aspects of CFD (the remaining 20% of problems) are planned for the future.

The seven principle chapters of the document address numerical, convergence and round-off errors; turbulence modelling; application uncertainties; user errors; code errors; validation and sensitivity tests for CFD models and finally examples of the BPG applied in practice. In the first six of these each of the different sources of error and uncertainty are examined and discussed, including references to important books, articles and reviews. Following the discussion sections, short simple bullet-point statements of advice are listed which provide clear guidance and are easily understandable without elaborate mathematics. As an illustrative example, an extract dealing with the use of turbulent wall functions is given below:

- Check the lower limit of y^+. In the commonly used applications of wall functions, the meshing should be arranged so that the values of y^+ at all the wall-adjacent integration points is only slightly above the recommended lower limit given by the code developers, typically between 20 and 30 (the form usually assumed for the wall functions is not valid much below these values). This procedure offers the best chances to resolve the turbulent portion of the boundary layer. It should be noted that this criterion is impossible to satisfy close to separation or reattachment zones unless y^+ is based upon y^*.
- Check the upper limit on y^+. In the case of moderate Reynolds number, where the boundary layer only extends to y^+ of 300 to 500, there is no chance of accurately resolving the boundary layer if the first integration point is placed at a location with the value of y^+ of 100.
- Check the resolution of the boundary layer. If boundary layer effects are important, it is recommended that the resolution of the boundary layer is checked after the computation. This can be achieved by a plot of the ratio between the turbulent to the molecular viscosity, which is high inside the boundary layer. Adequate boundary layer resolution requires at least 8-10 points in the layer.
- Exercise care when calculating the flow usingdifferent schemes or different codes with wall functions on the same mesh. Cell centred schemes have their integration points at different locations in a mesh cell than cell vertex schemes. Thus the y^+ value associated with a wall-adjacent cell differs according to which scheme is being used on the mesh.
- Check that the correct form of the wall function is being used to take into account the wall roughness. An equivalent roughness height and a modified multiplier in the law of the wall must be used.

All such statements of advice are gathered together at the end of the document to provide a 'Best Practice Checklist'. The examples chapter provides detailed expositions of eight test cases each one calculated by a code vendor (viz FLUENT, AEA Technology, Computational Dynamics, NUMECA) or code developer (viz Electricité de France, CEA, British Energy) and each of which highlights one or more specific points of advice arising in the BPG. These test cases range from natural convection in a cavity through to flow in a low speed centrifugal compressor and in an internal combustion engine valve.

Copies of the Best Practice Guidelines can be acquired from

Prof. A.G. Hutton
QinetiQ
Building 880
Ively Road
Farnborough GUI401X
UK
☎ 44.1252.395.568
Fax 44.1252.395.322
Email: aghutton@qinetiq.com

The price per copy (not including postage) is:

Non-ERCOFTAC Members	150EUR (discount price for academics 75EUR)
ERCOFTAC Members	100EUR (discount price for academics 50EUR)